FORSCHUNGSZENTRUM JÜLICH GmbH
KFA

Institut für Festkörperforschung

Magnetic Circular Dichroism and Resonant X-Ray Scattering at the $L_{2,3}$ Absorption Edges of 3d-Transition Metals in Magnetic Layer-Systems

Wolfgang Clemens

Magnetic Circular Dichroism and Resonant X-Ray Scattering at the $L_{2,3}$ Absorption Edges of 3d-Transition Metals in Magnetic Layer-Systems

Wolfgang Clemens

Abstract

Magnetic Circular Dichroism (MCD) at the $L_{2,3}$ absorption edges of 3d transition elements is studied with circularly polarized synchrotron radiation. The validity of sum rules, with which one can determine element specifically the spin- and orbital magnetic moments from the polarization dependent absorption spectra, is tested for the ferromagnets Fe, Co and Ni. We have investigated the differences in MCD of Fe, Co and Ni $L_{2,3}$ absorption edges measured with electron yield (EY) and fluorescence yield (FY) detection of the absorption signal. The experimentally determined spectra are compared to first-principle calculations. The magnetic coupling of Cr to Fe inside a Fe/Cr multilayer with one atomic layer of Cr between adjacent ferromagnetically coupled Fe films is shown to be antiparallel with a magnetic moment of Cr of about -0.3 μ_B. The dichroism signal of two atomic Cr layers in the same systems nearly vanishes, obviously due to magnetic frustration in the Cr film. In the fluorescence yield detection mode, resonant X-ray scattering effects are observed at Fe/Cr and Co/Mn multilayer systems and single Fe films depending on their structure (especially their thickness) and on the measurement geometry. These effects express themselves in additional intensity at the $L_{2,3}$ white lines, and the dichroism asymmetry can be enhanced drastically. X-ray reflection measurements on these systems have shown, that the dichroism signal can be strongly enhanced at the absorption edges in reflection. Apart from the absorption edges, additional structures are also found in the energy dependent reflection-spectrum, which are related to multilayer reflection peaks. This is verified by reflection calculations on these systems.

Magnetischer zirkularer Dichroismus und resonante Röntgenstreuung an den $L_{2,3}$-Absorptionskanten von 3d Übergangsmetallen in magnetischen Schichtsystemen

Magnetischer Dichroismus im Röntgenbereich hat sich in den letzten Jahren durch die zunehmende Verfügbarkeit intensiver und polarisierter Synchrotronstrahlung als neue leistungsfähige Methode zur elementspezifischen Bestimmung magnetischer und elektronischer Eigenschaften magnetischer Stoffe etabliert. Magnetooptische Effekte im sichtbaren Frequenzbereich sind schon seit dem vorigen Jahrhundert bekannt. Beispielsweise wird die Polarisationsrichtung von linear polarisiertem Licht in isotropen Medien unter Einfluß eines starken Magnetfeldes gedreht, dies ist der sog. Faraday-Effekt. Weit verbreitet zur Untersuchung der magnetischen Eigenschaften von Schichtsystemen ist der magnetooptische Kerr Effekt (MOKE), wo die Polarisationsrichtung linear polarisierten Lichts (z.B. Laserstrahlung), durch die Reflexion an einer magnetischen Oberfläche gedreht wird. Magnetischer Dichroismus im Röntgenbereich wurde dagegen erst 1975 zum ersten mal vorausgesagt [Erskine 75] und Ende der 80er Jahre zuerst beobachtet [Laan 86], [Schütz 87]. Er zeigt sich an unterschiedlichen Übergangswahrscheinlichkeiten (z.B. Absorptionskoeffizienten oder Photoemissionsintensität) ferromagnetischer Stoffe in Abhängigkeit der Orientierung der Magnetisierungsrichtung der Probe relativ zur Polarisation der anregenden Strahlung. Der magnetische zirkulare Dichroismus (engl.: magnetic circular dichroism, MCD) in der Röntgenabsorption äußert sich hierbei durch unterschiedliche Absorptionskoeffizienten, je nachdem ob die Magnetisierungsrichtung der Probe parallel oder antiparallel zur Helizität der anregenden zirkular polarisierten Strahlung ist. Durch die Entwicklung von Summenformeln [Thole 92], [Carra 93], hat man die Möglichkeit erhalten, elementspezifisch die Spin- und Bahn- Anteile magnetischer Momente direkt anhand von Absorptionsspektren zu bestimmen. Dies ist bisher durch keine andere Methode zu erreichen. Die klassischen Methoden zur Bestimmung magnetischer Momente, wie zum Beispiel Messungen mit der Faraday - Waage oder mit SQUID (superconducting quantum interferometer devices), ergeben nur die Gesamtmomente (Summe aus Spin- und Bahnanteil) und sind nicht elementspezifisch. Mit Neutronenstreuung hingegen kann man sehr wohl lokale magnetische Momente bestimmen und die Spin- und Bahn- Anteile trennen. Doch erreicht man dies nur durch Anpassung an Modellrechnungen, es ist also eine sehr indirekte Methode, die auch nicht elementspezifisch ist. Sie hat jedoch ihre Stärke in der Bestimmung von komplexen magnetischen Strukturen. Ähnliches gilt auch für die seit einigen Jahren aufgekommende Methode der magnetischen Röntgenstreuung im harten Röntgenbereich.

Zur Untersuchung der lokalen magnetischen Eigenschaften von heterogenen Systemen, wie zum Beispiel Legierungen, Verunreinigungen, aber auch magnetischen Vielschichtsystemen, bietet die Untersuchung mit MCD in der Röntgenabsorption eine neue sehr vielversprechende Methode. Zumal in jüngster Zeit die Entwicklung von magnetischen Vielschichtsystemen mit besonderen magnetischen Eigenschaften großes

Interesse erregt hat. Diese Eigenschaften sind zum Beispiel oszillierende parallele und antiparallele magnetische Kopplung von ferromagnetischen Schichten, in Abhängigkeit der Schichtdicke einer nichtmagnetischen Zwischenschicht. Interessant für magnetooptische Speicher- und Lesemedien sind ferner die senkrechte Anisotropie und große Magnetowiderstände in diesen Schichtsystemen. Eine besondere Rolle spielen hierbei Fe/Cr Vielfachschichten, an denen die antiferromagnetische Kopplung und der Riesenmagnetowiderstand zuerst entdeckt wurden [Grünberg 86], [Binasch 89]. Das System Fe/Cr dient deswegen vielfach als Modellsystem zur Untersuchung der magnetischen Eigenschaften der Vielfachschichtsysteme.

In dieser Arbeit werden die Effekte des magnetischen zirkularen Dichroismus an den $L_{2,3}$ Absorptionskanten von 3d Übergangselementen untersucht. Die Experimente wurden mit zirkular polarisierter Synchrotronstrahlung am SX700/3 Strahlrohr des Speicherrings BESSY, Berlin, durchgeführt. Die L-Kanten der 3d Übergangselemente liegen im Energiebereich von etwa 300 bis 1000 eV Photonenenergie, also im sogenannten weichen Röntgenbereich. Die Messung der Absorptionskoeffizienten kann auf verschiedene Arten erfolgen. Der direkte Weg ist die Bestimmung der Lichtintensität vor und nach dem Durchdringen der Probe. Dies ist jedoch im Weichröntgenbereich problematisch, da die Eindringtiefe der Strahlung hier nur bei einigen 1000Å liegt. Da die hier untersuchten Proben auf Einkristallsubstraten aufgedampft sind, beträgt ihre Gesamtdicke etwa 1 - 2 mm. Mit der direkten Messung ist es hierbei also nicht möglich, die Absorptionskoeffizienten zu messen. Deswegen wird hier das Absorptionssignal durch Messung von Sekundärprozessen wie der Elektronenausbeute oder der Fluoreszenzausbeute erhalten. Beide Methoden unterscheiden sich im wesentlichen durch unterschiedliche Informationstiefen. Während die Fluoreszenzstrahlung eine freie Weglänge von mehreren hundert Ångstrøm hat und man deswegen z.B. auch Informationen von vergrabenen Schichten erhalten kann, ist die freie Weglänge von Elektronen deutlich geringer, wodurch die Elektronenausbeute im wesentlichen zur Messung von Oberflächeneffekten herangezogen wird. Ferner sind Elektronen im Gegensatz zu den Fluoreszenzphotonen aufgrund ihrer elektrischen Ladung leicht beeinflußbar von angelegten elektrischen und magnetischen Feldern. Anhand von Fe, Co und Ni Schichten wurden diese beiden Methoden zur Messung der Absorptionskoeffizienten verglichen. Die so erhaltenen Spektren unterscheiden sich unter anderem im L_3/L_2 Intensitätsverhältnis der isotropen (gemittelt über alle Polarisationsrichtungen) als auch der Dichroismus-Spektren (Differenz der Spektren zwischen paralleler und antiparalleler Magnetisierungsrichtung zur Lichthelizität). Die Spektren werden verglichen mit neuen first-principles-Rechnungen. Die Gültigkeit der Summenregeln zur Bestimmung der magnetischen Momente wird anhand der Spektren im Vergleich mit Literaturdaten überprüft. Es zeigt sich, daß die Summenregeln im allgemeinen vernünftige Werte liefern, daß sie aber nicht uneingeschränkt anwendbar sind, und sich speziell für die verschiedenen Meßmethoden unterschiedliche Resultate ergeben. Es wird jedoch diskutiert, daß durch Vergleiche mit Referenzproben durchaus quantitative Ergebnisse erhalten werden können mit genügender Genauigkeit. Ferner kann das Verhältnis von Bahn- zu Spinmoment parameterfrei bestimmt werden.

Die Kopplung von Cr in einer Fe/Cr Vielfachschicht wird ebenfalls mit Hilfe von MCD untersucht. Es stellt sich heraus, daß 1 atomare Lage Chrom als Zwischenschicht in einem Fe/Cr System antiferromagnetisch zu Eisen koppelt. Mit Hilfe der Summenformeln wird ein magnetisches Moment von Cr von etwa -0.3 μ_B bestimmt. Rechnungen an demselben System ergeben ebenfalls eine antiferromagnetische Kopplung, allerdings mit einem Cr Moment von -0.652 μ_B. Der niedrigere experimentelle Wert läßt sich dadurch erklären, daß durch nicht-ideales Wachstum und Rauhigkeit der Grenzfläche das Moment erniedrigt werden kann. Der MCD Effekt für zwei atomare Lagen Cr im selben System ist vernachlässigbar gering. Dies läßt sich durch magnetische Frustration im Cr erklären, da zwei angrenzende Cr - Lagen das Bestreben haben, sich einerseits antiparallel zueinander auszurichten, aber auch antiparallel zur angrenzenden Fe Schicht. Dies ist aber gleichzeitig nicht möglich, da die angrenzenden Fe-Schichten parallel zueinander gekoppelt sind. Deswegen wird das magnetische Moment im Chrom in diesem Fall stark unterdrückt (magnetische Frustration).

In der Messung der Fluoreszenzausbeute muß man zusätzlich zum normalen Absorptionssignal noch Röntgenstreuung und -reflexion berücksichtigen. Die Größe dieser Effekte hängt ab vom Aufbau der untersuchten Probe (Materialien, Schichtdicken, Grenzflächen), aber auch von der Geometrie, in der die Messungen durchgeführt werden. Die Streueffekte können nur beobachtet werden, wenn sich der Detektor in der Streuebene befindet und das anregende Licht zumindest teilweise mit dem elektrischen Feldvektor senkrecht zur Streuebene polarisiert ist (s-polarisiert). Die Streuung äußert sich im wesentlichen durch einen Anstieg der Intensität an den $L_{2,3}$ Absorptionskanten, weswegen sie als resonante Röntgenstreuung bezeichnet wird. Sie wurde an Fe, Cr und Mn in Vielfachschichten, aber auch bei Fe in Einzelschichten gefunden. Die Größe der Streuintensität hängt im wesentlichen von der Schichtdicke des jeweiligen Elements ab. Die resonante Streuung hat bei Fe-Spektren starken Einfluß auf die Größe des MCD Effekts. So wird ein Anstieg der Asymmetrie (Verhältnis der Differenz der Absorptions-Intensitäten zwischen paralleler und antiparalleler Orientierung der Magnetisierung zur Lichthelizität und der Summe beider Intensitäten) an der Fe-L_3 - Kante von etwa 20% im Fall ohne Streuung auf etwa 40% mit Streuung beobachtet. Auch in der spekularen Reflexion kann eine Erhöhung der Asymmetrie beobachtet werden, für Fe-L_3 auf bis zu etwa 50%. Dabei muß noch berücksichtigt werden, daß die anregende Strahlung nicht vollständig zirkular polarisiert ist und die Magnetisierung der Probe nicht vollständig in Richtung der Lichthelizität zeigt. Diese Umstände verringern die Größe der Asymmetrie, weswegen man unter idealisierten Umständen noch wesentlich größere Asymmetrien erwarten kann. Diese großen Asymmetrien könnten beispielsweise dazu genutzt werden, linear polarisierte Strahlung durch Reflexion an diesen Schichten in Strahlung mit einem relativ großen Anteil an zirkular polarisierter Strahlung umzuwandeln. Bisher gibt es in diesem Energiebereich (Fe L_3 Kante = 707.5 eV) noch keine Polarisationsfilter. In der spekularen Reflexion erscheinen neben den Absorptionspeaks zusätzliche Strukturen in den Spektren. Sie sind durch normale Vielschichtreflexionen zu erklären, wie Rechnungen hierzu zeigen. Diese Reflexionsstrukturen zeigen keinen MCD Effekt.

I. Introduction

Magnetic dichroism in the X-ray regime has become a matter of great interest in the last few years. It describes the dependence of optical properties (e.g. absorption coefficients, photoemission intensities) on the relative orientation of the magnetization of a sample relative to the polarization direction of the exciting light. Magnetooptical effects in visible light are known already since the 19th century. A survey of these effects is given in ref. [Freiser 68]. For example, the polarization direction of linearly polarized light in an isotropic media is rotated in the presence of a strong magnetic field. This is the so-called Faraday effect. For the investigation of magnetic properties of magnetic films and multilayers the magnetooptical Kerr effect (MOKE) is widely used. Here the polarization direction of linearly polarized light, like for example laser light, is rotated by the reflection at a magnetic surface.

Magnetooptical effects in the X-ray regime have been demonstrated only recently. Magnetic dichroism in the X-ray absorption has been predicted in 1975 by Erskine and Stearn [Erskine 75] at the $M_{2,3}$ absorption edges of ferromagnetic Nickel. Magnetic circular dichroism (MCD) in the X-ray absorption is defined as the difference in the absorption coefficients for parallel and antiparallel orientation of the magnetization direction of the sample relative to the helicity of circularly polarized exciting light. A schematic setup of the absorption process is shown in Fig.1.1. It shows the absorption of circularly polarized light (hν) at the $L_{2,3}$ absorption edges of a 3d ferromagnet.

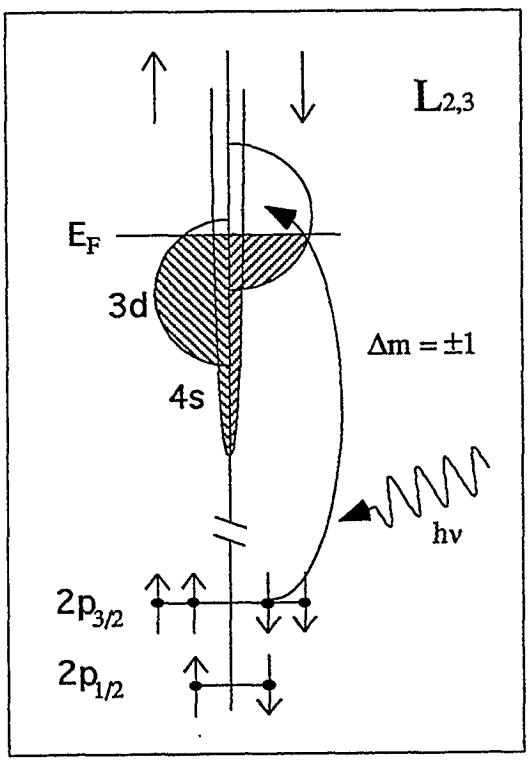

Fig. 1.1. Absorption of circularly polarized light in a ferromagnet.

The differences in the absorption spectrum are caused by the different transition probabilities for positive and negative helicity of the light for transitions from the core levels (e.g. $2p_{3/2}$: L_3 edge) into the unoccupied valence states of a ferromagnet (e.g. Fe), which are mainly of minority spin character.

The first experimental proof of magnetic X-ray dichroism was obtained with linearly polarized light by van der Laan et al. [Laan 86] in the $M_{4,5}$ absorption spectra of magnetically ordered rare-earth materials. The first experimental proof of magnetic X-ray dichroism with circularly polarized light (MCD) was in 1987 by Schütz et al [Schütz 87] at the K-absorption edge of ferromagnetic iron. The theoretical interpretation of these spectra were given by Ebert et al. in 1988 [Ebert 88]. The spectra in this case show relative differences for right and left circular polarization of several times 10^{-4} in magnitude. In the soft X-ray range magnetic circular dichroism has been detected for the first time at the $L_{2,3}$ absorption edges of nickel by Chen et al. [Chen 90]. The MCD signal at the $L_{2,3}$ edges of nickel was found to be approximately 2 orders of magnitude larger than those at the K edges of the transition metals. This can be understood because the $L_{2,3}$ absorption in the 3d transition elements is caused by transitions from the 2p core level to the magnetically relevant (exchange split) 3d states, while the K absorption is caused by transitions from the 1s core level to the p-like valence states, which are hardly polarized. The discovery of the large effects in the $L_{2,3}$ absorption of the 3d elements encouraged further experiments and thus a large number of publications on the MCD at the soft X-ray absorption edges of ferromagnets have appeared in the literature. Due to optimized experimental conditions (for example increasing of circular polarization of the light), the MCD effects could be increased, so that one finds MCD asymmetries at the Fe L_3 edge of about 20% by now.

For the interpretation of the spectra a simple "two step" model based on the single-particle band-structure approximation was developed [Schütz 90],[Stähler 93]. Based on an atomic model, sum rules were derived in 1992 by Thole et al. [Thole 92] and in 1993 by Carra et al. [Carra 93], which relate the intensity of the MCD signal to the ground-state expectation value of the magnetic field operators (orbital, spin and magnetic dipole) of the valence electrons. With the help of these sum rules, one is able to determine element specifically the magnetic moments of a sample separated by the spin- and orbital part. This is the only method so far, which can do this. In neutron scattering, the two contributions can be separated by fitting the measured form factors with a suitable model. In nonresonant X-ray diffraction, different polarization responses directly separate spin and orbital densities. However, all attempts to implement a quantitative separation experimentally have been, so far, inconclusive (see ref. [Thole 92]). There are also other spectroscopic methods, like spin resolved photoemission or spin resolved Auger spectroscopy [Kessler 76],[Feder 85],[FS 92], with which one can determine element specifically the magnetic structure of magnetic materials, but they cannot quantify the magnetic moments. The classical methods for the determination of the magnetic moments, like the Faraday balance or SQUID measurements give only the total magnetic moment (the sum of spin- and orbital contribution) and are not element specific.

The large effects and the possibility of element specific determination of magnetic moments, but also the development of new beamlines for circularly polarized synchrotron radiation in the soft X-ray range have encouraged a lot of experiments in the field of MCD in the last years. Here we can refer only to a limited list of publications in this field. Some examples are: The determination of enhanced orbital magnetic moments on Co atoms in Co/Pd multilayers [Wu 92]; Element-specific magnetic hysteresis as a means for studying heteromagnetic multilayers [Chen 93]; Induced spin polarization in Cu spacer layers in Co/Cu multilayers [Samant 94]; Circular magnetic X-ray dichroism of 3d impurities in Ni [Böske 94]. Furthermore, the geometric electronic structure can be determined by doing MCD measurements in EXAFS (extended X-ray absorption fine structure) measurements [Schütz 90]. The experiments are not limited to the 3d transition metals. There are also works on rare earth (4f) elements (see e.g. ref. [Rudolf 92]) and 5d-transition elements [Schütz 90]. Magnetic dichroism effects can also be used for element specific magnetic photoelectron microscopy (see e.g. [Stöhr 93],[Kachel 94], [Schneider 94]). Magnetic dichroism does not only occur in photoabsorption but it is also seen in photoemission and fluorescence emission. It was first observed in the photoemission spectra from the Fe 2p states in 1990 by Baumgarten et al. [Baumgarten 90]. There is also strong magnetic circular dichroism in 4f photoemission from rare earth elements like gadolinium metal [Starke 93]. Besides dichroism effects with circularly polarized light, linear dichroism is also seen in photoemission [Roth 93]. Magnetic dichroism in the X-ray fluorescence emission was predicted in 1991 by P.Strange et al. [Strange 91] and has first been observed in Fe $L_{2,3}$ X-ray fluorescence spectra in 1993 by Hague et al. [Hague 93]. Thus magnetic dichroism is present in all spectroscopic methods that measure the electronic structure of magnetic materials.

One aim of this work is to proof the validity of the sum rules on the absorption spectra of 3d ferromagnets Fe, Co and Ni determined by different methods, and in comparison with first-principle calculations. Next, MCD is applied to determine the magnetic structure of Cr layers inside a Fe/Cr multilayer. Further, the influence of resonant X-ray scattering and reflection of thin films and magnetic multilayers on the MCD effects is studied and possible applications are discussed.

In this work magnetic circular dichroism will be investigated in the $L_{2,3}$ absorption spectra of the 3d transition elements. The absorption spectra of Fe, Co and Ni are detected by measuring the electron yield (EY) and the fluorescence yield (FY). Both methods can be used analogously for the determination of the absorption coefficients. Differences in the spectra determined with both methods can be caused by the different nature of the electrons (electric charge, strong interaction with matter) and photons (no electric charge, rel. small interaction with matter) and by different transition probabilities in both cases. The electron yield detection is in general very suitable for the determination of surface effects, while the fluorescence detection is mostly used for the determination of bulk properties. The spectra obtained with both methods are compared and the validity of

the sum rules for the determination of the magnetic moments is checked for both cases. Furthermore first-principles calculations are presented of the same systems.

MCD is then applied to Fe/Cr multilayers in order to obtain the magnetic structure of Cr, in these systems. The magnetic properties of magnetic multilayers are of great interest for fundamental reasons but also as new recording and device applications [FS 93]. The Fe/Cr system can be treated as a model system, since here the antiferromagnetic coupling of adjacent Fe layers has been found, depending on the thickness of a Cr interlayer [Grünberg 86], [Carbone 87]. This has been found in the meantime on several other magnetic multilayer systems and the direction of the coupling is found to oscillate dependent on the thickness of non-magnetic interlayers [Parkin 90]. The magneto-resistance in antiferromagnetically coupled multilayers is found to be enhanced drastically compared to conventional bulk systems [Binasch 89]. For the interpretation of these effects, a microscopic understanding of the magnetic structure is important. The coupling behavior of Cr on Fe has been studied recently by several methods. It is found, that the first atomic layer of Cr couples antiparallel to Fe and the next layers couple antiferromagnetically to each other [Walker 92], [Unguris 93],[Jungblut 91],[Idzerda 93]. All these measurements have been done so far for Cr on an iron surface, but the coupling inside a real multilayer system has hardly been studied until now. In the work of Böske et al. [Böske 94b,c], the first atomic layer of Cr is found to couple antiparallel to Fe inside a Fe/Cr/Ag multilayer. But due to scattering effects in the spectra, the magnitude of the magnetic moment could not be determined. This will be done in this work.

Resonant X-ray scattering can influence the absorption spectrum measured in the fluorescence yield method. The wavelength of X-rays in the soft X-ray regime is in the typical thickness range of the investigated multilayer structures (some ten Ångstrøms). Therefore one can expect interference of the incidence light with the reflected or fluorescence light. Because the optical properties of matter are changing strongly at absorption edges, one can further expect interference or scattering intensities at the absorption edges, which causes resonant effects. These effects will be investigated systematically in relation to the dependence on the elements, film thickness and light polarization. Especially the influence on the MCD signal will be discussed. In specular reflection new structures appear in the energy dependent spectra due to multilayer reflections. They are studied on Fe/Cr multilayers and are compared to calculations. At the absorption edges the MCD signals are also strongly affected in reflection. This is also studied and possible applications are discussed.

II. X-Ray -Absorption, -Reflection, -Scattering

Most fundamental physical and chemical properties of matter (like conductivity, chemical bonding, magnetism, etc.) are caused by its electronic structure. Therefore the knowledge of the electronic structure is fundamental for a microscopic understanding of macroscopic properties. The interaction of light with matter can be used as a powerful tool for the determination of the electronic structure. Here we will discuss the interaction of matter with X-rays in the soft X-ray regime, that is the energy range of about $h\nu \approx 50$ - 2000 eV. The interaction with the electrons in the soft X-ray regime is of great interest for the determination of the electronic structure of many materials, because here are the excitation of the K (1s) shells of the light elements (C, N, O) and of the L (2p) shells of the magnetically relevant 3d transition metals (and the M shells of the 4f elements). This energy range can be covered experimentally with monochromatized synchrotron radiation, where also the polarization of the light can be chosen [Petersen 93]. An overview of the interaction of soft X-rays with matter, especially for the determination of the electronic structure is given in the book *"NEXAFS "* by J. Stöhr [Stöhr 92]. An overview of the use of synchrotron radiation for the investigation of condensed matter is given in ref. [FS 92]

The interaction of X-rays with matter results in direct and secondary processes. The interactions of the incident X-rays with the sample that result in "secondary" electrons is photoabsorption followed by Auger decay. The interactions of the incident X-rays with the sample that result in "secondary" photons are i) X-ray absorption followed by fluorescent decay, ii) coherent and incoherent scattering of X-rays, iii) specular reflection of X-rays and iv) diffuse scattering by surface irregularities. At first we discuss the photoabsorption, which gives information about the electronic structure of the investigated substance. The other effects are discussed in the second part of this chapter.

2.1 X-Ray Absorption

The intensity I of X-rays penetrating through matter decays due to the absorption of photons of the energy $h\nu$ after a penetrating length x according to the exponential law

$$I(h\nu, x) = I_0 \cdot e^{-\mu(h\nu)\, x} \quad , \tag{2.1}$$

where $\mu(h\nu)$ is the energy dependent linear absorption coefficient. This coefficient $\mu(h\nu)$ [cm^{-1}] is related to the absorption cross section $\sigma_x(h\nu)$ [cm^2/atom] by the atomic volume density of the sample n_V [atoms/cm^3] according to

$$\mu(h\nu) = n_V \, \sigma_x(h\nu). \tag{2.2}$$

The volume density is calculated from the mass density n_m [g/cm^3] by the relation $n_V = n_m \, L/A$, where $L = 6.022 \cdot 10^{23}$ [atoms/mole] is Avogadro's number and A

[g/mole] is the atomic weight. The X-ray absorption cross section σ_x of an atom is defined as the number of electrons excited per unit time divided by the number of incident photons per unit time per unit area. It therefore has the dimension (length)^2 and is usually given in units of cm^2 or barn (1cm^2 = 10^{24} barn). In the soft X-ray region values for $\sigma_x(h\nu)$ and μ ($h\nu$) have been tabulated [Palik 91],[Veigele 73],[Henke 82]. From these data the photon mean free path $1/\mu$ ($h\nu$) in most materials at $h\nu$ = 1000 eV is of the order of 1000Å.

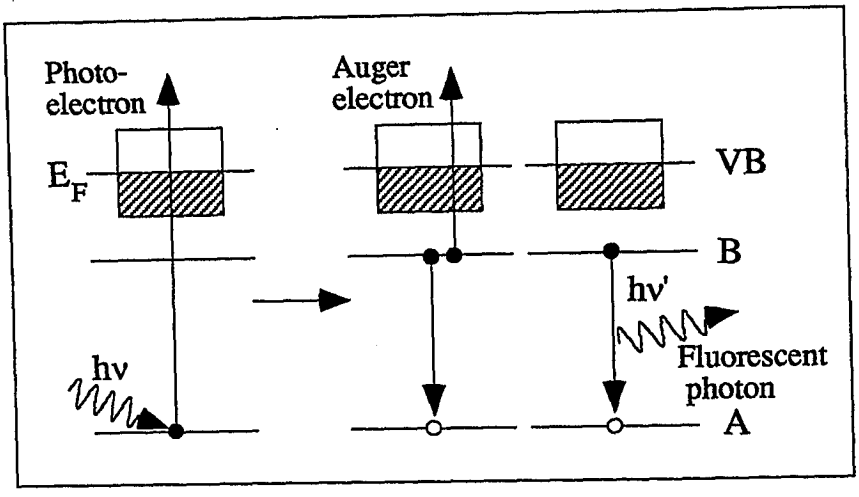

Fig. 2.1. Schematic diagram of a photon absorption process resulting in a photoelectron and a core hole (A). The hole is filled by an electron from a higher shell (B) either nonradiatively by emission of an Auger electron, or radiatively by emission of a fluorescent photon.

In the soft X-ray region the absorption of photons by emission of a photoelectron dominates by orders of magnitude over all other interactions (except reflectivity, which can be important under certain conditions, see below). The number of absorbed photons is directly proportional to the X-ray absorption cross section and, according to Fig. 2.1, so is the number of created core holes and photoelectrons. Fig. 2.1 suggests that the most direct method of measuring the X-ray absorption cross section is to monitor the intensity of the photoelectrons which constitute the primary excitation channel. However, this is not a valuable method since only those photoelectrons are measurable that have a higher energy than the vacuum level and most of them do not escape. The secondary deexcitation process occurs either nonradiatively, by Auger electron emission, or radiatively, by emission of a fluorescent photon. Both intensities are proportional to the absorption coefficient and therefore one can measure $\mu(h\nu)$ either by measuring the secondary electrons (electron yield detection (EY)) or photons (fluorescence yield detection (FY)). The fraction of the nonradiative decay rates relative to the total decay rate are called Auger yield ω_a and fluorescence yield ω_f, respectively, and satisfy the sum rule $\omega_a + \omega_f = 1$. The relative yields are a strong function of the atomic number Z, as shown for the the K- and L- shell fluorescence in Fig. 2.2.

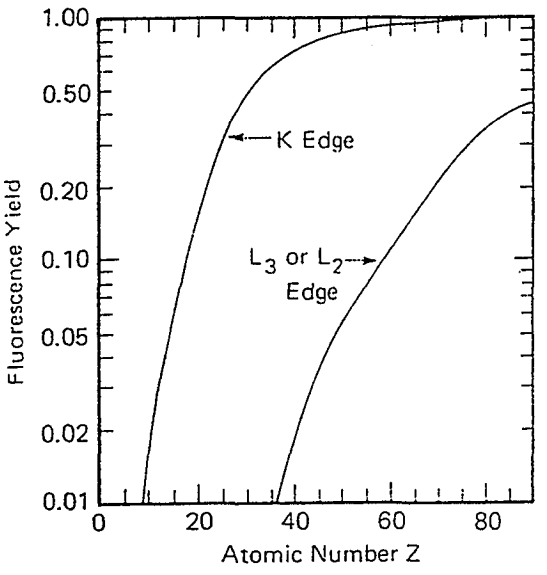

Fig. 2.2. Fluorescence yields following the excitation of K and L shells as a function of the atomic number Z, data taken from ref. [Krause 79].

The optical constants of materials fulfil various sum rules. Altarelli et al. [Altarelli 72] have given systematic derivations of those sum rules. One of them is

$$\frac{m\,c}{2\pi^2\,e^2}\cdot\frac{A}{\rho\,L}\cdot\int_0^{\omega_0}\mu(\omega)\,d\omega = n_{eff}(\omega_0)\ , \qquad (2.3)$$

where c is the vacuum speed of light, m the electron rest mass, e the electron charge, L Avogadro's number, A the atomic weight of the substance, ρ the density of the substance and $n_{eff}(\omega_0)$ the effective number of electrons per atom contributing to the optical transitions in the frequency range up to ω_0. This sum rule also states that the total absorption intensity over all energies (up to infinity) is equal to the number of electrons in the substance. This can be used for the normalization of calculated absorption spectra.

2.1.1 Near Edge X-Ray Absorption Fine Structure (NEXAFS)

Within the dipole approximation, which is valid for $k\cdot x << 1$ or $|x| << \lambda/2\pi$, where λ is the X-ray wavelength (and $k = 2\pi/\lambda$ the wavenumber) and x the characteristic shell diameter, the cross section is given by Fermi's golden rule

$$\sigma_x = \frac{4\,\pi^2\,e^2}{m^2\,\omega}\,|< f\,|\,\mathbf{e}\cdot\mathbf{p}\,|\,i >|^2\,\rho_f(h\nu)\ , \qquad (2.4)$$

where e is the electron charge, m the electron mass, ω the frequency of the electromagnetic wave, **e** the unit vector, $\mathbf{p} = \Sigma\mathbf{p}_i$ the sum of the linear momentum operators of the electrons, and ρ_f (hν) is the energy dependent density of the final states.

The term ρ_f (E) shows that the absorption signal near the absorption edge is proportional to the density of unoccupied states. But due to the dipole selection rules, one can detect only shell sensitive density of states. The selection rules for the electric dipole radiation in LS - coupling are

$$\begin{aligned} &\Delta J = \pm 1, 0 \quad \text{but not } J = 0 \rightarrow J' = 0 \\ &\Delta S = 0 \\ &\Delta L = \pm 1, 0 \quad \text{but not } L = 0 \rightarrow L' = 0, \text{ and } \Delta L = 0 \text{ is very weak} \end{aligned} \tag{2.5}$$

for single electrons holds:: $\Delta l_i = \pm 1, \quad (\Delta l_{j \neq i} = 0)$

This means that in the absorption of a K (1s) shell one can only have excitations into the p final states and for the L (2p) shell into s- and d- final states. For the X-ray absorption at the 3d transition metal K and L - absorption edges the following transitions are allowed due to the dipole selection rules:

$$\begin{aligned} &K: \quad 1s \quad \rightarrow \quad 4p_{1/2} \\ &L_2: \quad 2p_{1/2} \quad \rightarrow \quad 3d_{3/2}, 4s \\ &L_3: \quad 2p_{3/2} \quad \rightarrow \quad 3d_{3/2,5/2}, 4s \end{aligned} \tag{2.6}$$

In appendix ii) the absorption energies in the soft X-ray regime of the K-, L- and M-edges of some selected elements (especially the 3d transition metals) are given.

The intensity ratio between the L_3 and L_2 edge is expected due to the statistical ratio to be

$$\frac{(2l+1)_{L_3}}{(2l+1)_{L_2}} = \frac{2}{1} \tag{2.7}$$

In the near edge absorption fine structure (NEXAFS) spectroscopy one detects the X-ray absorption coefficient at an absorption edge in the energy range of up to about 50 eV above the edge. According to (2.4) this signal is directly proportional to the unoccupied density of states, thus it should give detailed information about the electronic structure of the material. But as shown by Fink et al. [Fink 85] the absorption spectra at the $L_{2,3}$ edges of the 3d elements do not always describe the density of unoccupied states. The interaction of the valence band with the core hole (correlation effects) has to be taken into account. Nevertheless NEXAFS spectroscopy can give detailed information about the electronic structure of the investigated substances [Stöhr 92].

In the extended X-ray absorption fine structure (EXAFS) spectroscopy, one detects the absorption signal in an energy range up to several hundred eV above the absorption edge, where the absorption coefficient shows oscillations which give information about the geometrical structure of the absorbing material [FS 92].

2.1.2 Electron Yield (EY) Detection

Absorption of X-rays leads to the creation of photoelectrons and Auger electrons. On their way to the surface these electrons are scattered inelastically by electron-electron and electron-plasmon interactions and quasi-elastically by electron - phonon interactions. This is shown schematically in Fig. 2.3a. The relative importance of the scattering mechanism depends on the kinetic energy and on whether the material is a metal, a semiconductor or an insulator. Nevertheless, the electron scattering length or mean free path as a function of kinetic energy follows a "universal curve" shown in Fig. 2.3b., where the dashed region indicates the variation found in different materials.

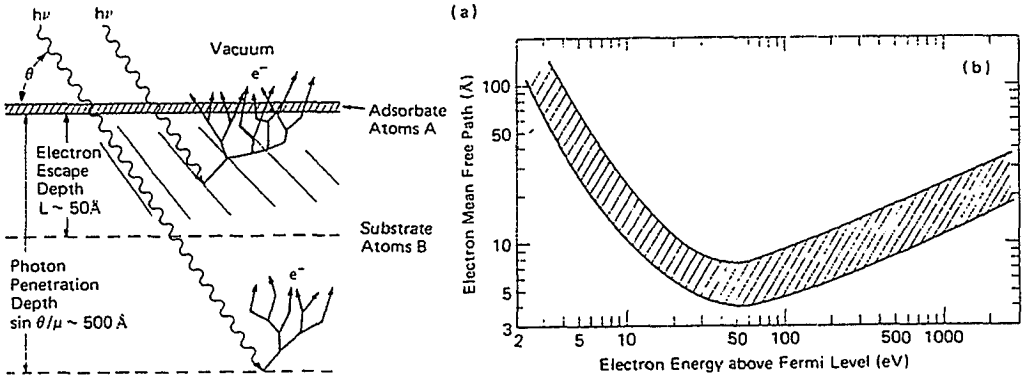

Fig. 2.3. a) Photoabsorption and electron production in a sample. b) Electron mean free path in solids as a function of the electron kinetic energy above the Fermi level. The shaded area represents the distribution typically found for different materials [Stöhr 92].

In particular, absorption of X-rays in the soft X-ray regime leads to primary photoelectrons and Auger electrons with a mean free path of typically less than 10 Å. The inelastical scattering of these primary electrons results in an electron cascade. The number of electrons escaping from the surface is directly proportional to the absorption coefficient μ. The electrons can be detected for example by a channeltron which amplifies the signal to a measurable current, or directly by measuring the sample current. This is discussed in more detail in chapter IV (Setup).

When the cascade reaches the surface only those electrons will escape into vacuum which have sufficient energy to overcome the surface potential barrier. This limits the origin of the total Electron Yield (EY) signal to an effective escape depth L (see Fig. 2.3a.) since electrons generated deeper inside the sample will have insufficient energy to

escape. Therefore the electron detection method is very surface sensitive and information of buried layers like in multilayers is hardly available, only if the cover layers are quite thin. On the other hand electron yield detection is ideal to study signals from the surface, as for example from adsorbates.

2.1.3 Fluorescence Yield (FY) Detection

The absorption coefficient μ can also be measured by detecting the fluorescence photons excited by the core hole decay. As mentioned above, the penetration depth of photons in the soft X-ray regime is typically 1000 Å. Therefore the detection of the fluorescence yield gives more information about the bulk properties of the sample compared to the electron yield detection which is very surface sensitive. The relatively large penetration depth can cause saturation effects, called self absorption. This effect is discussed in detail by Eisebitt et al. [Eisebitt 93]. If one considers a flat sample with thickness d, where photons of the energy hν enter the sample with incident glancing angle α, a core hole can be produced in a level x if the photon energy is sufficiently high. The core hole decays by the emission of a photon with energy hν'. If the photon leaves the sample, it can be detected at a takeoff angle β by the detector. Let μ_x be the absorption coefficient associated with the production of a core hole in the investigated level x; $\mu_{tot} = \mu_x + \mu_{other}$ is the total absorption coefficient of the sample, while μ_{other} describes absorption due to shallower core levels, valence levels, and other atomic species. The measured intensity is given by [Eisebitt 93]

$$I_x(h\nu) \propto \frac{\mu_x(h\nu)}{\mu_{tot}(h\nu) + \mu_{tot}(h\nu')\frac{\sin\alpha}{\sin\beta}} \cdot \left[1 - e^{-\left(\frac{\mu tot(h\nu)}{\sin\alpha} + \frac{\mu tot(h\nu')}{\sin\beta}\right)d}\right] \quad . \quad (2.8)$$

This shows that the fluorescence yield signal is not directly proportional to the absorption coefficient but also depends on the detection geometry and the sample thickness. Due to the self absorption effect, the spectra become more broad and the structure is lost. But it is possible to detect absorption spectra ($\mu_x(h\nu)$) without self absorption effects measuring the fluorescence yield. One way is to detect the signal under two different angles, as it is described in ref. [Eisebitt 93]. Another way is to measure under complete grazing takeoff angle β so that the exponential factor becomes small. But the most efficient way is to take thin films as samples (small d). Then the exponential factor can be changed by $e^{-x} \approx 1 - x$, and eq. (2.8) reduces to

$$I_x(h\nu) \propto \mu_x(h\nu)\frac{d}{\sin\alpha} \quad , \quad (2.9)$$

and the fluorescent signal is directly proportional to μ_x. In Fig.2.4 the effects of self absorption on the absorption spectrum of the $L_{2,3}$ edges of an iron film for different film thicknesses and different detection angles are shown. It is clearly seen in Fig. 2.4b, that

the thick film (250 Å) shows self absorption at grazing in - normal out geometry (geometry II), while the structure is sharp (no self absorption) for grazing in - grazing out geometry (geometry I). In Fig. 2.4a, the same is shown for a thin film (50 Å). Here the structure is normal in both geometries. This shows that for the detection of the absorption coefficient with fluorescent detection one should choose thin films (remarkably less than the penetration length of the light) in the right geometry (grazing takeoff angle (geometry I)).

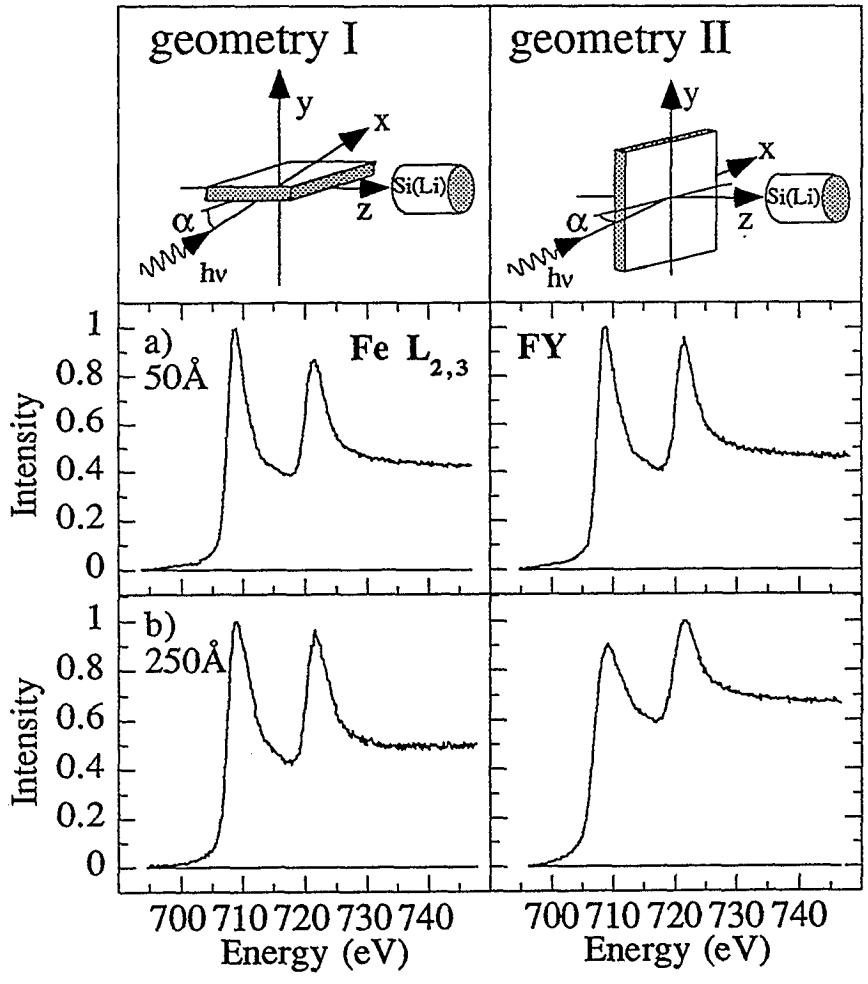

Fig. 2.4. Fe $L_{2,3}$ absorption spectra detected in fluorescence yield (FY) mode for grazing(geometry I) and normal (geometry II) takeoff angle. a) 50Å film, b) 250Å film.

Fluorescence yield measurements are mostly carried out by gas proportional counters or semiconductor diodes (Si(Li) or Ge). Both detectors offer energy discrimination capabilities and reasonable detection efficiencies [Timothy 83]. But one can use also channeltrons for fluorescence detection, as described in chapter IV (Setup).

2.2 X-Ray -Reflection and -Scattering

Here we discuss the interactions of the incident X-rays that do not result in photoabsorption but in reflection, transmission, and scattering.

The energy of the light is related to the wavelength by $h\nu = h\,c\,/\,\lambda$ (where ν is the frequency, c is the velocity and λ is the wavelength of the light), which gives the relationship

$$\lambda\,[\text{Å}] \cdot h\nu[\text{eV}] = 12398.52 \qquad (2.10)$$

linking X-ray energy $h\nu$ (in units of eV) with X-ray wavelength λ (in units of Å). Therefore in the soft X-ray region the wavelength is much larger than the atomic diameter, it is in the range of ≈ 6 - 250 Å, thus in the range of the thickness of thin evaporated layers typically used in magnetic multilayer systems [FS 93] or transmission multilayers used as monochromators or polarization analyzers [Schäfers 93]. Therefore, scattering of soft X-rays is more important in thin layer and multilayer structures, than on the atomic scale.

This is also shown in Fig. 2.5, where the different cross sections for Cu (Z = 29) are plotted as a function of the photon energy. It is clearly shown that in the soft X-ray region the photoelectric or X-ray absorption cross section σ_x is dominating over all the others, like the coherent (Rayleigh) scattering cross section σ_{cs}, the incoherent (Compton) scattering cross section σ_{is}, the cross section for pair production σ_{pair}, and the nuclear photoabsorption cross section σ_{nucl}. The total cross section σ_{tot}, the sum of all others, is nearly identical with σ_x in the soft X-ray region, and only from about 10^5 eV photon energy on, the other cross sections dominate. But one has to take care not to neglect the scattering cross sections completely, because due to the intense synchrotron light used they might still influence the spectrum, especially in the fluorescence yield detection and in resonant processes.

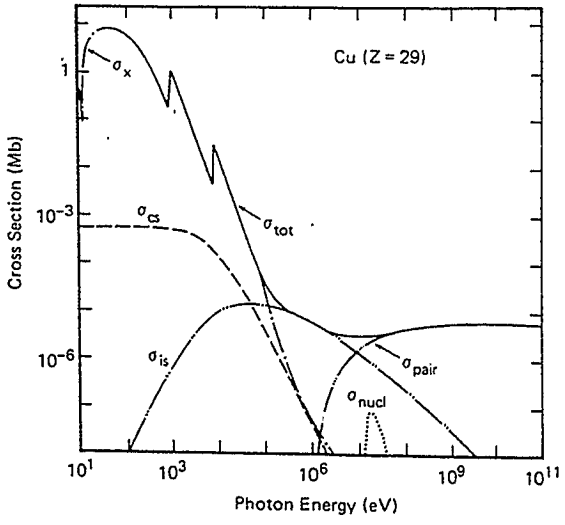

Fig. 2.5. X-ray cross sections for different interactions with a copper (Z = 29) atom. σ_X is the photoelectric or X-ray absorption cross section, σ_{CS} is the coherent (Rayleigh) scattering cross section, σ_{IS} is the incoherent (Compton) scattering cross section, σ_{pair} is the cross section for pair production, and σ_{nucl} ist the nuclear photoabsorption cross section. The total cross section σ_{tot} is the sum of all others. Data taken from ref. [Hubbel 80]

As mentioned above, the reflection, transmission, and scattering in thin film and multilayer structures is of great importance in the soft X-ray region. The most important value for optical properties is the refraction index n_c. It is defined as

$$\sqrt{\varepsilon(\omega)} = n_c(\omega) = n(\omega) + i\,k(\omega) \quad , \tag{2.11}$$

where $\varepsilon(\omega)$ is the energy dependent dielectric function. $n_c(\omega)$ is a complex number where $n(\omega)$ is the real part and $k(\omega)$ the imaginary part. In the soft X-ray regime the refraction index is near $n_c = 1$, therefore it is often also described by $n_c(\omega) = 1 - \delta(\omega) - i\,\beta(\omega)$.

The refraction indices are correlated with the absorption coefficients $\mu(\omega)$ by the Kramers Kronig relations. The Kramers-Kronig relations connect real and imaginary part of certain complex functions describing the optical behaviour of solids [Altarelli 72]. The real part $n(\omega)$ of the complex refraction index is obtained by the Relation

$$n(\omega_o) = 1 + \frac{c}{\pi} P \int_0^\infty d\omega \, \frac{\mu(\omega)}{\omega^2 - \omega_o^2} \, , \tag{2.12}$$

where P denotes the Cauchy principle value of the integral and ω the angular frequency ($2\pi\,\nu$, where ν is the frequency) of the radiation. As long as the reflectivity R of the sample used is small ($R << 1$, $k^2 << n^2$, which is valid for the soft X-ray regime), $\mu(\omega)$ and the imaginary part k of n_c are connected by the expression

$$k(\omega_o) = \frac{c}{2\,\omega_o}\,\mu(\omega_o) \, . \tag{2.13}$$

The values for $n_c(\omega)$ are tabulated for most materials and over a wide energy range, for example in ref. [Palik 91], [Henke 82] or [Hagemann 74]. But in the energy range near absorption edges, the values are not well known, and if one needs the precise indices in those energy ranges, one has to fit absorption curves to the tabulated values in that range in order to obtain the absolute numbers.

The reflection of radiation of an incidence angle α rel. to the surface normal of an interface (see Fig. 2.6a) is described by the Fresnel formula. They describe the reflection coefficient R (quotient of incoming and reflected light intensity), if the electrical field vector **E** is perpendicular to the reflection plane (R_s), and if the electrical field vector is parallel to the reflection plane (R_p):

$$R_s = \frac{(a - \cos\alpha)^2 + b^2}{(a + \cos\alpha)^2 + b^2} \tag{2.14}$$

$$R_p = R_s \cdot \frac{(a - \sin\alpha\,\tan\alpha)^2 + b^2}{(a + \sin\alpha\,\tan\alpha)^2 + b^2} \tag{2.15}$$

with

$$a^2 = \frac{1}{2}[\sqrt{(n^2 - k^2 - \sin^2\alpha)2 + 4n^2k^2} + (n^2 - k^2 - \sin^2\alpha)] \quad (2.16)$$

$$b^2 = \frac{1}{2}[\sqrt{(n^2 - k^2 - \sin^2\alpha)2 + 4n^2k^2} - (n^2 - k^2 - \sin^2\alpha)] \quad (2.17)$$

During the reflection there is apart from the change of the amplitude of the light wave also a phase shift δ_s or δ_p. The phase shift difference $\Delta = \delta_p - \delta_s$ between the two phase shifts is given by

$$\tan\Delta = \frac{-2\,b\,\sin\alpha\,\tan\alpha}{a^2 + b^2 - \sin^2\alpha\,\tan^2\alpha} \,. \quad (2.18)$$

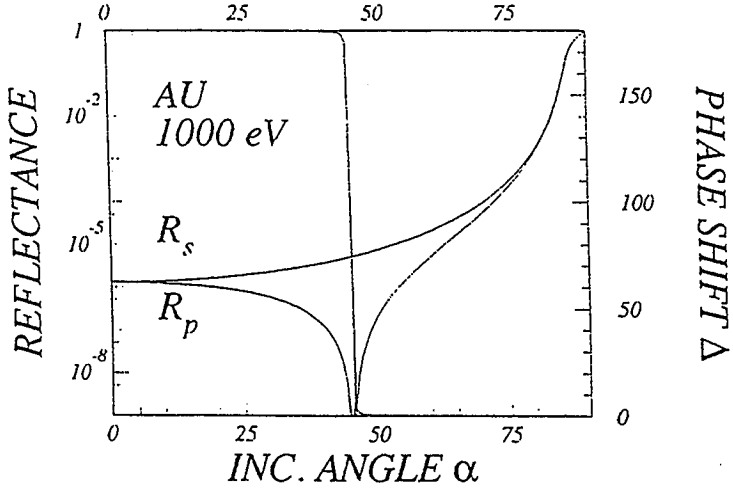

Fig.2.6. Reflectivities R_s and R_p and phase shift Δ at hv = 1000 eV for an Au surface as a function of the angle taken relative to normal incidence [Petersen 93].

The reflectivities R_s and R_p for a Au surface at hv = 1000 eV are given in Fig. 2.6 as a function of the angle taken relative to normal incidence α. One can clearly see that the reflectivities for both polarizations are equal for normal incidence ($\alpha = 0°$) and total grazing incidence ($\alpha = 90°$). While the reflectivity for s-polarized light (R_s) increases monotonously from about 10^{-6} to 1 changing α from 0 to 90°, the p-polarized light is nearly not reflected at all at 45°. But for grazing incidence angles $\alpha \approx$ 75-90°, both reflectivities are quite the same and sufficiently high; this means that reflection at grazing angles does hardly change the intensity and polarization of the incidence light. This is important for optics in the soft X-ray regime, such as monochromators. Similar to the formula for the reflectivity there exist also Fresnel formula for the Transmission T (quotient of incidence and transmitted light intensity) depending on the refractive indices and the incidence angle.

At a real surface there is not only specular reflectivity, but also diffuse scattering due to the roughness of the surface. The specular reflected intensity is found only at the exact reflection position (incidence angle = take-off angle). But diffuse scattered light is found over a wide range of angles around the specular take-off angle. The intensity is higher in the reflection plane than perpendicular to it. This is shown for the scattering off a polished Pt(111) single crystal by Fischer et al. [Fischer 89], shown in Fig. 2.7.

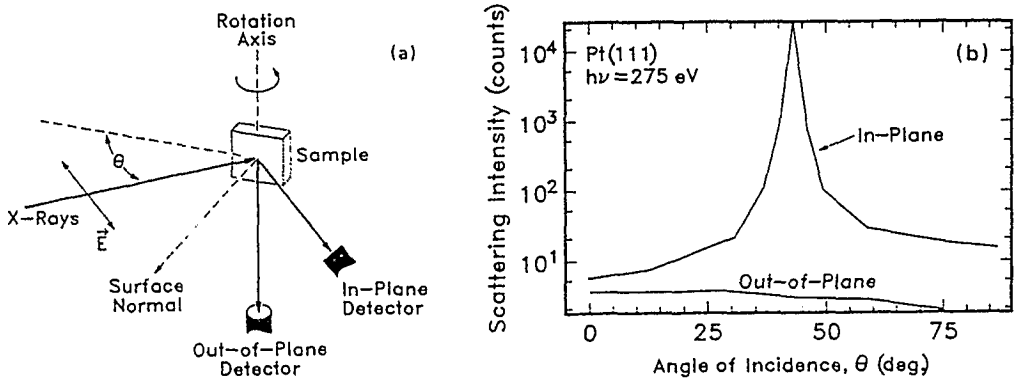

Fig. 2.7. a) experimental arrangement used by Fischer et al. [Fischer 89]. b) measured scattered light intensity for in-plane and out of plane detector positions of scattered light off a polished Pt(111) single crystal at hν = 275 eV.

For in-plane orientation the large peak around 45° is due to the specular reflected beam. It is important that at all angles the out-of-plane detection intensity is lower than the in-plane detection intensity. Therefore, the out-of-plane detection geometry should be preferred in measurements, where the scattering of the light disturbs the measured signal.

Because the wavelength of the light in the soft X-ray regime is of the order of the layer thickness in multilayer systems, interference effects of the transmitted and reflected light, which might cause additional scattered intensity depending on the detection geometry, may occur.

III. Magnetic Circular Dichroism (MCD) in X-Ray Absorption

Stimulated through the advent of synchrotron light sources with the possibility to obtain polarized light of high intensity over a broad spectral range in the last decades, it was possible to study magneto-optical effects in magnetically ordered substances in the X-ray regime. This photon energy regime covers optically induced core and valence transitions in the magnetically relevant rare earths and transition metals. After the experimental discovery of magnetic X-ray dichroism in the late 80's (see also introduction, chapter I), there appeared simple models for the interpretation of the circular dichroism spectra for the K-absorption edges [Schütz 90],[Stähler 93], where the dichroism spectra can be related to the local magnetic structure. In 1992 Thole et al. [Thole 92] published a sum rule based on an atomic model, which relates the circular dichroism spectra of an absorption edge to the local orbital momentum, and in 1993 another sum rule based on the same model came out by Carra et al. [Carra 93], which relates the spin magnetic moment to the dichroism spectra. Therefore one is able now with the help of these sum rules, to determine element specifically the local magnetic moments of a ferromagnet from near edge absorption spectra taken with circularly polarized light. This can give new insight into the magnetic structure of complex systems and the separation of orbital and spin part of the total magnetic moment, which was until now possible only indirectly by neutron scattering experiments.

3.1 Fundamental Spectra

The absorption coefficient μ in the case of the absorption of polarized light in a magnetized sample depends on the orientation of the magnetization (**M**) relative to the light polarization direction. This effect is called magnetic dichroism. There are some special conditions, where one obtains the absorption spectra for the transition of one special value of the magnetic quantum number Δm. The spectra taken under these conditions are called the fundamental spectra. The designations of the fundamental spectra are given according to the notation of v.d. Laan and Thole [Laan 91].

In the case of circularly polarized light (σ), the light polarization is given by the helicity (photon spin direction) **S**. **S** can either be parallel or antiparallel to the light penetration direction, which is represented by the wave vector **k** ($\sigma^+ := \mathbf{S} \uparrow\uparrow \mathbf{k}$ = positive helicity = right circularly polarized light and $\sigma^- := \mathbf{S} \uparrow\downarrow \mathbf{k}$ = negative helicity = left circularly polarized light). Here one has the following fundamental spectra:

absorption coefficient	Magnetization	Δm	name
μ^+	$\mathbf{M} \uparrow\uparrow \mathbf{S}$	+1	R
μ^-	$\mathbf{M} \uparrow\downarrow \mathbf{S}$	-1	L

Table 3.1. Fundamental spectra for circularly (σ) polarized light; **M** denotes the Magnetization direction and **S** the photon spin vector (helicity),respectively.

In the case of linearly polarized light (π) the polarization is defined by the electrical field vector **E**, which is always perpendicular to **k**. The fundamental spectra in this case are:

absorption coefficient	Magnetization	Δm	name
μ^z	$\mathbf{M} \parallel \mathbf{E}$	0	Z
$\mu^{\pm}$	$\mathbf{M} \perp \mathbf{E}$	± 1	R+L

Table 3.2. Fundamental spectra for linearly (π) polarized light; **M** denotes the Magnetization direction and **E** the electrical field vector, respectively.

According to the Δm - selection rules $\mu^{\pm}$ is equal to 1/2 ($\mu^+ + \mu^-$). Linear and circular dichroism are defined by the differences

Circular Dichroism (R - L) : $\mu^{mcd} = \mu^+ - \mu^-$

Linear Dichroism (Z - 1/2(R+L)) : $\mu^{mld} = \mu^z - \mu^{\pm}$

The isotropic spectrum μ^I is the sum of all fundamental spectra :

Isotropic Spectrum (R+L+Z) : $\mu^I = \mu^z + \mu^+ + \mu^-$

In circular dichroism measurements one usually detects μ^+ and μ^- not directly. In the case of non-parallel orientation of the magnetization (**M**) and light polarization (**S**), the relative angle α has to be taken into account (see also ref. [Laan 86]). The exciting light is not completely circularly polarized in the real case, but usually elliptically polarized. Therefore one has to include a factor for the degree of circular polarization P (with P = 0: no circular polarization; in the case of a bending magnet at a synchrotron light source: linearly polarized. |P| = 1: completely circular polarized). The magnetization m of the sample might also not be complete . In the case of circular dichroism the *real* dichroism spectrum ($\mu^+ - \mu^-$) is then given by the experimental one ($\mu^+ - \mu^-$)^{exp} according to

$$\mu^+ - \mu^- = \frac{1}{P \cos^2\alpha \; m} (\mu^+ - \mu^-)^{exp} = \frac{1}{C} (\mu^+ - \mu^-)^{exp} \quad , \qquad (3.1)$$

with $C = P \cos^2\alpha \, m$.

With linearly polarized light one also has to take into account the direction of the **E** - vector relative to the incidence plane. The light is **p** - polarized, if **E** is *in* the incidence

plane (only achievable by off-normal incidence) and it is s - polarized, if **E** is *perpendicular* to the incidence plane(and in normal incidence).

3.2 Models and Sum Rules

In calculating soft-x-ray core-level absorption and MXD spectra in the 3d transition elements, it is essential to take relativistic effects into account. For a simple model, however, one can treat only the core-levels relativistically (spin-orbit-split levels). This approach has been advanced by Erskine and Stern using a simplified exchange-split representation of the 3d valence band [Erskine 75]. We shall refer to this approach as the Erskine-Stern model, and it is described below in Sec. 3.2.1. In a second approach one can incorporate spin-orbit splitting into both the core and valence levels. This fully relativistic model is described in Sec. 3.2.2.

3.2.1 Erskine-Stern Model

The simplest available model of core-level x-ray absorption cross sections and associated MXD is that of Erskine and Stern [Erskine 75]. They point out that for Ni the unoccupied 3d states lie in a narrow energy range just above the Fermi level E_f and (in the absence of spin-orbit coupling) are exclusively of minority ($\downarrow$) spin, as indicated in Fig. 1.1. We therefore need to consider only the set of squared-dipole-matrix elements shown in appendix iii) (see Ref. [Smith 92]).

Summing over the entire manifold of unoccupied $d^{\downarrow}$ states, one obtains for the total cross section ($\mu^+ + \mu^-$) and the CMXD cross section ($\mu^+ - \mu^-$) at the L_2 and L_3 absorption edges:

$$L_3\,(p_{3/2} \rightarrow d^{\downarrow}) \begin{cases} (\mu^+ + \mu^-) = \frac{4}{3}A + \frac{4}{3}B + \frac{4}{3}C \\ (\mu^+ - \mu^-) = -\frac{2}{3}A + \frac{2}{3}C \end{cases}$$

$$L_2\,(p_{1/2} \rightarrow d^{\downarrow}) \begin{cases} (\mu^+ + \mu^-) = \frac{2}{3}A + \frac{2}{3}B + \frac{2}{3}C \\ (\mu^+ - \mu^-) = \frac{2}{3}A - \frac{2}{3}C \end{cases} \qquad (3.2)$$

where A, B, and C are defined in appendix iii). No matter how the A, B, C terms are weighted, however, the model predicts that the L_3 to L_2 ratio for the total cross section ($\mu^+ + \mu^-$) and the CMXD cross sections ($\mu^+ - \mu^-$), respectively, should be:

$$\frac{(\mu^+ + \mu^-)\,(L_3)}{(\mu^+ + \mu^-)\,(L_2)} = \frac{2}{1}, \qquad \frac{(\mu^+ - \mu^-)\,(L_3)}{(\mu^+ - \mu^-)\,(L_2)} = -\frac{1}{1}. \qquad (3.3)$$

For A, B and C one gets, according to ref. [Smith 92] $\frac{4}{5}R^2$, $\frac{2}{5}R^2$ and $\frac{2}{15}R^2$, respectively, (R: standard integral, see appendix iii)). Therefore one obtains for the MCD asymmetry at the L_3 and L_2 - edge:

$$\frac{(\mu^+ - \mu^-)}{(\mu^+ + \mu^-)}(L_3) = -\frac{1}{4}\ (=-25\%)\,, \quad \frac{(\mu^+ - \mu^-)}{(\mu^+ + \mu^-)}(L_2) = +\frac{1}{2}\ (=+50\%) \qquad (3.4)$$

The energy diagram for the (2p -> 3d) $L_{2,3}$ absorption of 3d transition elements for circularly polarized light is shown in Fig. 3.1. Indicated are the matrix elements for the individual transitions according to the Erskine Stern model (see appendix iii) and ref. [Smith 92]).

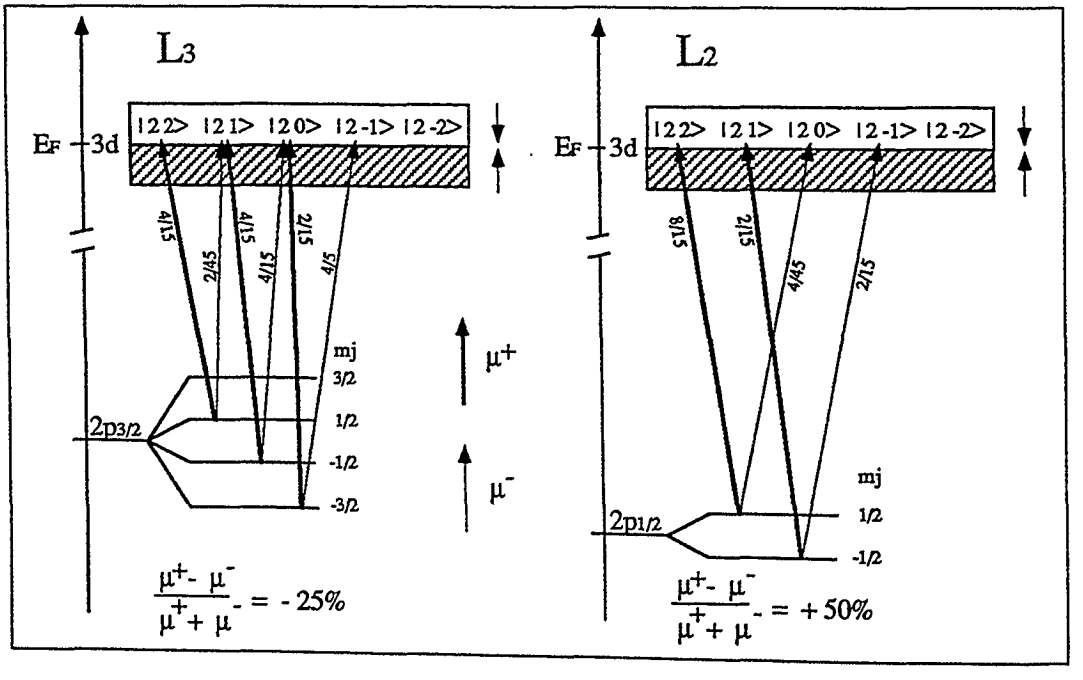

Fig 3.1. Magnetic circular dichroism in the Erskine Stern model for a 3d ferromagnet.

3.2.2 Fully Relativistic Models

The MCD ratios of eqs. (3.3) and (3.4) are valid only in the simple model described above. In realistic systems, they differ from these values due to spin-orbit interaction in the valence band. In order to include this, one has to use fully relativistic models (relativistic in the core level *and* in the valence band). This is discussed in this chapter. One can distinguish between atomic models and band structure models.

The Erskine-Stern Model provides a perfect symmetry between the $Y^{\downarrow}_{2\,2}$ and $Y^{\downarrow}_{2\,-2}$ and between the $Y^{\downarrow}_{2\,1}$ and $Y^{\downarrow}_{2\,-1}$ wave-functions. This symmetry is removed if the final states are treated relativistically, that is to say, if valence-band spin-orbit coupling is included. The physics here was anticipated in a 1949 paper by Mott [Mott 49]. Spin-orbit splitting will enhance $j = \frac{5}{2}$ over the $j = \frac{3}{2}$ character near the top of the valence d band, and this will favour the intensity of the L_3 over the L_2 absorption edge. This means, that the L_3/L_2 ratios from eqs. (3.3) and (3.4) change slightly in favor of L_3. Especially the CMXD ratio of L_3/L_2 becomes bigger than -1/1. A detailed calculation is given in ref. [Smith 92] for MCD at Ni. A theoretical interpretation of the main principles of magnetic dichroism measured with soft X-rays is given by ref. [Jo 92].

Atomic models:

The X-ray absorption spectrum is composed of hundreds of dipole transitions from the ground state to the accessible final states. On the basis on an atomic like model, van der Laan and Thole [Laan 90] have calculated the magnetic dichroism in the X-ray absorption branching ratio, also by including a crystal field. They also calculated the absorption spectra depending on the spin-orbit parameters (and on the symmetry) [Laan 91b].

Band structure models:

Recently, relativistic, spin-polarized band calculations of magnetic circular dichroism MCD (and magnetic linear dichroism MLD) have come out. With the full potential linearized augmented plane wave (FLAPW) method used to calculate MCD of 3d transition metal surfaces [Wu 94] or with the spin polarized, relativistic linear muffin-tin orbital (SPR-LMTO) method for 3d bulk and multilayer structures [Guo 94a] one is able to calculate efficiently MCD of complex systems. With the help of these calculations, one can determine the electronic and magnetic properties and the MCD spectra separately for each layer and each element, so that one can compare them well to experimentally determined spectra. In Fig. 3.2 a calculated $L_{2,3}$ absorption spectrum of Fe is shown [Guo 94]. The energy scale is set to the first inflection point of the L_3 edge. The spectra for parallel (R) and antiparallel (L) coupling of the magnetization to the light helicity are

shown as well as the sum (R + L) and the difference (R - L), the MCD spectrum. The spectra are convoluted by a Lorentzian (with 0.9eV FWHM at the L_3 edge and 1.4 eV FWHM at the L_2 edge) and a Gaussian (with 1eV FWHM) curve, to represent the experimentally determined signal.

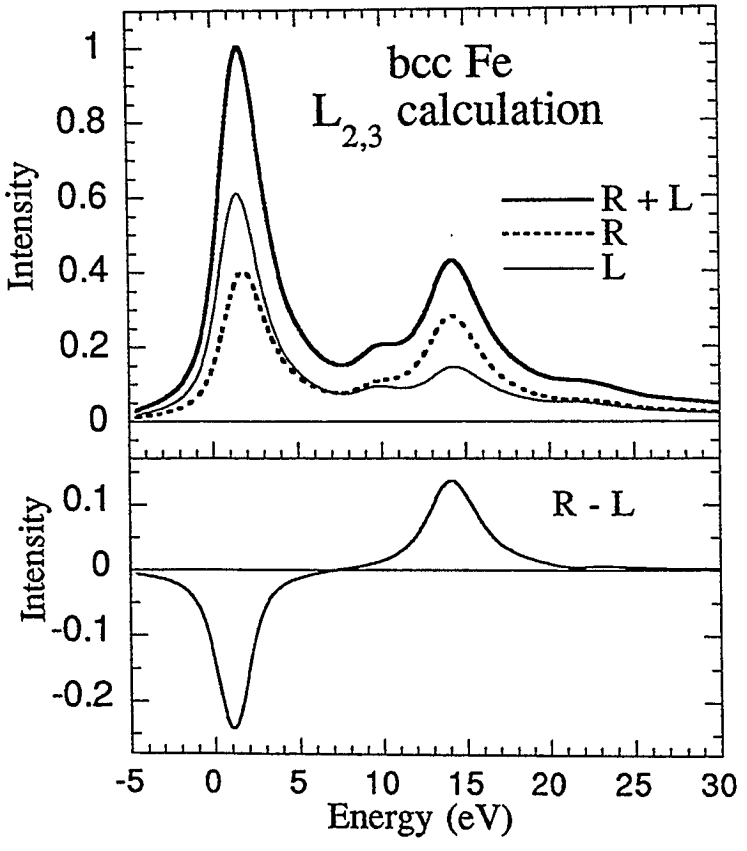

Fig. 3.2. Calculated Fe $L_{2,3}$ absorption spectra for parallel (R) and antiparallel (L) coupling of the magnetization to the light helicity, as well as the sum (R + L) and the difference of both spectra (R - L).

As seen already in the Erskine-Stern model, the intensity of the difference curve (R-L) is negative at the L_3 edge while it is positive at the L_2 edge. The MCD ratio between L_3 and L_2 is not -1/1, as predicted in this simple model, because the spin orbit interaction in the valence band cannot be neglected. This leads to the orbital moment and to a different ratio in the MCD spectrum.

3.2.3 Sum Rules

For magnetooptical absorption there is a very fundamental sum rule [Bennett 65], which says, that the CMXD signal ($\mu^+ - \mu^-$) integrated over the whole energy range shall vanish:

$$\int_0^\infty (\mu^+ (\omega) - \mu^- (\omega)) \, d\omega = 0. \qquad (3.5)$$

As mentioned above, the L_3/L_2 ratio for CMXD ratio differs from the -1/1 value of the Erskine-Stern model in real (fully relativistic) materials. This seems to be in contradiction to the above mentioned sum rule. But it must be considered, that the integral in Eq. (3.5) is over *all* energies and not only over the $L_{2,3}$ edges. If one integrates only over the $L_{2,3}$ edge-energies, one can get information about the local spin- and orbital moments, as mentioned below.

In the last few years there have been developed sum rules for the absorption of circularly polarized light by ferromagnets on the basis of atomic models. With the help of these sum rules one obtains the ground state expectation values of $\langle L_Z \rangle$ [Thole 92] and $\langle S_Z \rangle$ [Carra 93]. A detailed description of the sum rules is given in the appendix iv). Here are given the formula that can directly be used for our measurements, i.e. the $L_{2,3}$ absorption edges of the 3d elements:

MCD at the $L_{2,3}$ absorption edges of the 3d elements: 2p->3d excitation

As mentioned above one has to include the calibration factor C into the experimentally determined dichroism spectra. Then we obtain for the determination of the orbital moment:

$$\langle L_Z \rangle = 2 \frac{n_h}{C} \frac{I^l_{mcd}}{I_t} \qquad (3.6)$$

and for the determination of the spin moment:

$$\langle S_Z \rangle + \frac{7}{2} \langle T_z \rangle = \frac{3}{2} \frac{n_h}{C} \frac{I^s_{mcd}}{I_t} \qquad (3.7)$$

with the number of holes in the 3d band n_h, the magnetic dipole operator T ($T_z = S_z (1 - 3 \cos^2\Theta)/2$), and the integrals

$$I^l_{mcd} = \int_{L3+L2} dE(\mu^+ - \mu^-),$$

$$I^s_{mcd} = \int_{L3} dE(\mu^+ - \mu^-) - 2 \int_{L2} dE(\mu^+ - \mu^-),$$

and

$$I_t = \int_{L3+L2} dE(\mu^+ + \mu^- + \mu^z).$$

Due to the shell and element selectivity, the MCD spectra are likely able to determine the orbital ($\mu_l = -\mu_B \langle L_z \rangle$, where μ_B is the Bohr magneton $\mu_B = \frac{e\hbar}{2m}$) and the spin (if T_z is negligible) magnetic moment ($\mu_S = -2\,\mu_B \langle S_z \rangle$) separately for each atom due to these powerful sum rules (3.6) and (3.7).

In relation to circular dichroism, linear dichroism can be neglected in the systems investigated here. This will be discussed later. Therefore $\mu^z = \frac{1}{2}(\mu^+ + \mu^-)$ and the isotropic spectrum $(\mu^o + \mu^+ + \mu^-)$ becomes $\frac{3}{2}(\mu^+ + \mu^-)$, thus it can be written as

$$I_t = \frac{3}{2} \int_{L_3+L_2} dE(\mu^+ + \mu^-).$$

The ratio $\langle L_z \rangle / (\langle S_z \rangle + \frac{7}{2} \langle T_z \rangle)$ is independent of the number of d-holes n_h, the normalization by the isotropic spectrum, and the experimental constant C; thus this value contains no more variable and is therefore very well useful for the independent comparison of magnetic properties. From equations (3.6) and (3.7) one gets this ratio by

$$\frac{\langle L_z \rangle}{\langle S_z \rangle + \frac{7}{2} \langle T_z \rangle} = \frac{4}{3} \frac{I^l_{mcd}}{I^s_{mcd}} \quad . \tag{3.8}$$

The ratio of $\langle L_z \rangle$ and $\langle S_z \rangle$ is connected with the magnetic moments by $\frac{\langle L_z \rangle}{\langle S_z \rangle} = 2 \frac{\mu_{orb}}{\mu_{spin}}$. If T_z is negligible, these ratio can be compared directly to the one determined by the sum rules (3.8).

3.2.4 Comparison of Sum Rules with First Principle Calculations

The sum rules (3.6) and (3.7) are very powerful for the determination of element specific magnetic moments, but they are based on an atomic model and it is still questionable so far whether eqs. (3.6) and (3.7) derived from such a simple model can be applied to complex real metals with their strongly hybridized multi-band structure. For example it is not clear, whether the dipole moment T_z in Eq. (3.7) can be neglected in the solid state, as mentioned by Carra et al. [Carra 93]. Recent calculations of Fe and Co multilayer systems by Guo et al. [Guo 94b] show that the calculated magnetic dipole moment is small in the Co systems, but is comparable to the orbital magnetic moment in Fe systems. But for bulk bcc Fe they found that T_z can be neglected completely ($\langle 2T_z \rangle < 0.001\ \mu_B$) and for bulk hcp Co T_z was also found to be negligibly small ($\langle 2T_z \rangle < -0.003\ \mu_B$).

The comparison of the magnetic moments determined with the sum rules compared to the ones obtained by first principles band structure calculations by Wu et al. [Wu 94] and Guo et al. [Guo 94a], shows that the orbital sum rule (3.6) is found to give orbital magnetic moments too small by a about 5-10% [Wu 94a] or 20-35% [Guo 94a]. For each ion species there is a simple linear relationship between the integrated MCD signal and the orbital moment of an ion in magnetic solids. The spin magnetization sum rule (3.7) is found to give rather accurate spin magnetic moments for the Co systems (errors within 15%). However, it does not hold qualitatively for higher anisotropic systems such as Fe multilayers [Guo 94a], or at surfaces [Wu 94b].

The band structure calculations are made in the single particle picture in the ground state, which does, of course, not represent exactly the real case. The effects of a photo-induced core hole on the determination of the magnetic moments are determined in the case of Nickel by Wu et al. [Wu 94a]. They found that these core holes are strongly screened, which induces an enhancement of $\langle L_z \rangle$. In a recent paper by Alouani [Alouani 94] the effect of a core hole on the absorption spectra of 3d ferromagnets is discussed in detail. The main results are: i) in the presence of a core hole, the spin magnetic moment of the excited atom is substantially smaller than the ground state value, and ii) the white line of Fe is shifted by about 1 eV toward the Fermi edge (3). These effects can therefore cause differences in the calculated magnetic moments and spectra, if no core hole has been taken into account in the calculations.

IV. Experimental Setup

The experiments have been performed in a ultrahigh vacuum (UHV) stainless steel chamber, it was connected to the SX700/3 beamline at the BESSY storage ring, Berlin, for using circularly polarized synchrotron radiation. The absorption signal is detected either in the electron yield method by detecting the photo current from the sample or in the fluorescence yield mode by detecting the fluorescence yield emission from the sample with the help of a Si(Li) semiconductor diode.

4.1 Beamline for Circularly Polarized Soft X-Rays

The measurement of magnetic circular dichroism at the L-edges of the 3d transition metals demands tuneable, circularly polarized soft X-rays. This can practically only be achieved with synchrotron radiation. The general properties of synchrotron radiation can be seen for example in ref. [FS 92]. We have chosen the SX700/3 soft X-ray beamline (monochromator) at the BESSY synchrotron light source, Berlin for the production of circularly polarized soft X-rays (CSX) [Petersen 93]. This beamline is adapted to a dipole magnet in the electron storage ring. The polarization of the synchrotron radiation in the plane of the storage ring is linearly polarized with the electrical field vector parallel to this plane ($I_{\parallel}$). With increasing off-plane angle ψ, there is an increasing amount of intensity with the electrical field vector perpendicular to this plane ($I_{\perp}$). This leads to elliptically polarized light at off-plane angles, which are accepted by the beamline. In Fig. 4.1 the off-plane distribution of the radiation from a BESSY dipole together with the SX700/3 acceptance window is shown at three different positions.

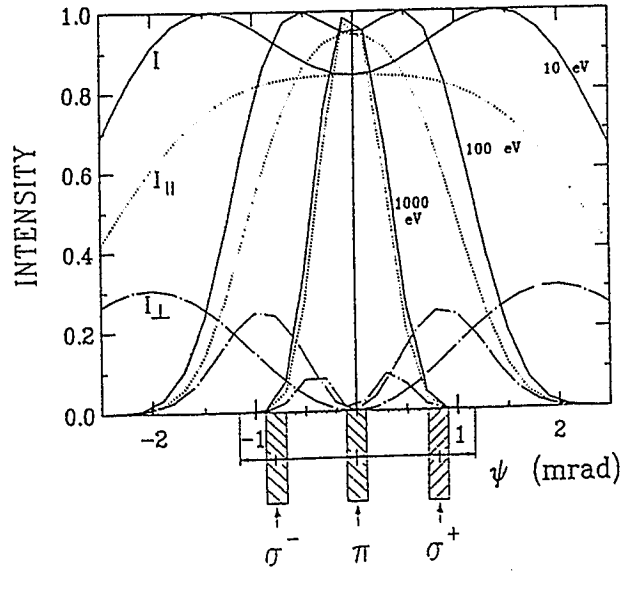

Fig.4.1. $I_{\parallel}$ and $I_{\perp}$ as a function of the off-plane angle ψ for three different photon energies at a BESSY dipole magnet [Petersen 93]; included are the SX700/3 acceptances for $\psi = 0$ and for $\sigma^{\pm}$ - light. The total intensity $I = I_{\parallel} + I_{\perp}$ is also given.

The beamline layout is shown in Fig.4.2. The radiation is accepted by one of two plane mirrors and reflected at a grazing angle into the SX700/3. The mirrors can be moved vertically to accept σ^- (first mirror) and σ^+ (second mirror) radiation. The σ^+ light passes through a tunnel in the σ^- mirror.

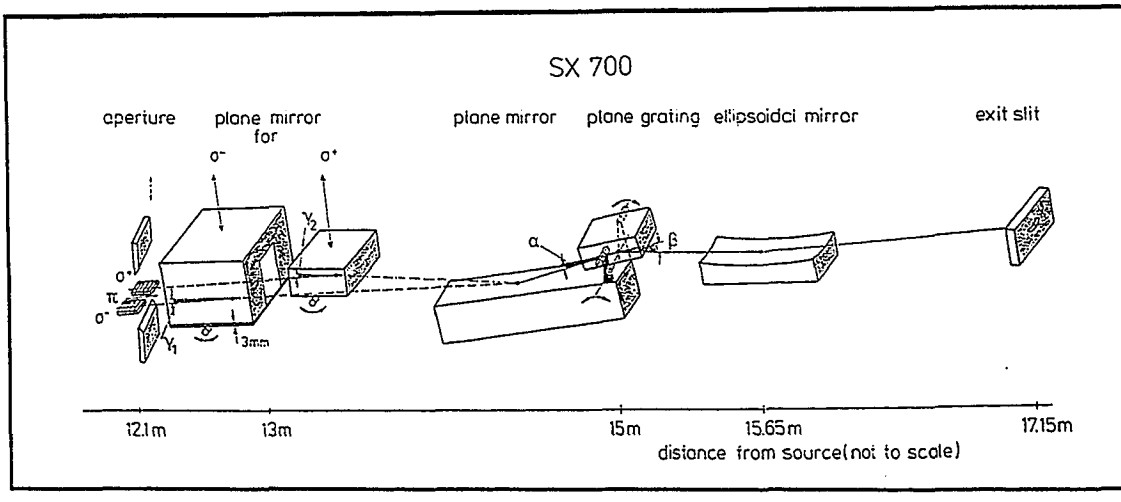

Fig. 4.2 Scheme of the optical configuration of the SX700/3 beamline

Circularly polarized light can be produced at the SX700/3 in the broad energy range 30-2000eV. This range can be covered because the optics do always stay in a grazing angular range, all grazing angles are ≤ 13° for the 1200 lines/mm (plane-) grating. As shown in Fig. 2.6 for 1000 eV photon energy the phase shift differences Δ due to reflections of s- and p- polarized light is always small for these angles and the high degree of synchrotron radiation polarization accepted off-plane by the first optical element is therefore conserved by the optics to a large extend, i.e., depolarization effects are small. The greater the off-plane angle ψ is, the greater is the degree of circular polarization P_{circ}. At a dipole magnet, P_{circ} is given by the light intensities ($I_{\parallel}$ and $I_{\perp}$) according to

$$P_{circ} = 2\frac{\sqrt{I_{\parallel} \cdot I_{\perp}}}{I_{\parallel} + I_{\perp}} \quad . \tag{4.1}$$

If one normalizes the total intensity $I_{\parallel} + I_{\perp} = 1$, the ratio $I_{\parallel} / I_{\perp}$ is then given by

$$\frac{I_{\parallel}}{I_{\perp}} = \frac{1 + \sqrt{1 - P_{circ}^2}}{1 - \sqrt{1 - P_{circ}^2}} \quad . \tag{4.2}$$

At a typical value of $P_{circ} = 0.7$ is $I_{\parallel} / I_{\perp} = 5.996$, this means, that even at this relative high degree of circular polarization , the intensity $I_{\parallel}$ is about 6 times higher than $I_{\perp}$.(For $P_{circ}=1$, $I_{\parallel}$ is equal to $I_{\perp}$, of course).

Because the total intensity decreases with increasing ψ (and thus with increasing P_{circ}), one must find an optimum between a high degree of circularly polarization and sufficient high light intensity. We have chosen typically an off-plane value of $\psi = -0.6$ mrad. At this angle, the light intensity is about 1/3 of the intensity at $\psi = 0$. According to calculations [Peterson 93] this results in $P_{circ} > 0.8$ in the energy range of about 500 - 1000 eV, which covers the L absorption edges of the 3d transition elements. In this energy range, P_{circ} , is nearly constant, it is just smoothly increasing with photon energy. The real value of P_{circ} in this energy range is not known, because measurements for the determination of the Stokes parameters can be done only for energies up to about 100 eV. At 800 eV photon energy P_{circ} was estimated from photoemission experiments at the Fe 2p state [Baumgarten 90] to be in the range of 60 - 80% for $\psi = 0.3$ mrad.

4.2 MCD Measurements with Fluorescence and Electron Yield Detection

The measurements discussed here are done under ultra high vacuum (UHV) ($p < 4 \cdot 10^{-9}$ mbar) conditions for several reasons. First, the beamline is working under UHV conditions (to avoid absorption of the soft X-rays and contamination of the optical elements and because it is directly connected to the electron storage ring) and the measurement chamber is directly connected to the beamline. On the other hand, the detection of electrons requires good vacuum and the fluorescence detector must be kept under good vacuum conditions, too. We have mainly studied ex situ prepared and covered samples, but if one studies surface properties, the vacuum conditions must be even better ($p < 1 \cdot 10^{-9}$ mbar), depending on the system. To achieve the UHV conditions, the measurement chamber is made of stainless steel, and pumped by a turbomolecular pump and an ion getter pump. After pumping down the chamber primarily to a pressure in the 10^{-7} mbar range, the whole chamber is baked for about 24h at an elevated temperature of about 180°C in order to remove adsorbates (especially water) from the chamber - surfaces. The UHV conditions are then reached after cooling down of the chamber to room temperature. In order to change the samples without braking the vacuum, we used an additional lock chamber which is working only at high vacuum (10^{-7} mbar range). Here the samples are put in from normal pressure, they can be stored and they can be transferred into the UHV chamber by a magnetic transfer system. Thus we are able, to change the samples and even to put samples from outside into the UHV chamber within a short time (approximately 15 min). Fig. 4.3 shows a schematic setup where one can see the sample in the middle of the figure. It can be magnetized by two permanent magnets (made of a CoSm alloy) parallel or antiparallel to the light penetration direction x (and thus parallel or antiparallel to the light helicity). The incoming photons (hν) must pass a gold mesh before they reach the sample under the incidence angle α. The emitted photocurrent from the gold mesh is measured by a picoamperemeter and is used for the normalization of the spectra (to avoid noise on the goldmesh current, the gold mesh is put to a negative potential of about -20V by a battery). The fluorescent photons from the sample hν' are detected by a Silicon fluorescence detector (Si(Li)), which is positioned 90° to the light penetration direction (z

direction). The sample is also electrically connected to a picoamperemeter (and like the goldmesh put to about -20V by a battery) in order to detect the electron yield.

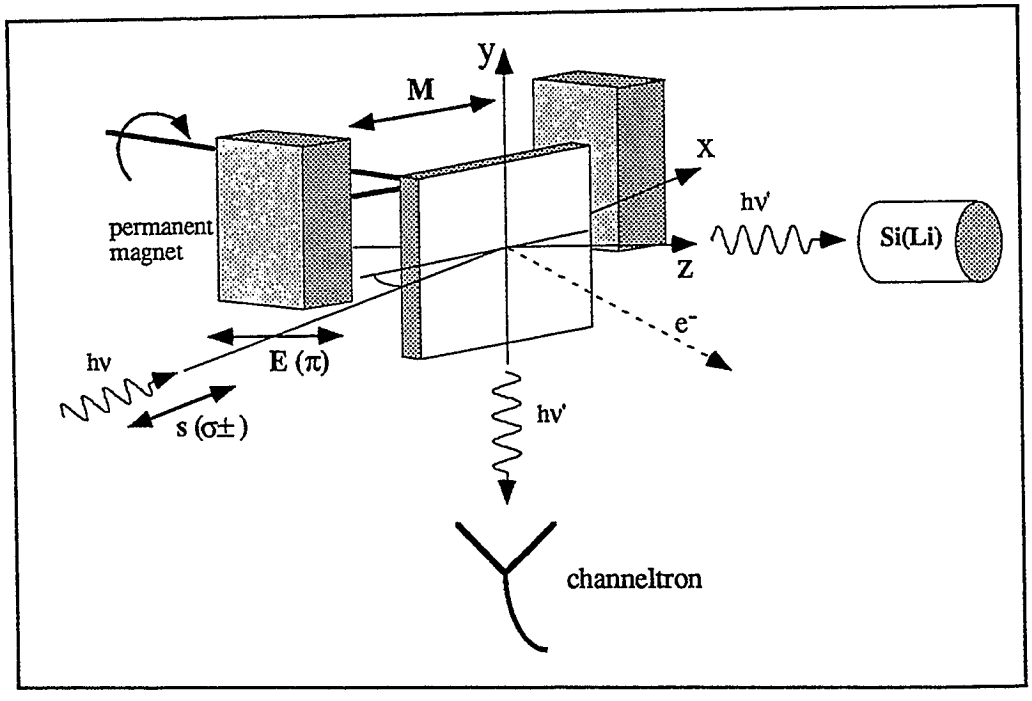

Fig. 4.3 Schematic setup of the experiment

The semiconductor Si(Li) diode is suitable for soft X-ray fluorescence studies down to photon energies of about 200 eV. The schematic setup of the Si(Li) detector is shown in Fig. 4.4:

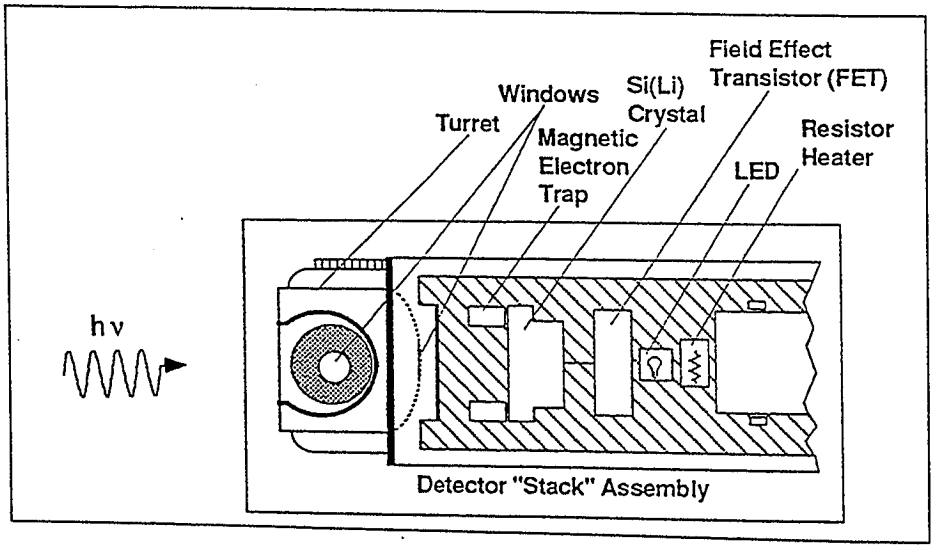

Fig. 4.4. Schematics of a Si (Li) fluorescence detector used in this work

We use a Tracor Pioneer Ultra detector. It mainly consists of a Li drifted Si crystal which is kept at liquid nitrogen temperature. The incoming X-rays produce electron-hole pairs. The number of these pairs is proportional to the X-ray energy. X-rays of approx. $h\nu \geq 190$ eV (Boron emission) can be detected by this diode. The signal is amplified by a field effect transistor connected to the detector. The signal is furthermore amplified by a Tennelec TC 245 amplifier and then analyzed by a Tennelec PCA-multiport multichannel analyzer. The count rate of semiconductor detectors is limited to about $5 \cdot 10^4$ cts/s. This detector offers energy discrimination capabilities and reasonable detection efficiency (see also [Stöhr 92]). Fig. 4.5 shows the energy resolved fluorescence spectra taken with the Si(Li) detector from a Co/Cu multilayer sample (a $Cu_{30Å}$ $Co_{25Å}$ $Cu_{30Å}$ trilayer structure on a saphire (Al_2O_3) substrate) for different incident photon energies.

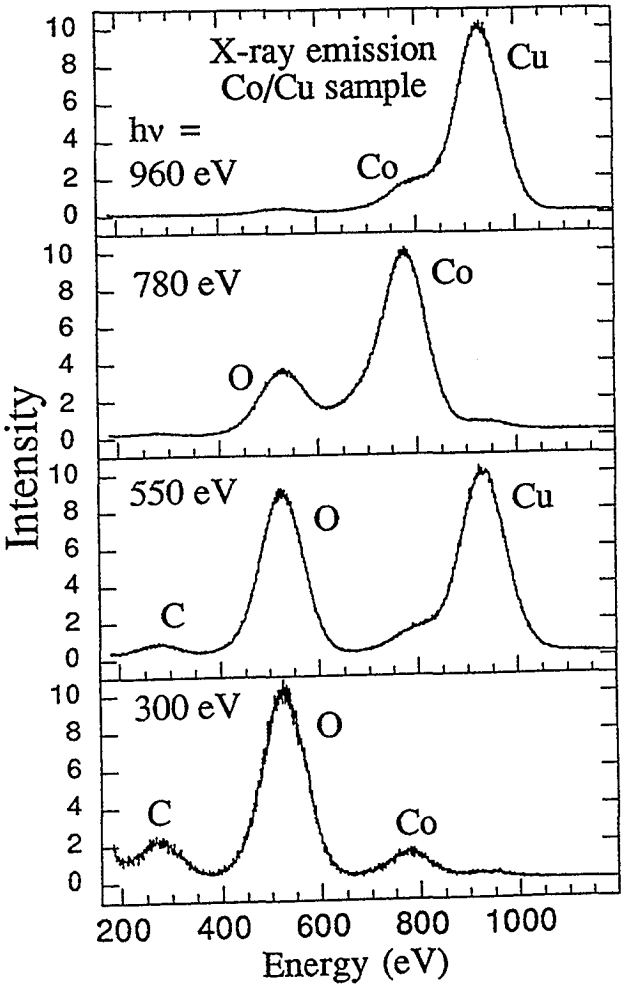

Fig. 4.5. Fluorescence spectra of a Co/Cu/Co trilayer structure taken with a Si(Li) fluorescence detector for different excitation energies.

At an excitation energy of $h\nu = 300$ eV, one can see the fluorescence emission of Carbon (C) at about 280 eV, which is due to contamination on the surface. Additionally one can see emission from Oxygen (O) (from the substrate and from surface contamination), around 520 eV and from Co around 780 eV (L-emission). The higher

energy peaks can be seen, because the exciting light contains also the second and higher orders (with lower intensity), with the double (or n-times) of the determined (first order) photon energy. At an excitation energy of 550 eV one can clearly see the oxygen peak and with approximately the same intensity the Copper L-emission peak around 930 eV (due to second order light). At 780 eV the Cobalt emission is dominating, while at 960 eV there is nearly only Copper emission seen in the spectrum. The energy resolution of the Si(Li) detector is about 100 eV in this energy range, which is not enough to resolve structures in one emission peak (for example L_α and L_β). But it is sufficient enough to discriminate between the different elements. For the detection of an absorption spectrum with fluorescence yield detection we put a window of sufficient width around the corresponding emission peak and count the intensity within this area dependent on the excitation energy. By doing this, one can increase the peak to background ratio compared to the total yield detection, because all the emission from the other elements (contamination, higher order peaks) and scattered light, that is not within this window, is not detected.

The electron yield is measured by detecting the photocurrent from the sample with a Keithley picoamperemeter. Because this is a very small signal (typically in the 10^{-10}A range), the signal is very sensitive to electromagnetic noise. Therefore we put a battery between the Amperemeter and the sample, which puts the sample to a negative potential of about -20V. All connections and cables, including the battery are carefully shielded and the distances are kept as short as possible. We compared this signal to the one detected with a channeltron and found the same spectrum, as long as the permanent magnets are not near the sample. But during one MCD measurement, the magnets are close to the sample, and then we found, that the signal from a channeltron is very strongly disturbed by this, while the signal measured with the sample current is hardly affected.

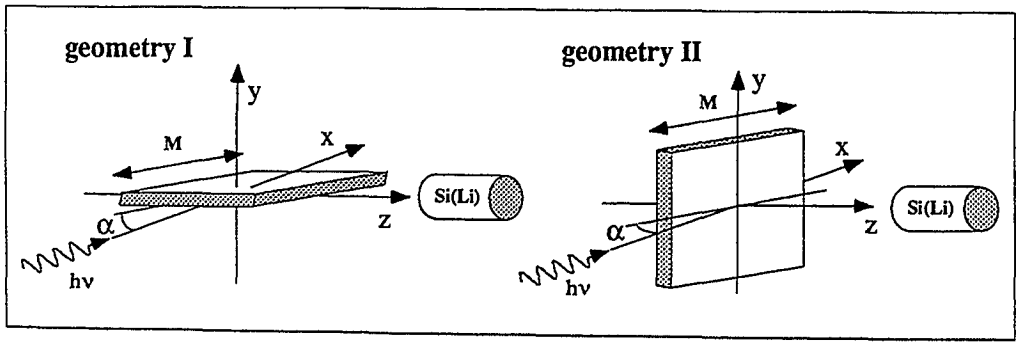

Fig. 4.6. Geometries used for the experiment. (detection direction (Si(Li)) : z)

As mentioned in chapter II, the scattered light from the sample can influence the signal detected in fluorescence yield. In order to avoid this, we have taken the absorption spectra in the FY mode normally in a geometry, where the detector is out of the scattering plane, geometry I in Fig.4.6. The Si(Li) fluorescence detector is always in z - direction, i.e., perpendicular to the penetration direction of the incoming photons (x). The light reaches the sample in grazing incidence and the emitted fluorescence light is detected perpendicular to this at grazing take off. Besides the low scattered light intensity, this geometry also has advantages because self absorption effects in thick films are reduced in this geometry (see chapter II). On the other hand, the intensity detected by the Si(Li) detector is decreased in this geometry compared to a normal take off angle (geometry II), because of the grazing exit angle. Therefore, for very thin films (like Fe/Cr multilayers with Cr in the monolayer range), for systems, where self absorption effects and scattering are negligible, or if one especially wants to study scattering effects and reflection, geometry II can be chosen . Here the detector is in the scattering plane and the emission signal is taken normal from the sample.

V. MCD of 3d Transition Metals in Magnetic Layer Systems

In this chapter the results of the magnetic circular dichroism (MCD) measurements and the comparison with calculations will be discussed. The first part is the quantitative comparison of the $L_{2,3}$ absorption spectra of the 3d elements taken in the electron yield (EY) and fluorescence yield (FY) detection method. Both methods are compared to new first-principle calculations. The circular magnetic dichroism spectra of the 3d ferromagnets Fe, Co and Ni is discussed in detail. It will be shown, that the results are quite different for those cases. In the next part the coupling of Cr as a monolayer in a Fe/Cr multilayer system will be discussed.

All the experiments described in this chapter are carried out at the SX700/3 beamline of the BESSY storage ring in Berlin [Petersen 93], using circularly and linearly polarized soft X-rays, see chapter IV.

5.1 MCD at the $L_{2,3}$ Absorption Edges of the 3d-Elements Measured With EY and FY Detection Compared To First Principle Calculations

The x-ray absorption can be measured in different ways, as described in chapter III. The exact way to determine the absorption coefficient is to measure directly the difference of light intensity in front of the sample and behind the sample. In the soft x-ray regime the penetration depth of the light is in the range of some 1000 Å. Therefore it is not possible to detect the penetrated light of a sample of about 1-2 mm thickness. But this is the typical thickness of the samples investigated here. Here we investigate thin epitaxial films of 50 - 100 Å thickness, evaporated on a single crystal substrate. The epitaxial growth is important for the comparison with theory, where a special structure is assumed; but it is also experimentally relevant, because in this case, the thin films are completely magnetized in plane, with a very low saturation field (less than 100 G) and with certain, well known easy magnetization axes (in plane). These thin epitaxial films can only be prepared by evaporation onto single crystal surfaces, this defines the total thickness of the sample. So, the direct measurement is not possible, but as discussed in chapter III, there are other methods to determine the relative absorption coefficients. One of them is the electron yield method (EY), where all the electrons are detected that are excited by Auger decay and by the corresponding secondary (scattered) electrons. As discussed in chapter III, this signal is proportional to the absorption coefficient. But this method is very surface sensitive, with a mean free path of typically 5 - 50 Å. Therefore it is hardly possible to detect signals from buried layers. The other method is the fluorescence yield (FY) method, where the secondary photons are detected that are excited by filling the hole coming from the photoemission by electrons from higher levels. This method has the advantage of relatively long information depth (mean free path of the light) of typically 1000 Å in the soft x-ray regime, so that also the signal of buried layers can be detected. This has the advantage that the samples can be prepared ex situ and can be covered to avoid oxidation. One disadvantage of this method is a saturation effect, the so called self

absorption. Because of this, the investigated films must be quite thin (typically less than 100 Å) thick. One can avoid or minimize the self absorption effect also by choosing a suitable geometry, as discussed in chapter II. Another effect that occurs in the FY detection mode is that light scattered from the sample cannot be distinguished from secondary photons coming from the absorption process, but this effect can also be minimized by choosing a geometry, where the detector is out of the scattering plane (geometry I, see chapter IV).

So it is shown that each of the two methods (EY and FY) to measure the relative absorption coefficients has advantages and disadvantages depending on the investigated system. The EY mode is most widely used and accepted for the determination of the absorption spectra. Now it is important to see whether the absorption spectra determined by the FY mode are similar, or in how far they are different. If one takes care for the special conditions for each method discussed above one could expect the same results, but this needs to be checked. Especially it must be seen if the dichroism effects are the same in both methods. This is important because there are some systems like buried layers or impurities, where one cannot use the EY detection mode, and where only the FY detection mode can be used for the determination of the absorption spectra. In order to see how reliable the data are taken in the FY mode a direct comparison of both methods is important.

Because of the different conditions for EY and FY detection, it is not simple to find systems, where one can use both methods simultaneously. But this is important for a direct comparison. We have chosen thin films of 40 - 80Å thickness. These films have been prepared under UHV conditions by sputtering (Ni, Co) or electron-beam evaporation (Fe) on a single crystal surface (Co, Ni: sapphire (Al_2O_3); Fe: GaAs+1500Å Ag). To avoid oxidation, these films have been covered by thin inert films on top (Co: 18Å Cr, Ni: 20Å Au, Fe: 35Å Cu). The easy magnetization axes of all films are in plane with a very small coercitive field of less than 100 G.

5.1.1 Isotropic Spectra

The isotropic absorption spectra contain contributions of all possible transitions for Δm (± 1 and 0), they are the conventional absorption spectra. It is of interest, how the $L_{2,3}$ absorption spectra change within the 3d transition elements. Here we compare the experimental data to new first-principle calculations of the absorption spectra. This method is described in chapter 3.2.3. It is of interest, how far the calculations describe the experimental results or what kind of differences are observed. This helps for a better understanding of the electronic structure of the elements, and it is further interesting for the interpretation of the MCD data, described in the next chapter. The experimental data are detected in two different modes, the fluorescence yield (FY) and the electron yield (EY) detection mode. The FY has been detected with the help of a Si (Li) solid state detector with an energy resolution of about 100 eV (see chapter IV), here we have taken

the energy window around the corresponding emission lines to maximize the peak to background ratio of the signal. The EY was detected as the total sample current.

The general trend of the shape of the absorption spectra in the 3d series has been discussed already by Fink et al. [Fink 85]. There the spectra have been measured by electron energy loss spectroscopy (EELS) and the results have been compared to density of states (DOS) calculations. They found a deviation from the expected 2:1 statistical weight for the ratio of the L_3 to L_2 peak intensities and differences in the shape of the L_3 and L_2 spectral regions between the EELS spectra and the DOS.

To achieve isotropic spectra, one has to take the average over all fundamental spectra, as discussed in chapter III. But we found, that the difference between the fundamental spectra Z ($\Delta m = 0$) and (R+L)/2 ($\Delta m = \pm 1$) are negligible small in our cases (this means that there is no magnetic linear dichroism), so that we present here the average of the spectra taken with circularly polarized light with magnetization direction **M** parallel to the helicity **S** of the incident circularly polarized light, and **M** antiparallel **S**; this represents the isotropic spectrum.

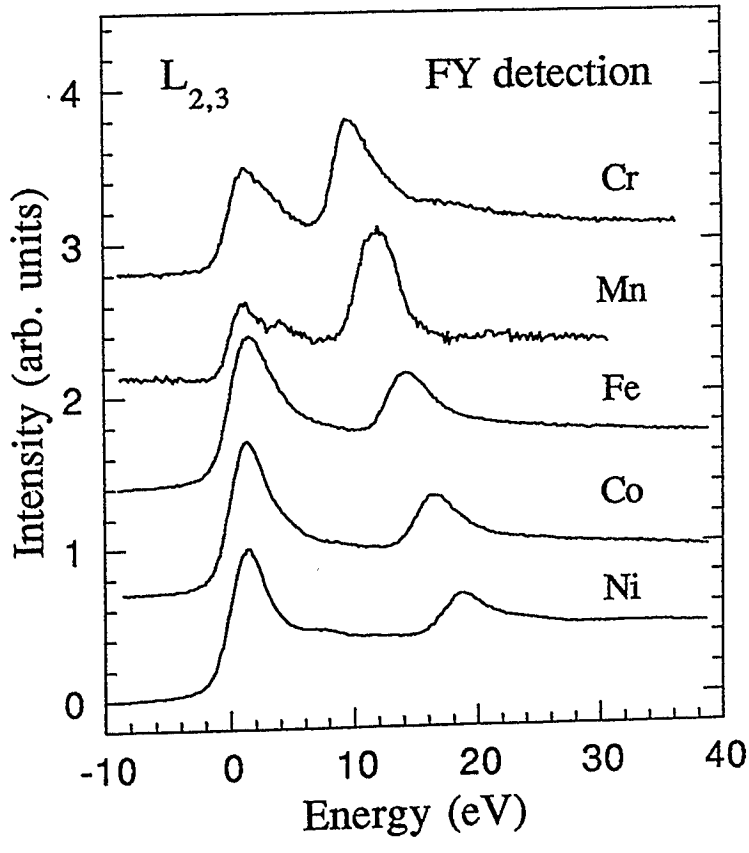

Fig.5.1. Isotropic spectra of Cr, Mn, Fe, Co, Ni taken in fluorescence yield (FY).

In Fig. 5.1 the isotropic $L_{2,3}$ absorption spectra of the 3d elements Cr, Mn, Fe, Co and Ni are shown, measured in the FY mode. In all the cases the samples are thin films in the thickness range of 40 - 80 Å, covered with about 30 Å Cu, Cr or Ag to avoid oxidation. The spectra are taken in geometry I, as described in chapter IV, where the detector is out of the scattering plane, to avoid scattering and self absorption effects. The energy scale is set to the first inflection point of the L_3 edges. The real absorption energies are in the range of 575 eV (Cr L_3) up to 870 eV (Ni L_2); the absorption energies are given in detail in appendix ii). The original spectra are divided by the gold mesh signal and a constant background is subtracted. Then the spectra are normalized to 1 at the peak maximum.

One can clearly see two trends in the spectra. First the spin-orbit splitting (energy difference between L_3 and L_2) is increasing with increasing atomic number, from 8 eV in Cr up to 16.8 eV in Ni. This is due to the increasing spin-orbit interaction within the 3d series. The other trend is more interesting. The branching ratio (ratio of the intensity of L_3 peak and the sum of $L_2 + L_3$ peaks) is increasing within the 3d series, too. According to the statistical ratio in the core level occupation, it should always be $2/(1+2) = 0.666$. But this ratio in these spectra is different from the statistical one, as it has already be seen by Fink et al. [Fink 85]. Especially for the early 3d elements Cr and Mn it is strongly reduced. The origin of the non statistical branching ratio in these spectra is due to initial-state spin-orbit splitting and electrostatic interactions between core hole and valence electrons [Thole 88]. But the branching ratio in these FY spectra are even more different from the statistical one than the EELS spectra by Fink et al.

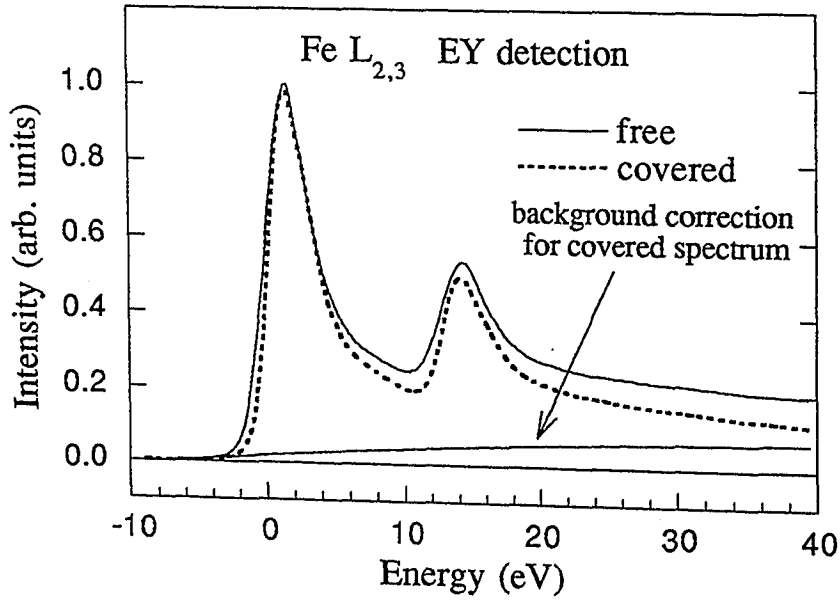

Fig. 5.2. Fe $L_{2,3}$ absorption spectra taken in EY mode from a clean surface and a buried layer.

In order to obtain more quantitative results for the branching ratio, we have compared the spectra for Fe, Co and Ni taken in the FY mode to those taken in the EY mode and to new first principle calculations. But as mentioned above, a comparison of spectra in FY and EY mode is not simple, one has to choose samples where no self absorption or scattering changes the spectrum in the FY mode and where the investigated layer is not buried too deep so that the signal can still be detected in the EY mode. We have chosen thin films of 50-60Å thickness, which are prepared ex situ. Therefore they had to be covered to avoid oxidation. The cover layer in our case is in the range of 20-35Å thickness of Cu,Cr or Au. Here the EY signal is already weaker because the electrons are scattered in the cover layer; the FY signal is not influenced by a cover layer of this thickness. Because we want to compare spectra of the same samples, in the same geometry, we have to see at first how the cover layer influences the EY spectrum. Therefore we have compared EY spectra of the buried layers to ones from a clean, not covered surface. The clean Fe spectrum was taken from a 200Å Fe film, which was deposited on a sapphire substrate. This film was also prepared ex situ and therefore covered with 20Å Au. This cover layer has been removed in situ by Argon sputtering to achieve the free and clean surface. This comparison is shown for the Fe $L_{2,3}$ spectrum in Fig. 5.2.

Fig. 5.2 shows the spectrum from a clean Fe surface compared to the spectrum of a 60Å Fe film which is covered by 35Å Cu. The spectra are normalized to the L_3 peak maximum. The cover layer causes that the Fe absorption spectrum is lying on a smoothly decreasing background on the Fe absorption spectrum. We have added a quadratic background to the spectrum of the covered film, as shown in the figure, then the spectra are quite the same. This kind of background was used also for the Co and Ni spectra.

Fig. 5.3 shows the comparison of the isotropic spectra of Fe, Co and Ni taken in FY and EY mode compared to first-principles calculations.

For a direct comparison of the spectra taken in FY and in EY mode, the spectra have been taken from the same samples in the same geometry. Because the samples are capped with a top layer of about 30-50 Å Ag or Cu, the spectra for the EY yield are lying on a smooth decreasing background. By comparing these data to those taken from clean surfaces, we found that the EY data from these buried films can be corrected by a quadratic background to have the same shape of the clean surfaces. Therefore the EY spectra shown are corrected by this background.

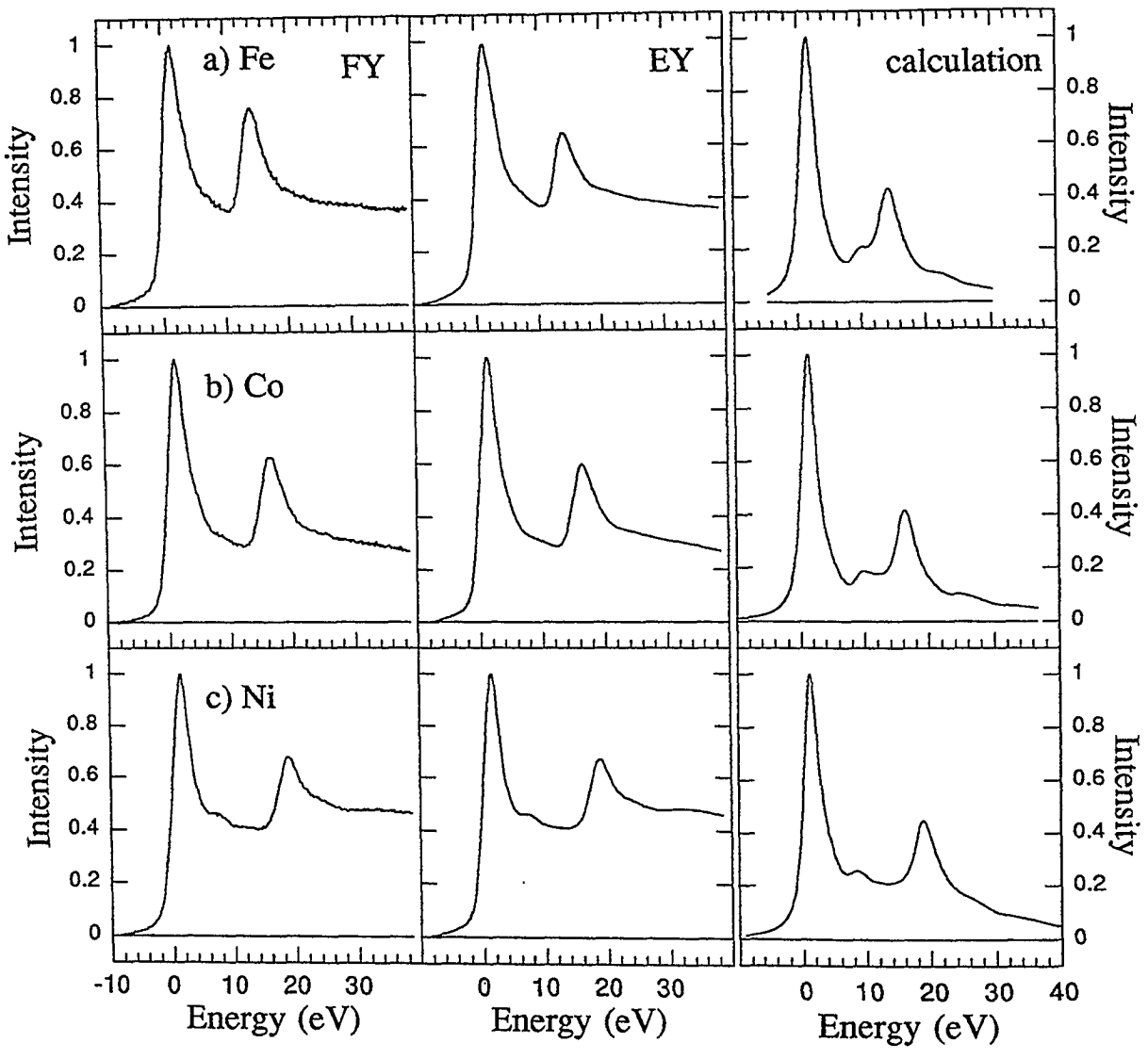

Fig. 5.3. Isotropic spectra of Fe, Co and Ni, a) taken in FY mode, b) taken in EY mode and c) first principles calculations.

The L absorption edge consists of transition from the 2p core levels to the 3d and 4s valence levels (see Fig.1.1 and chapter II). The 3d contributions are represented by the main peaks in the spectrum (corresponding to the unoccupied densitiy of states DOS) while the 4s states have less structure in the valence band and therefore they give rise to a step-like background in the spectrum. For a comparison of the d-state branching ratios in the different spectra, the s-parts need to be subtracted from the original spectrum. This is shown in Fig.5.4. in the case of Fe. The original isotropic spectrum is shown on the top, together with the steplike s-background. For the s-states we estimated the statistical ratio of $L_3/L_2 = 2/1$, because there is no spin-orbit interaction in these states [Thole 88]. The

step can be described by an arc tan function positioned at the inflection point (IP) of the original spectrum [Stöhr 92]:

$$I_{step} = \left[\frac{1}{2} + \frac{1}{\pi}\arctan\left(\frac{E\text{-}IP}{\Gamma/2}\right)\right] \qquad (5.1)$$

This implies the convolution of a square step with a Lorentzian, i.e., an integral of a Lorentzian function, which yields an arctan function. Here, IP is the position of the inflection point of the step (= IP of the original spectrum); H is the step height of the function, E is the independent variable, energy, and Γ is the width of the step, which is fitted to the width of the increasing edge. Another description of the step function is the so-called error function (erf), which practically yields to analogous results. The position of the IP of the step in the case of the L_2 edge cannot unambiguously taken from the

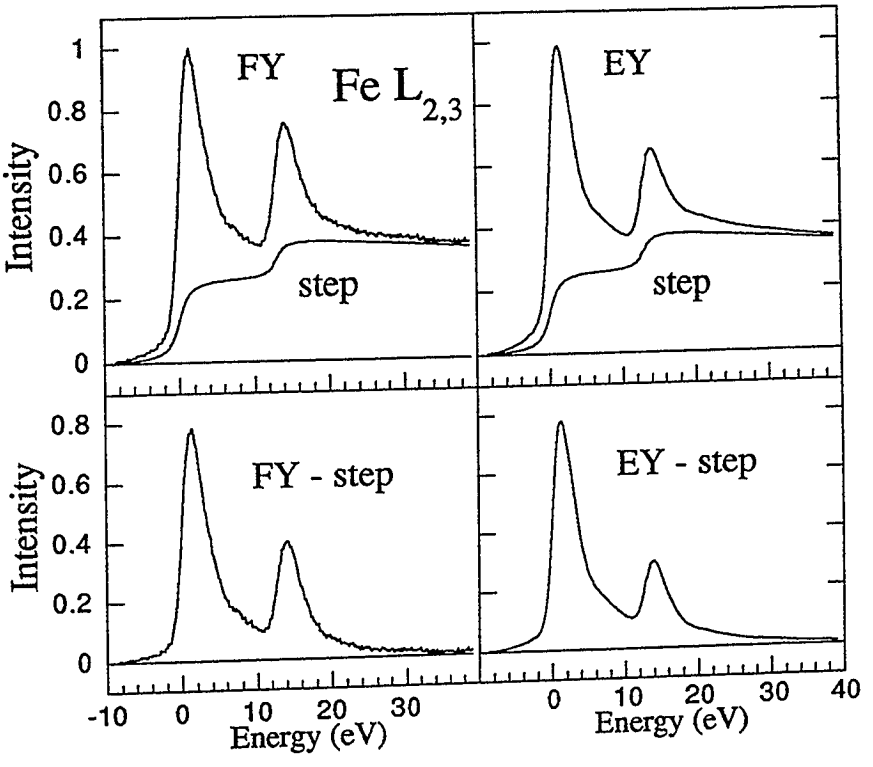

Fig. 5.4. Isotropic $L_{2,3}$ absorption spectrum of Fe taken in FY and EY mode, together with the step-like background due to the s states. The difference, which corresponds to transitions into the 3d states, is shown on the bottom of the figure.

absorption spectra, because there is an overlap of the tail of the L_3 intensity at the L_2 white line, which might shift the IP of the original spectrum. But the spin-orbit splitting of the $L_{2,3}$ edges are well known (for example from photoemission experiments, see also appendix ii)), and in the case of Fe, Co and Ni the spin-orbit splitting between L_3 and L_2 is already quite large, so that the overlapping tail of the L_3 edge hardly influences the position of the IP of the L_2 edge. A second complication to modelling the continuum step is that the steps are usually not constant above the edge but exhibit a decay due to decreasing overlap between the initial and final states in the electronic transition. To model this decline, the step function given by (5.1) is multiplied by a very weak exponential decay (see also ref. [Stöhr 92]).

The isotropic spectrum together with the step according to (5.1) is shown in Fig. 5.4 in the case of Fe in FY and EY mode. The subtracted spectrum, which corresponds to the transition of the 3d states, is shown on the bottom of the figure.

From the spectra with the subtracted s states, as shown in Fig.5.3, we have determined the $L_{2,3}$ branching ratio from the integrals over the L_3 and L_2 white lines, respectively:

$$B = \frac{L_3}{L_2+L_3} \tag{5.2}$$

This should be (2/(1+2)) = 0.667 due to the statistical ratio, but due to spin-orbit interaction in the d states, this ratio can vary from the statistical one [Thole 88]. In Table 5.1 the $L_{2,3}$ branching ratios for the d-states are given.

$\frac{L_3}{L_2+L_3}$	Fe (bcc)	Co (hcp)	Ni (fcc)
calc.	0.689	0.704	0.697
this exp. EY	0.669±0.003	0.678±0.003	0.674±0.003
this exp. FY	0.607±0.003	0.667±0.003	0.681±0.003

Table 5.1. $L_{2,3}$ branching ratio of the isotropic spectra for Fe, Co and Ni measured in FY and EY mode compared to first principle calculations [Guo 94].

One can see, that the branching ratios are close to the statistical one, but are different for each element and also depend on the detection mode. The branching ratios are shown graphically in Fig. 5.5 for a better comparison.

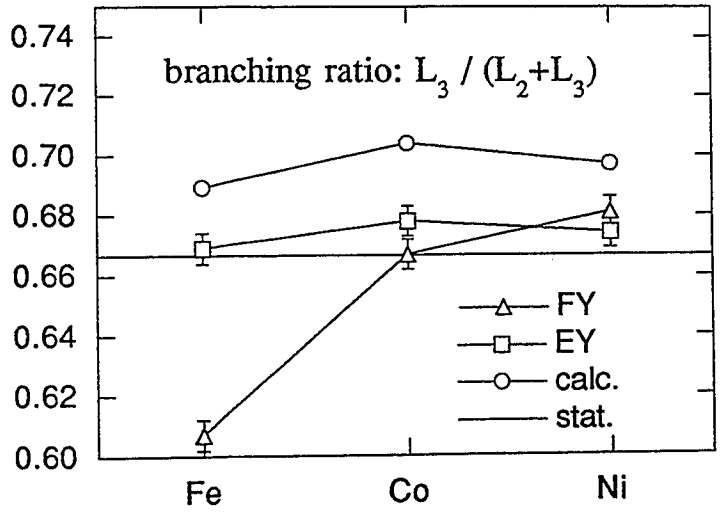

Fig 5.5. $L_{2,3}$ branching ratio of the isotropic spectra for Fe, Co and Ni measured in FY and EY mode compared to first principle calculations.

The branching ratios measured in the FY mode are different from those measured in EY mode. In the case of Fe and Co, it is smaller in the FY mode and for Ni it is a little higher. The differences in the branching $L_{2,3}$ ratios between electron- (EY) and fluorescence yield (FY) can have different origins. The FY spectrum might be changed for example by diffuse scattering or by self absorption effects, as described in chapter II. But because the geometry was chosen so that the detector was perpendicular to the scattering plane, diffuse scattering can be neglected in this case. The thickness of the samples is also chosen in a way that no self- absorption changes the spectrum, as discussed above. It is more reliable that the differences are caused by different fluorescence rates Γ_x at the L_2 (Γ_{x2}) and L_3 (Γ_{x3}) edge compared to the Auger rates (Γ_{A2},Γ_{A3}, respectively). The total transition rate Γ_{tot} can be set to the Auger rate in this energy regime.

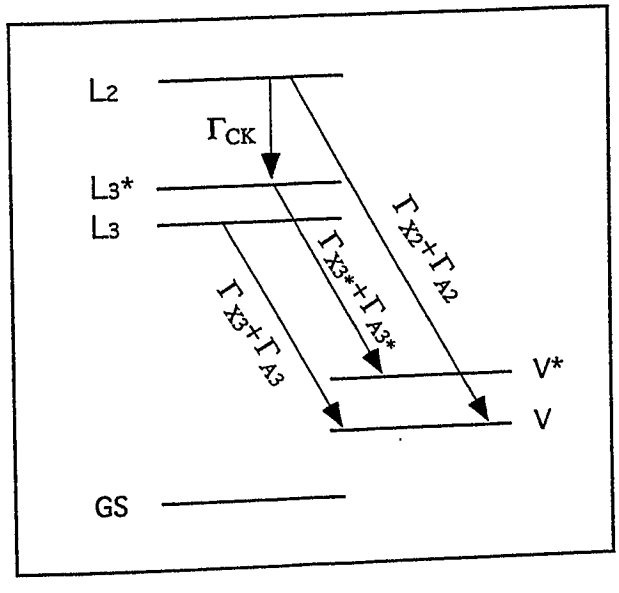

Fig.5.6. Energy scheme for the excitation and decay of the L_2 and L_3 absorption edges by fluorescence- and Auger decay with the corresponding transition rates Γ_x and Γ_A, respectively.

At the L_2 edge the core hole can be filled, besides the direct decay, also by a Coster Kronig (CK) transition as shown schematic in Fig.5.6. A Coster Kronig transition is an Auger transition in which the initial vacancy and one of the electrons that fills this vacancy are in a shell with the same principal number (in this case the L shell) (see e.g. ref. [Carlson 75]). This results in an extra valence hole compared to the normal Auger transition. Because of the large overlap of the wave functions, Coster Kronig transitions are more than an order of magnitude larger than normal Auger processes. In this special case, the L_2 core hole is not directly filled by a valence electron but by an electron from the L_3 shell and then the L_3 hole is filled by a valence electron. Thus an extra electron with the energy difference of the L_2 and L_3 edges is excited from the valence band.

The total transtition rate Γ_{tot} is the sum of the electron (Auger) rate Γ_A and of the fluorescence rate Γ_x (and in the case of Coster Kronig processes also of the Coster Kronig rate Γ_{CK}). Because the electron rate is orders of magnitude larger than the fluourescence rate one can set $\Gamma_{tot} \approx \Gamma_A$ at the L_3 edge. Therefore, for the electron yield, the intensities (I) at the L_3 edges are given by the corresponding absorption cross sections σ. At the L_2 edge the Coster Kronig rate needs to be taken into account. The extra electron which is excited by the Coster Kronig process results in extra intensity at the L_2 edge; but the energy of this extra electron is quite small, so that it hardly produces secondary electrons, in contrast to the primarily excited Auger electron with several hundred's eV energy, which produces a corresponding large number of secondary electrons. Therefore in a first approach the EY intensity at the L_2 edge is also proportional to the absorption cross section σ:

$$I_{L3}(EY) \propto \sigma_{L3}, \qquad I_{L2}(EY) \propto \sigma_{L2} \tag{5.3}$$

The fluorescence yield (FY) - intensity at the L_3 edge is related to the absorption cross section σ by

$$I_{L3}(FY) \quad \propto \quad \sigma_{L3} \cdot \frac{\Gamma_{x3}}{\Gamma_{tot3}} \quad \approx \quad \sigma_{L3} \cdot \frac{\Gamma_{x3}}{\Gamma_{A3}} \; . \tag{5.4}$$

At the L_2 edge the FY - intensity is given by

$$I_{L2}(FY) \propto \sigma_{L2} \cdot \left[\frac{\Gamma_{x2}}{\Gamma_{tot2}} + \frac{\Gamma_{CK}}{\Gamma_{tot2}} \frac{\Gamma_{x3*}}{\Gamma_{tot3*}} \right] \approx \sigma_{L2} \cdot \left[\frac{\Gamma_{x2}}{\Gamma_{A2}+\Gamma_{CK}} + \frac{\Gamma_{CK}}{\Gamma_{A2}+\Gamma_{CK}} \frac{\Gamma_{x3*}}{\Gamma_{A3*}} \right] . \tag{5.5}$$

because of the additional Coster Kronig process. Thus the $L_{2,3}$ intensity ratio for FY is given by

$$\frac{I_{L3}}{I_{L2}}(FY) \quad = \quad \frac{\sigma_{L3}}{\sigma_{L2}} \cdot \left[\frac{\frac{\Gamma_{x3}}{\Gamma_{A3}}}{\frac{\Gamma_{x2}}{\Gamma_{A2}+\Gamma_{CK}} + \frac{\Gamma_{CK}}{\Gamma_{A2}+\Gamma_{CK}} \frac{\Gamma_{x3*}}{\Gamma_{A3*}}} \right] \tag{5.6}$$

and the difference in the $L_{2,3}$ intenstity ratios between EY and FY detection is given by

$$\frac{\frac{I_{L3}}{I_{L2}}(FY)}{\frac{I_{L3}}{I_{L2}}(EY)} = \left[\frac{\frac{\Gamma_{x3}}{\Gamma_{A3}}}{\frac{\Gamma_{x2}}{\Gamma_{A2}+\Gamma_{CK}} + \frac{\Gamma_{CK}}{\Gamma_{A2}+\Gamma_{CK}} \frac{\Gamma_{x3*}}{\Gamma_{A3*}}} \right] \quad . \qquad (5.7)$$

This becomes 1 (numerator = denominator) if $\Gamma_{x3} = \Gamma_{x2} = \Gamma_{x3*} = \Gamma_x$ and $\Gamma_{A3} = \Gamma_{A2} = \Gamma_{A3*} = \Gamma_A$, which is, of course, not very likely to happen.

One possible explanation for the differences in the FY and EY detection would be that $\frac{\Gamma_{x3*}}{\Gamma_{A3*}} > \frac{\Gamma_{x3}}{\Gamma_{A3}}$, that means, that an extra valence hole has less influence on Γ_x than on Γ_A. This could result in a smaller $L_{2,3}$ branching ratio for FY than for EY, as we have seen in the experiment. This could also explain the systematic changes in the 3d series, because in a pure band picture, an extra hole should not change the transition rates, while in an atomic model it does. Within the 3d series, there is a tendency from the earlier to the later elements from more atomic like to more bandlike behaviour.

5.1.2 Magnetic Circular Dichroism (MCD) of Fe, Co, Ni

Magnetic circular dichroism exhibits itself by the different absorption coefficients for parallel (μ^+, R) and antiparallel (μ^-, L) orientation of the magnetization of the sample (**M**) relative to the photon helicity (**S**), as described in chapter III. In Fig.5.7 these fundamental absorption spectra (R and L) of Fe are shown, detected by the different methods, FY and EY. The spectra in the center of the figure show the fundamental absorption spectra (R, L). Both spectra are taken independently by changing the magnetization direction. The spectra have been first divided by the goldmesh current (I_0) for normalization, and then a constant background has been subtracted. After this the spectra are normalized far above the edge to the same height and finally normalized in the way, that the sum of both spectra at the L_3 peak maximum is 1. The top of the figure shows the sum of both spectra, after subtraction of a step-like background of the s-like states, which is also indicated in the middle of the figure. The difference R-L (the MCD spectrum) is shown on the bottom of the figure. Here one can clearly see that the spectra detected with FY and EY are not only different in the isotropic spectrum, but also in the MCD spectrum. The shape and intensity at the L_3 edge is nearly identical, as it was already seen in the isotropic spectrum, but the most striking difference is the MCD intensity between the L_3 and L_2 edges. It is nearly zero in the EY and also in the calculated spectrum, but it is clearly positive in the FY spectrum. The MCD intensity at the L_2 peak is higher in FY than in EY; this is, of course, due to the higher L_2 intensity in FY than in EY.

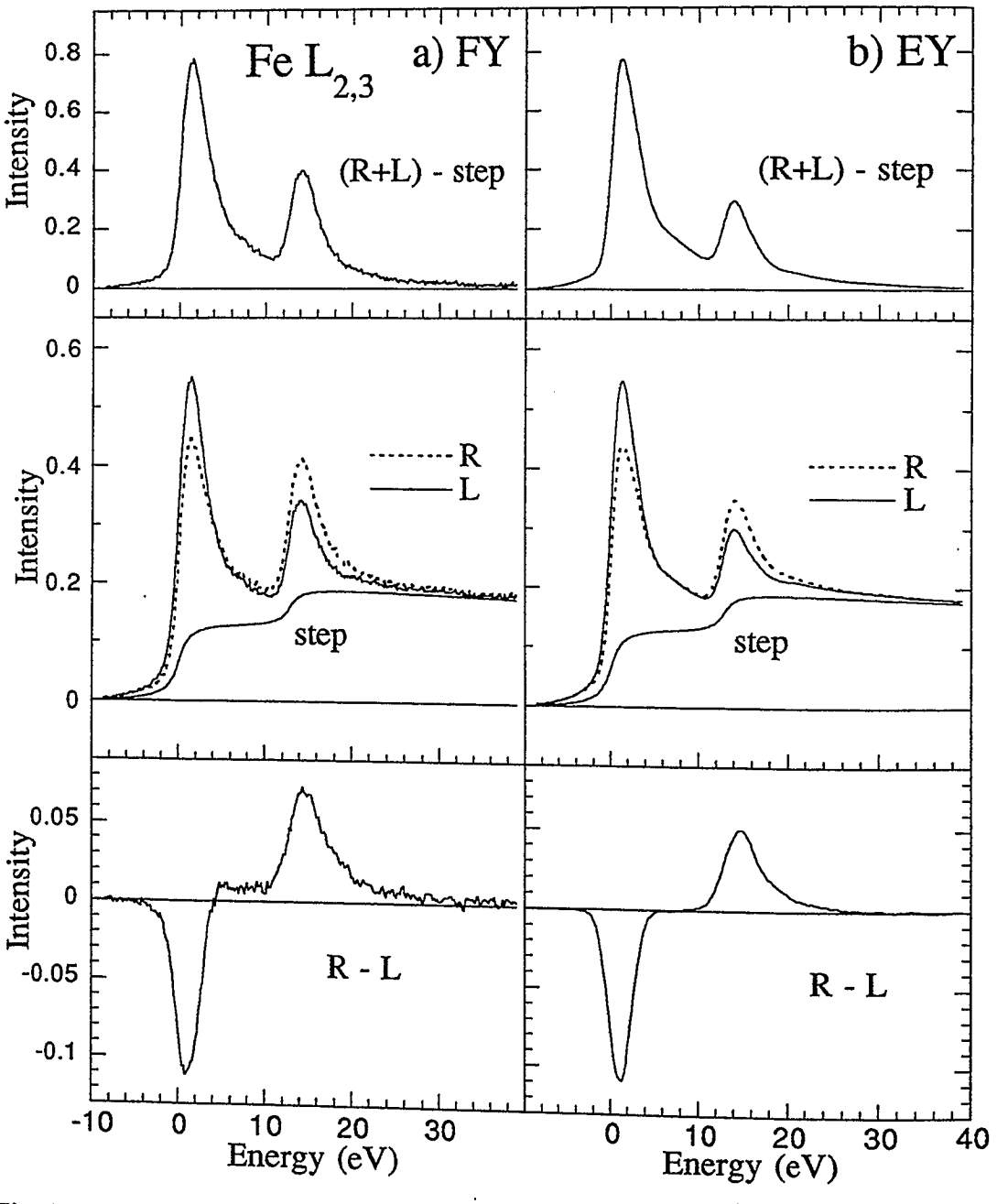

Fig.5.7. $L_{2,3}$ absorption spectra of Fe taken in a) FY and b) EY mode. top: isotropic spectrum after subtraction of a step-like background; center: fundamental spectra R (μ^+, **M** ↑↑ **S**), L (μ^-, **M** ↑↓ **S**) and steplike background; bottom: MCD spectra R-L.

The MCD spectra for all 3d ferromagnets (Fe, Co, Ni) are presented in Fig.5.8, again in comparison of FY and EY detection and calculation. The original spectra have in all cases been normalized in the way shown in Fig.5.6, i.e., R+L = 1 at the L_3 peak maximum. Therefore, the intensity in the MCD spectrum at this point (but only at this point!) is directly the asymmetry (R-L / R+L). The experimental MCD spectra have less intensity compared to the calculated ones. This is mainly due to the experimental conditions (not parallel coupling of **M** and **S**, not completely polarized light). This difference will be compensated by the factor C described in chapter III.

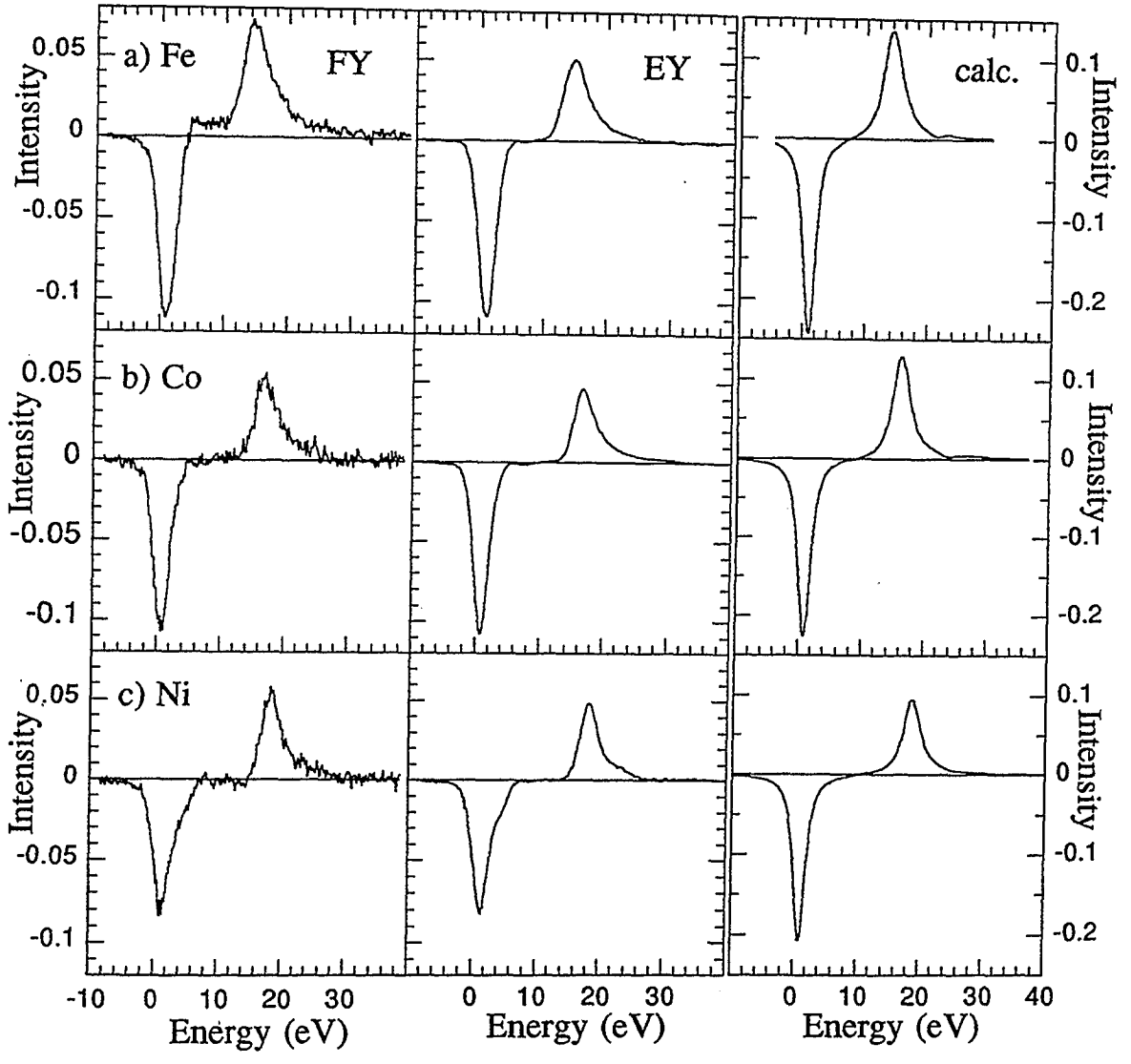

Fig.5.8. MCD spectra (R-L) of the $L_{2,3}$ absorption edges of Fe, Co and Ni detected in the FY and EY mode compared to first principle calculations. The original spectra R and L are normalized so, that R+L = 1 at the L_3 peak maximum (see Fig. 5.3).

One can see in Fig.5.8, that the general shape of the MCD spectra is the same in all cases. The intensity at the L_3 edge is negative and at the L_2 edge positive and between the edges the MCD intensity is very small. But in detail, there are striking differences. The most important difference between the spectra detected in FY and EY mode in the case of Fe the non vanishing intensity in the FY MCD spectrum, as mentioned above. This can be caused by magnetic circular dichroism in the Fe $L_{2,3}$ X-ray fluorescence spectra, which was predicted in 1991 by Strange et al. [Strange 91]. Experimentally, this was also found by Hague et al. [Hague 93]. It expresses itself by different fluorescence

intensities for different light polarizations, and the $L_{2,3}$ fluorescence spectrum shown by Hague et al. shows a non vanishing difference in the MCD emission spectrum also between the absorption edges. This effect is hardly seen for Co and Ni. Within the statistical noise, the MCD intensity is nearly zero between the edges. The MCD intensities at the L_3 edge are nearly identical in EY and FY mode, while the intensity at the L_2 edge is different, like in the isotropic spectra. The tail of the L_2 intensity to higher energies is longer in FY than in EY. But this might be caused simply by the higher MCD intensity in the FY L_2 peak. In the MCD spectrum of Ni one can see a shoulder at about 4eV in the L_3 peak. This structure, which has no counterpart in the density of states, has been observed already by Chen et al. [Chen 91] in electron yield data; here it is also seen in the fluorescence yield data. This feature has been discussed by Chen et al. [Chen 91] as a representation of a shake-up or shake-off phenomenon analogous to the 6eV hole-hole correlation satellite in photoemission. This shoulder is not present in the calculated spectrum, which is again a sign for a correlation effect, which is not taken into account in the calculations. For a quantitative analysis of the differences between the EY and FY detection modes and the calculations, we use the sum rules described in chapter III.

As discussed in chapter III, the knowledge of the d-state occupation number is of essential importance for the determination of the magnetic moments with the help of the sum rules, because they are directly proportional to it. On the other hand, the ratio $\langle L_z \rangle / \langle S_z \rangle$ (by neglecting T_z) is independent of this, the experimental factor C, and the normalization by the isotropic spectrum; therefore, this ratio is ideal for an independent comparison of the different systems. The integrals over the edges are taken 3 eV before the inflection point (IP) up to the energy, where the MCD spectrum reaches approximately zero. This is at the L_3 edge approx. 7.5 eV and at the L_2 edge approx. 15 eV above IP. In the following Table, these ratios are listed for Fe, Co and Ni. One can get the numbers also directly from the magnetic moments by $\langle L_z \rangle / \langle S_z \rangle = 2\, \mu_{orb}/\mu_{spin}$.

$\frac{\langle L_z \rangle}{\langle S_z \rangle}$	Fe (bcc)	Co (hcp)	Ni (fcc)
[Stearn 86], exp.	0.12	0.14	0.17
[Guo 94a] calc	0.05	0.11	0.17
[Guo 94a] sum rules*	0.04	0.09	0.16
[Carra 92]*	0.13	0.13	0.19
this exp. EY*	0.12 ± 0.01	0.15 ± 0.01	0.18 ± 0.02
this exp. FY*	(-0.09 ±0.02)	0.12 ± 0.01	0.11 ±0.02

Table 5.2. $\langle L_z \rangle / \langle S_z \rangle$ ratios for the experiment and theory compared to the data determined from the MCD measurements with the help of the sum rules.*In the cases where the sum rule has been used, the magnetic dipole operator T_z (see Eq.(3.7)) has been neglected.

The data from ref [Stearn 86] are experimental data from neutron scattering experiments. The data from ref. [Guo 94] are from first principle relativistic calculations,

where calc. means that these are directly the data from the calculations and sum rules means that there the sum rules have been applied to the calculated MXD spectra. The differences between these two methods have been discussed in detail in ref. [Guo 94], see also chapter 3.2.4. The data for Ni are new calculations, which are not in the given reference. The data from ref. [Carra 92] are experimental data evaluated with the help of the sum rules, and the last two rows contain the data evaluated from this experiment with the help of the sum rules. In all cases (except Ni, FY) one can see the tendency of increasing ratios from Fe to Ni. The EY data fit quite well to the corresponding neutron scattering data. But the FY data for Fe is completely wrong, it even gives a negative value. This is of course due to the positive MCD intensity between the edges in this case. The Co ratio from the FY measurement fits quite well and the Ni ratio is smaller. The sum rule gives good values for the $\langle L_z \rangle / \langle S_z \rangle$ ratio in the EY mode (the data of ref. [Carra 92] are also taken from EY spectra), but in the FY mode it is only good for Co. Besides the special case in iron, this might be due to the different branching ratios in the absorption and MCD spectra. Due to the Coster Kronig decay, the FY data do not represent the real branching ratio and therefore also give different results in the sum rules. The calculated values of Guo et al. are significantly smaller for Fe and Co than the experimental data, and the values determined by the sum rules from the calculated spectra (third row) are even smaller. Thus, the atomic model and the band structure calculation are not consistent for these elements. For Ni the calculated data fit quite well.

Usually one is interested in the magnetic moments and not in their ratio. For this, one needs some parameters to evaluate these numbers from the sum rules. An important parameter is the d state occupation number of the solid, respectively the number of d-holes in the valence band ($n_h = 10 - n_d$) which must be known according to eq. (3.6) and (3.7) to evaluate the magnetic moments.

	Cr (bcc)	Mn (cubic)	Fe (bcc)	Co (hcp)	Ni (fcc)
atomic number Z	24	25	26	27	28
n_d (atom)	5	5	6	7	8
n_d			6.57	7.57	8.63
$n_h = 10 - n_d$			3.43	2.43	1,37

Table 5.3. d-state occupation numbers n_d and number of 3d holes ($n_h = 10 - n_d$) of the 3d elements calculated for the typical solid state structures from first-principles calculations [Guo 94a], compared to the atomic case.

The d-state occupation numbers for the 3d elements are shown in Table 5.2. It can be seen, that the d-state occupation numbers of the 3d elements in the solid state are larger than in the atom, this is due to a hybridization of the d with s- or p- like states.

Additionally to this, one needs to know the experimental conditions, which are combined in the factor C in eqs. (3.6) and (3.7). At first there is the geometrical factor, the angle α between the photon spin direction and the magnetization, which has been

explained in chapter IV, it is 30° in our case. The samples in our case have been thin epitaxial films, which can be magnetized completely with a very low magnetic field (less than 100 G), this means, that all the samples have been fully magnetized and this factor (m) is equal to 1. The last factor, the degree of circular polarization of the light P, is much more critical. The light is taken off the axis of the synchrotron under an angle of -0.6 mrad and is not completely polarized [Petersen 93]. The degree of circular polarization can be calculated and is about 90 % for an off-plane angle of 0.6 mrad in the energy range of 500 -900 eV [Petersen 93]. P increases with increasing photon energy and increasing off-plane angel, but above approximately 300 eV the energy variation of P is very weak, so that one can estimate it to be constant for the energy range of 500 - 900 eV, the range of the $L_{2,3}$ absorption edges of the 3d magnetic elements. Experimentally there is a lack of data for the soft x-ray regime. There is one publication about photoemission of the Fe 2p states [Baumgarten 90], where the authors estimate a polarization degree of 60 - 80% for an off-plane angle of 0.3 mrad. This is not precise enough, and it is also for a different off plane angle than we have used (0.6 mrad). With the help of a reference sample with known magnetic moment one can use MCD measurements to evaluate P (or a factor C', which includes all experimental coefficients and the number of d-holes). This has been done in ref. [Böske 94a] for a thin Co film. Assuming that the sum rules are valid, the polarization degree was found to be 48 % for an off axis angle of -0.3 mrad at the Co $L_{2,3}$ absorption edges. For our conditions so far, there are no reliable data for P, therefore we calibrate our data to the average data of Fe, Co and Ni determined from the sum rules compared to the experimentally known magnetic moments. From this, we get an experimental factor C = 0.54. With $\alpha = 30°$ ($\cos^2 30° = 0.75$), we estimate an average polarization factor of P = 72%. We take this value for all measurements. The results of these evaluations (including the calculated numbers for n_d from table 5.2) are listed in table 5.3.

magnetic moments (μ_B)	Fe (bcc)		Co (hcp)		Ni (fcc)	
	μ_{spin}	μ_{orb}	μ_{spin}	μ_{orb}	μ_{spin}	μ_{orb}
[Stearns 86]	2.25	0.14	1.86	0.13	0.656	0.055
[Guo 94] calc.	2.214	0.053	1.581	0.084	0.598	0.052
[Guo 94] sumrule*	1.882	0.034	1.524	0.068	0.549	0.043
this exp. EY*	2.03	0.12	1.53	0.12	0.79	0.07
this exp. FY*	2.72	(-0.15)	1.59	0.10	0.93	0.05

Table 5.4. Magnetic spin (μ_{spin}) and orbital (μ_{orb}) moments (in units of μ_B) of the 3d ferromagnets Fe, Co and Ni. *In the cases where the sum rule has been applied, the magnetic dipole operator T_z (see Eq.(3.7)) has been neglected. The experimental factor C was estimated to be C = 0.54 in the last two rows.

The magnetic moments are derived from the sum rules (3.6) and (3.7) with neglecting the magnetic dipole operator T_z and estimating that linear dichroism is negligible compared to circular dichroism. The first point is important for the determination of the magnetic spin moment. Within the atomic model, this can be justified [Carra 93] in cubic systems. But also in new first principles calculations by Guo et al. [Guo 94b] it was found, that this is true for the bulk systems; but in magnetic multilayer systems, T_z might become more important. Whereas neglecting linear dichroism is important for the normalization of the MCD spectra by the isotropic spectra. With circularly polarized light one can only obtain the absorption spectra with the selection rules $\Delta m = +1$ and -1 but not $\Delta m = 0$, which is also needed for the isotropic spectrum. But we have also performed measurements with linearly polarized light, and we found that the linear dichroism effect is really negligible compared to the circular dichroism in these bulk systems. Therefore, the isotropic spectrum can be taken from those ones determined with circularly polarized light by 3/2 (R+L) as discussed in chapter III.

The values obtained from first principle calculations [Guo 94a] are always smaller than the ones experimentally determined [Stearns 86] (see also ref. [Eriksson 90] for a comparison of experimental an theoretical determined magnetic moments in Fe, Co and Ni). And comparing the magnetic moments obtained from first principle calculations to those obtained from the calculated spectra with the help of the sum rules it is found that the values obtained with the sum rules are always smaller than the calculated ones, as discussed in chapter 3.2.4.

The magnetic moments determined from our experimental spectra in the EY and FY mode vary for each element from the literature data [Stearns 86]. The most striking difference is the orbital moment of Fe obtained from the FY data. Here one even obtains a negative value for μ_l. This is of course caused by the non-vanishing MCD intensity between the edges in the case of Fe taken in FY mode. The data for Co and Ni are much more reliable, although there is still a difference in EY and FY mode. The values for the spin moments in the FY mode are in all cases larger than the ones in the EY mode, whereas the values for the orbital moments are smaller (especially in the case of Fe). This is probably mainly caused by the enhanced L_2 intensity in the FY data. And in the case of Fe also by the non-vanishing MCD signal between the edges.

Summarizing the MCD data it can be concluded, that with the help of the sum rules one can determine the local spin- and orbital- moments of the 3d ferromagnets, at least semi-quantitatively. The values for the EY and FY data are not identical, especially in the case of Fe. For Co and Ni the numbers are more close. If one wants to make precise measurements, one should take a reference sample of the same element with a known magnetic moment and compare the results to this reference sample. One can not simply take the calibration factor C (which might in reality not only contain the experimental factors mentioned above, but also correction factors for the sum rules, different for each element) from another element, if one wants to get absolute values for the magnetic moments. (Also the number of d-holes n_h is a not well known factor, which is directly

proportional to the moment.) These problems, one gets rid of by using a reference sample. Then the use of the sum rules is a very powerful tool for the determination of element specific local moments. This has been shown for example by Wu et al. [Wu 92], and Weller et al. [Weller 94], where the enhancement of the orbital moments of Co in multilayers has been studied in comparison to a bulk Co sample. The use of EY or FY detection mode is then mainly given by the sample one wants to study and by the experimental conditions. The measurement of buried films and impurities in an applied (probably changing) magnetic field is of course a domain of the FY detection (see e.g. ref. [Böske 94a]). Of special interest is the element specific determination of magnetic hysteresis curves in heteromagnetic systems (like multilayers). Chen et al. [Chen 93] have shown this for a Fe/Co multilayer, where the hysteresis curves of Fe and Co have been separately determined by measuring the MCD signal at the L_3 edge in the FY mode as a function of the applied magnetic field. The measurement of the magnetic properties of surfaces and adsorbates is better done with EY detection. Recently it was found by Vogel et al. [Vogel 94] that also the absorption signal in EY detection is polarization and angle dependent; so one must take care in comparing data taken from different geometries not only in FY but also in the EY detection mode. For a better quantitative understanding of the FY data, calculations of the absorption signal in the FY detection mode should be performed.

5.2 MCD at the $L_{2,3}$ Absorption Edges of Cr in Fe/Cr Multilayers

Fe/Cr multilayers are a model system for magnetic multilayers. The Fe/Cr system was the first multilayer system, where the oscillating behavior of the magnetization of adjacent Fe layers in dependence on the Cr spacer thickness [Grünberg 86], [Carbone 87],[Unguris 91] and a giant magneto-resistance is reported for antiparallel ordered Fe layers [Baibich 88],[Binasch 89]. Recently, the coupling behavior of Cr on Fe has been studied with spin-polarized electron energy-loss spectroscopy (SPEELS) [Walker 92] and with scanning electron microscopy with polarization analysis (SEMPA) [Unguris 92]. With SEMPA it was possible to obtain the orientation of the topmost Cr layer(s) on Fe for a wedge-like structure with a polarization analysis of the scattered secondary electrons. Both in SPEELS and SEMPA, the Cr signal oscillates with a short period of about two atomic layers. A significant deviation is reported [Unguris 93] for low coverages. With spin-polarized photoemission from the Cr 3p core level of Cr on Fe (100) [Jungblut 91] it was possible to deduce an antiparallel average spin orientation of Cr relative to Fe up to about 2 atomic layers. The authors find a decreasing polarization with increasing Cr coverage up to 2 Cr layers, presumably due to antiferromagnetic coupling of the second Cr layer to the first one.

A magnetic circular dichroism experiment for Cr overlayer coverages down to 0.25 atomic layers [Idzerda 93] directly shows the initial antiferromagnetic coupling of Cr to Fe. The authors find decreasing Cr moments with increasing layer thickness and the

magnetic structure of Cr is found to be consistent with antiferromagnetic coupling between adjacent Cr layers. The magnetic moments of one Cr monolayer on top of Fe is estimated by Jungbluth et al. [Jungbluth 91] and Idzerda et al. [Idzerda 93] to be in the range of 0.6 - 1 μ_B/atom. In a recent publication by Turtur and Bayreuther [Turtur 94], the magnetic moment of a monolayer Cr on Fe (100) is found to be 3 μ_B, by in situ magnetometer measurements. The coupling of Cr to Fe *within* a multilayer system has first been investigated recently by Böske et al. [Böske 94b,c]. Since mostly Cr overlayers (with one interface to vacuum) have been investigates so far, and keeping in mind, that the magnetic coupling takes place in buried magnetic structures, the examination of the coupling of Cr to Fe in an actual multilayer is of reasonable interest. Böske et al. have used the fluorescence yield mode to detect the Cr absorption, because this is the most suitable method for buried systems in the soft X-ray regime. They studied systems of 1, 2 and 3 atomic layers of Cr in a (Fe/Cr/Ag/Cr/Fe) structure with a buffer layer of 30Å Ag between the adjacent Fe/Cr structures to avoid magnetic frustration between the adjacent Cr layers. They showed, that also inside a multilayer, the first Cr layer couples antiparallel to Fe and that their results are consistent with layerwise antiferromagnetism of Cr. But the magnitude of the spin moments could not be obtained experimentally, because the Cr $L_{2,3}$ FY spectra show strong contributions of scattered intensity in their case, which makes an accurate determination of the moments with the help of the sum rules impossible. They also performed first principle calculations of the system and found a magnetic spin moment of -0.398 μ_B for the Cr layer at the Fe/Cr interface.

Here we also want to study the magnetic coupling of Cr to Fe within a Fe/Cr multilayer system. We have chosen samples of $(Fe_{20Å}\ Cr_x)_4Fe_{20Å}$ with x = 1 and 2 monolayers ML (1 ML Cr = 1.45 Å) epitaxially grown on a GaAs (100) substrate. In a first step, 10Å Fe and 1500Å Ag were grown at an elevated temperature of 100°C on clean GaAs. This ensures layer-by-layer growth and minimizes interdiffusion [Etienne 90]. The further step consisted of growing the desired layers on this substrate. Cr layers of 1 and 2 ML thickness were grown on 20Å Fe. This structure is repeated four times, then covered again with 20Å Fe and finally with about 50Å Cu, to avoid oxidation. A schematic setup for the samples is shown in Fig.5.9

Structural properties and quality of the samples have been checked with reflection high energy electron diffraction (RHEED). From conversion electron Mößbauer spectroscopy (CEMS) the Cr interface roughness is determined to be in the range of 1 - 2 atomic layers for similar samples [Landes 90]. Both samples investigated here are made simultaneously on the same substrate, to achieve exactly the same conditions. After the preparation process, the sample has been cut into two pieces. The easy magnetization axes are in-plane.

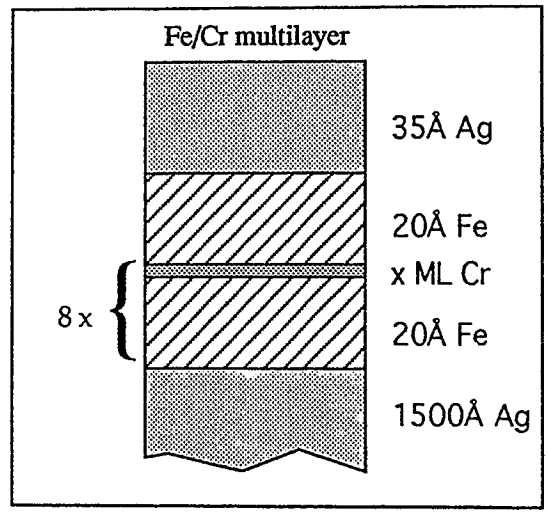

Fig. 5.9. Structure of the Fe/Cr samples used (substrate: GaAs(100))

For the detection of the Cr absorption edges we have chosen again the fluorescence yield, in order to achieve information from inside the sample. The geometry was as shown in geometry II from chapter IV. In this geometry the detector is in the scattering plane, so that scattered light contributes to the spectrum, but because the total thickness of the Cr films is very small (4 ML), this geometry gives more intensity than geometry I, which has the advantage that the detector is out of the scattering plane. The $L_{2,3}$ absorption spectra of Cr for the 1 and 2 ML sample are shown in Fig. 5.10. The Fe layers are aligned ferromagnetically in both cases. In the top row of Fig. 5.10 the isotropic spectra of Cr of 1 and 2 ML Cr in the Fe/Cr multilayer are shown, respectively. The energy is set to the first inflection point of the L_3 edge. The bottom of the figure shows the corresponding MCD spectra. The MCD spectrum of 1ML Cr clearly exhibits a positive peak at the L_3 edge; this proves unambiguously, that this layer couples antiparallel to Fe. But there is hardly any structure in the MCD spectrum at the L_2 edge. Compared to this spectrum, the MCD spectrum of the 2ML sample (Fig.5.10b) shows nearly no intensity. This can be caused either by antiferromagnetic coupling of the adjacent Cr layers, but it can also be caused by magnetic frustration of the Cr layers, which is more likely in this case. If there is an even number of Cr layers in-between ferromagnetically coupled Fe layers, and the Cr layers want to couple antiparallel to Fe at the interface and also antiparallel to each other, the magnetic Cr moments frustrate, i. e., they vanish, because this kind of coupling is not possible in such a geometry (see also refs. [Hasegawa 91] and [Xu 93] and references therein).

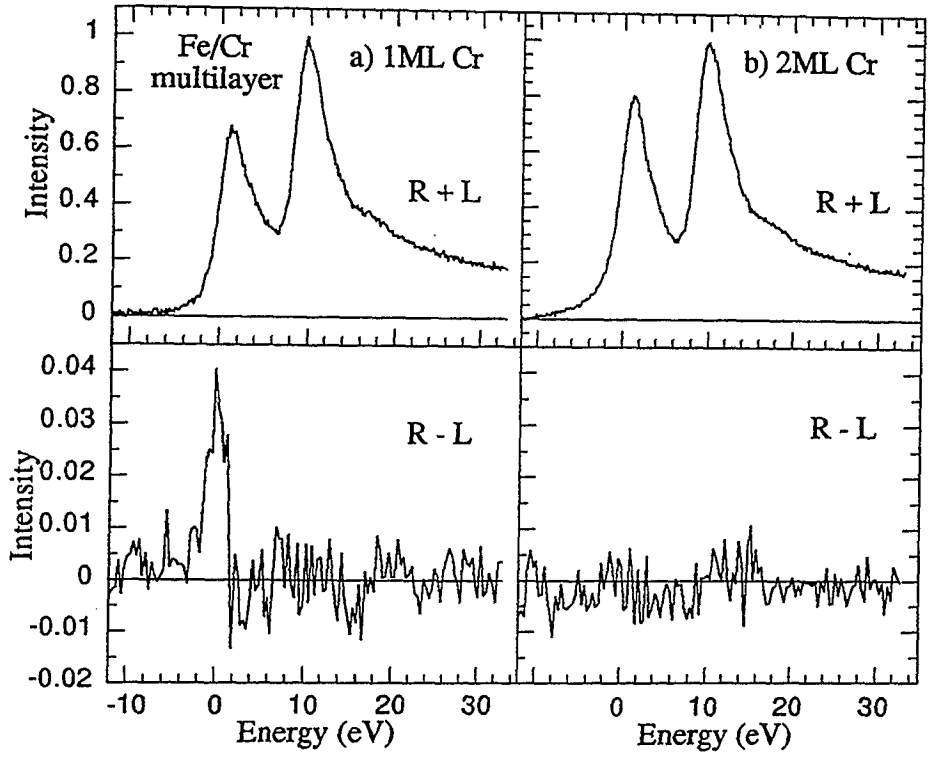

Fig. 5.10. Cr $L_{2,3}$ absorption spectra, a) 1ML and b) 2ML Cr in a Fe/Cr multilayer system. Top: Isotropic spectra, bottom: MCD spectra (R-L)

The isotropic spectra for the 1 and 2 ML Cr samples are also slightly different. The L_3 peak intensity in the 2ML spectrum is higher than the one of the 1 ML spectrum. The comparison of the averaged spectra taken with circularly polarized light compared to spectra taken with linearly (p-polarized) light (not shown) gives the same spectrum in the 1ML case, but is different in the case of the 2 ML spectrum (it is similar to the 1ML spectrum). This is a sign of appearance of resonant scattering in the 2 ML spectrum, as will be discussed in the following chapters.

Our aim is a quantitative determination of the magnetic moment of Cr in the 1 ML sample. This can be done with the help of the sum rule of Eq. (3.7). For using this sum rule it is important to have a spectrum without scattering effects, like the 1 ML spectrum is. In Fig. 5.11 we show this MCD spectrum again, compared to a first principles calculation of Cr in the same geometry.

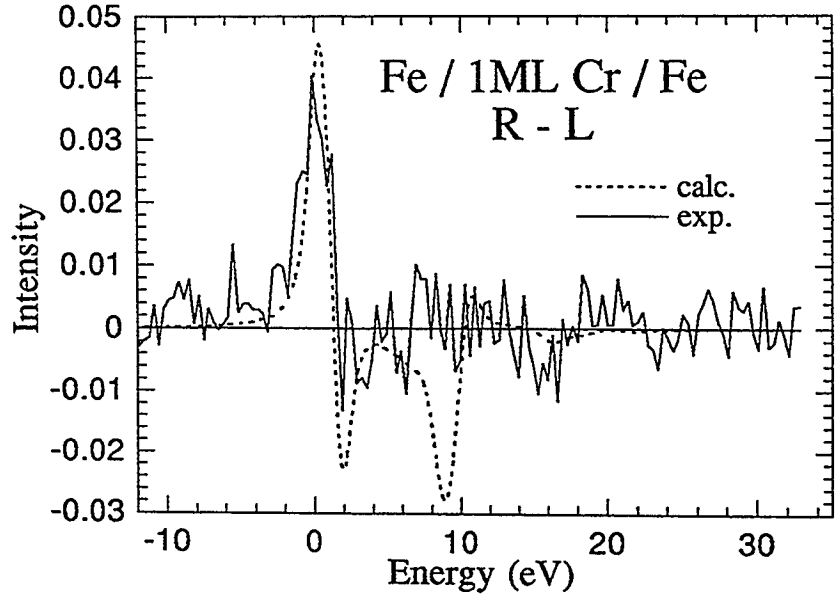

Fig.5.11. Cr $L_{2,3}$ MCD spectrum of 1ML Cr in a Fe/Cr multilayer. solid line: experimental spectrum, dashed line: first principle calculation

Fig.5.11 shows the comparison of the experimentally determined Cr spectrum compared to a first principle calculation. In both cases, the isotropic spectrum (R+L) is normalized to 1 at peak maximum. The positive intensity at the L_3 edge is clearly seen in both spectra, but the calculated spectrum shows much more structure than the experimental one. One reason might be due to the statistical noise in the experimental spectrum. The Cr spectrum of Böske et al [Böske 94b] has a comparable noise in the spectrum, but there is also seen more structure, like in the calculation. Another reason for the big L_3/L_2 ratio in the experimental MCD spectrum can be a large orbital moment. For a quantitative determination we use the sum rules (3.6) and (3.7). For this, the steplike background has to be subtracted from the isotropic spectrum. Because we have no reference sample, we have to estimate the factors needed for the sum rules: The number of d-holes is calculated to be $n_h = 6.74$, the angle between magnetization and light helicity is 23°, and the degree of polarization is estimated to be 70%. Then we obtain with the help of the sum rules a magnetic spin moment of $\mu_s = -0.3\ \mu_B$ for 1 ML Cr in Fe/Cr. This is a reasonable value; the first principles calculation gives a spin moment of $-0.652\ \mu_B$ at the interface. Due to interface roughness, interdiffusion and not ideal epitaxial growth the

Cr moment decreases (see e.g. ref. [Stoeffler 91]), which is, of course, true in the real sample.

To summarize, we have found that 1 ML Cr between two adjacent Fe layers inside a Fe/Cr multilayer couples antiferromagnetically to Fe, with a magnetic spin moment of about -0.3 μ_B. Calculation of the same system leads to qualitatively the same results but larger moments are predicted because of the ideal system in the calculation. The moments of 2 ML Cr in the same system vanish because of magnetic frustration. The isotropic spectrum for the 2 ML sample shows contributions to resonant scattering at the L_3 edge.

VI. Resonant X-Ray Scattering and X-Ray Reflection in Magnetic Layer-Systems

In this chapter we will show, how resonant X-ray scattering and X-ray reflection at single films and multilayers, detected with the fluorescence yield (FY) detection mode, can influence the shape of the spectra, especially at the L_3 edges. The magnitude of the scattering depends on the kind of the samples, on the experimental geometry and on the polarization of the light. Due to scattering not only the shape of the isotropic spectrum changes, but also the dichroism (MCD) signal. For example, the dichroism effect at the Fe L_3 edge is enhanced, under certain conditions, very drastically.

In the last several years magnetic X-ray scattering experiments using synchrotron radiation have been performed on a steadily growing number of magnetic systems. (see ref. [Blume 88], [Vettier 94] and the references therein) These experiments have included high-resolution studies of the pure magnetic scattering in antiferromagnets as well as of the interference between charge and magnetic scattering in ferromagnets. For example, using the high degree of linear polarization of the incident beam, it has been possible in synchrotron experiments to distinguish between charge scattering peaks, arising from lattice modulations, and magnetic peaks, in a spiral magnetic structure. Magnetic-resonance exchange scattering at the iron L_2 and L_3 edges has been reported by Kao et al. [Kao 90]. They find large changes in the specular reflectivity of p-polarized light near the Fe $L_{2,3}$ absorption edges from a single-crystal iron film with an external magnetic field perpendicular to the scattering plane. A theoretical analysis of magnetic dichroism in the X-ray-resonance scattering of cubic systems at the K and L edges is given recently by Rennert [Rennert 93]. He has analyzed how to measure different contributions independently by observing Bragg peaks in and outside the scattering plane and by changing the polarization of the incoming and of the scattered photon.

All these investigations deal with the scattering within the lattice structure. But in the soft-X-ray regime, one also has to take into account scattering caused by the interfaces in thin films and multilayers. As mentioned already in chapter II, the wavelength in the range of the $L_{2,3}$ absorption edges of the 3d elements (about 500 - 800 eV) is in the thickness range of typical thin film and multilayer structures (around 20Å). Thus, for example standing waves can form themselves within the layers, especially near the absorption edges, where the optical constants are drastically changed. This might cause additional scattering effects, which can influence the absorption spectra. All the spectra shown in this chapter are taken in the fluorescence yield (FY) mode, if not mentioned else, because the scattered light intensity can only be measured in this mode.

6.1 Fe/Cr Multilayers and Single Fe-Films

In chapter V the magnetic structure inside Fe/Cr multilayers was discussed. Here we want to study resonant X-ray scattering effects on this system. We have investigated a number of different samples, which are all grown on a GaAs (100) substrate with a silver buffer layer. They are all prepared in the same way as the Fe/Cr system described in chapter V. Thus the samples consist of epitaxial layers grown in the bcc (001) direction with the easy magnetization direction in the plane. The roughness of the interfaces is in the order of 1-2 atomic layers, which means that they are very sharp interfaces. In Fig. 6.1 the samples discussed in this chapter are shown schematically.

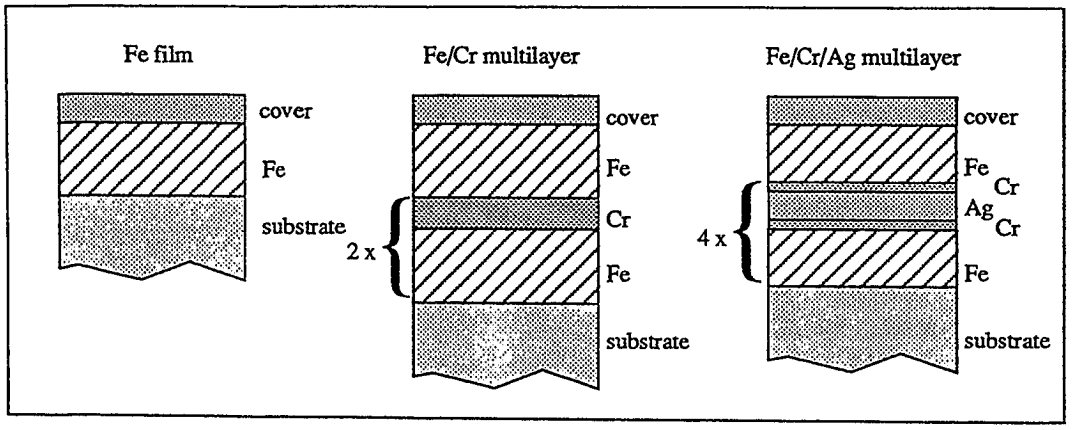

Fig. 6.1. Schematic setup of the Fe-films and Fe/Cr multilayers discussed in this chapter. All samples are grown on a GaAs (001) substrate with a 1500Å Ag (001) buffer layer. the cover layers are either 500Å ZnS or Ag or Cu films with a thickness of about 30Å.

Fig. 6.2 shows the Fe $L_{2,3}$ absorption spectrum taken with circularly polarized light of a Fe/Cr multilayer compared to the spectrum of a single Fe film. The structure of the Fe/Cr multilayer is $[Fe_{20Å}\ Cr_{18Å}]_2Fe_{20Å}$. The Fe films in this multilayer are ferromagnetically coupled, this has been seen from magnetic hysteresis curves taken with MOKE measurements (not shown). The single Fe film has an Fe thickness of 50Å. Both samples are covered with 500Å ZnS to avoid oxidation. The spectra are taken in geometry II, mentioned in chapter IV. In this geometry the detector is in the plane of the scattered light. The angle of incidence α is 22±1° and the detector is positioned at 90 degrees relative to the incidence light. The bottom of the figure shows the absorption spectra averaged over the different magnetization directions taken with linearly and circularly polarized light, normalized to the same background far above the edges. The spectra of the single film are nearly identical, as it is expected from the selection rules ($\Delta m = \pm 1$ in both cases). But the spectra of the multilayer are quite different. Especially

the intensity at the L_3 edge is much higher in circularly polarized light than the one in linearly polarized light.

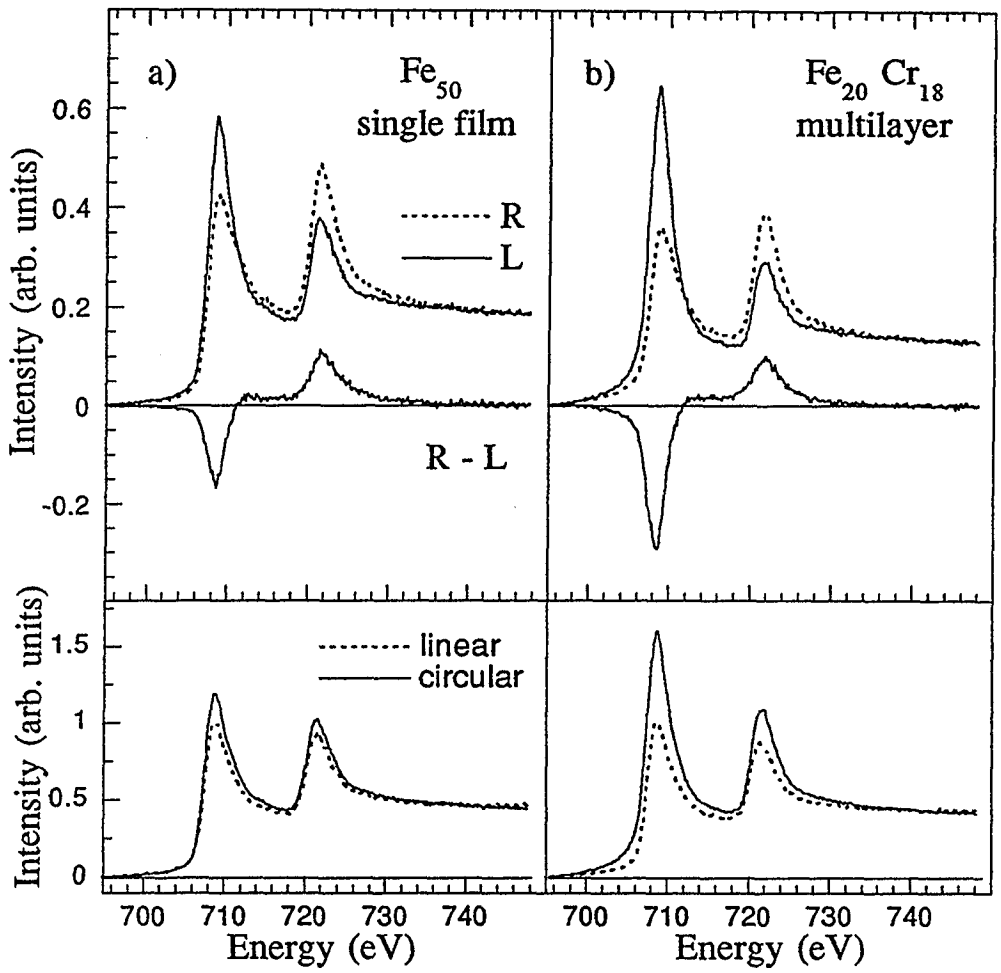

Fig. 6.2. Fe $L_{2,3}$ absorption spectra taken from a 50Å Fe film (left) and an Fe/Cr multilayer (right) (in geometry II). Top: Fundamental spectra R and L and MCD spectra (R-L). Bottom: comparison of spectra taken with linearly and circularly polarized light.

The top of fig 6.2 shows the spectra taken with circularly polarized light (σ^-, -0.6mrad off plane) and the MCD spectrum (difference between spectrum of parallel and antiparallel coupling of sample magnetization to light helicity). The spectrum of the single film shows the normal MCD spectrum, as already discussed in chapter V. The MCD asymmetry ((R-L)/(R+L)) at the L_3 edge is about -17% and about +11% at the L_2 edge. Compared to this, the MCD asymmetry for the multilayer is much higher, namely -30% at the L_3 edge and about +14% at the L_2 edge. Thus, the dichroism signal is strongly influenced by the increased intensity at the absorption edge in the multilayer spectrum. The enhanced MCD signal could be caused by an increased magnetic moment in the multilayer sample. But such a strong enhancement would be surprising in this kind of multilayer. In Co/Pd multilayers such an enhancement was observed by Wu et al. [Wu 92]; but in the case of Fe/Cr, one would not expect this, because Cr tends

to decrease the magnetic moments of Fe at the Fe/Cr interface [Hasegawa 91]. Therefore we have determined the total magnetic moment (sum of spin and orbital moment) of both samples separately with SQUID (Superconducting Quantum Interferometer Device) measurements. The magnetic moment is 2.31±0.1 $\mu_{B/atom}$ for the single film and 2.16±0.1 $\mu_{B/atom}$ for the multilayer. The error in the data is mainly caused by the uncertainties in the thickness of the films. So we could not find an enhancement of the magnetic moment in the multilayer, it is even a little smaller than in the single film. Therefore the enhancement of the dichroism asymmetry cannot be caused by magnetic circular dichroism in the absorption. Already from the comparison between circularly and linearly polarized light (bottom of Fig. 6.2), it is clear, that the enhanced intensity in the multilayer spectrum is caused by something else than the absorption signal. In order to understand, whether the enhanced intensity is caused by X-ray scattering, we have taken spectra under different geometrical conditions, as shown in Fig.6.3.

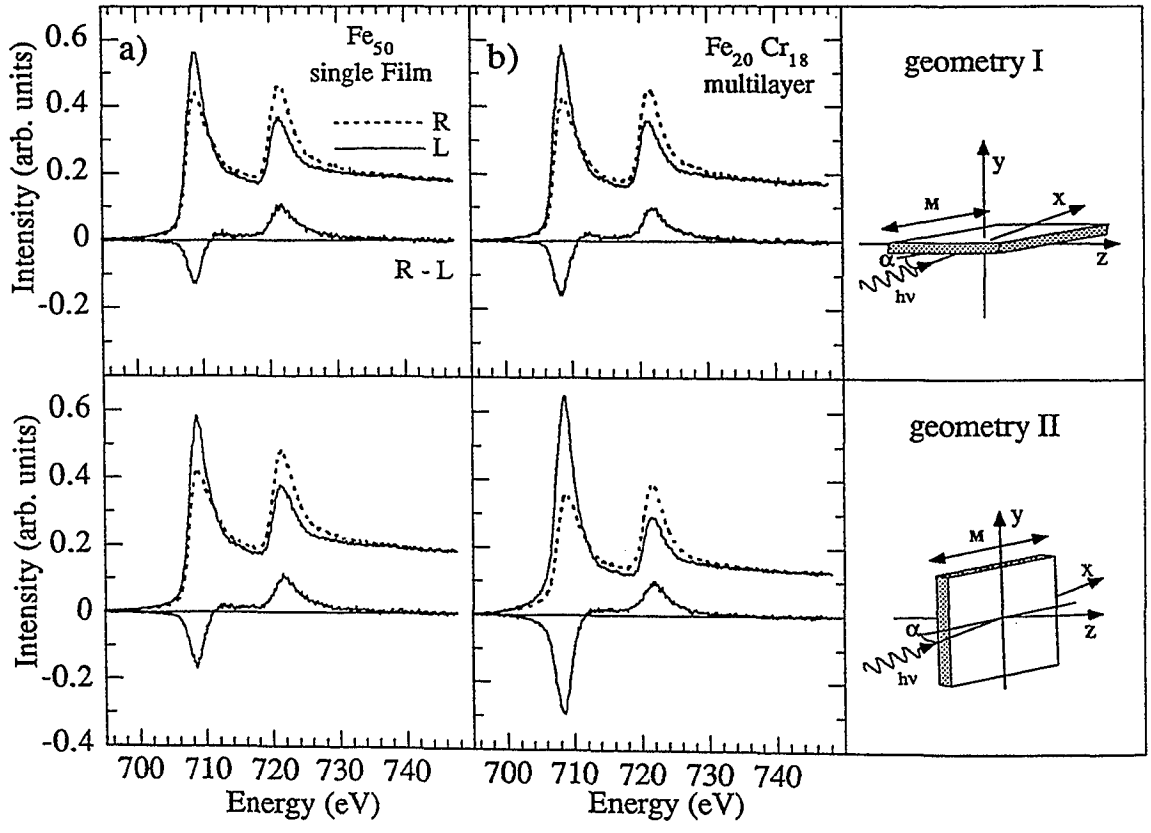

Fig. 6.3. Fe $L_{2,3}$ absorption spectra of a) a 50Å Fe film and b) an Fe/Cr multilayer measured in different geometries (I and II).

The intensity of scattered light from a sample is mainly observed in the scattering plane, which is defined by the direction of the incident light and the surface normal. This has been discussed already in chapter II. The spectra of Fig. 6.2 have been taken in geometry II, which means, that the detector is in the scattering plane. If the enhanced intensity in the multilayer spectrum is caused by scattering effects, the enhancement should strongly depend on the measurement geometry. This geometry dependence is shown in Fig. 6.3. On the left side of the figure the spectra of the 50Å Fe film are shown, while the ones from the multilayer are on the right side. On the bottom of the figure the spectra taken in geometry II are shown, with the detector in the scattering plane; these are the same spectra as shown in Fig.6.2. One can clearly see the differences in the multilayer spectrum, as discussed above. But if one detects the same spectra in geometry I, where the detector is out of the scattering plane (top of fig.6.3), the spectra of the single film and the multilayer are nearly identical; there is no more additional intensity in the multilayer spectra and also not in the MCD spectrum. The spectra of the single film are identical in both geometries (this also shows, that self absorption in the fluorescence can be neglected completely in this sample). Thus, the enhanced intensity in the multilayer spectrum is probably due to light scattering. This is a resonant process, because the intensity is mainly enhanced at the absorption edge, but it cannot be caused by the atomic structure of the samples, because this is identical in the single film as well as in the multilayer. It is obvious that the scattering depends on the layer thickness. Therefore the dependence of the resonant X-ray scattering is studied on the film thicknesses in the multilayer. This is shown in Fig. 6.4.

In Fig. 6.4 the Fe $L_{2,3}$ absorption spectra of Fe/Cr multilayers with different Fe and Cr thicknesses are presented. The multilayers have the structure $Cr_n[Fe_m\ Cr_n]_2Fe_m$, with a) n=18Å, m=30Å, b) n=18Å, m=20Å and c) n=10Å, m=20Å. The samples are covered with 35Å Ag to avoid oxidation, they are made on the same substrate at the same time to be sure to have identical growth conditions. After the preparation, the samples have been cut. The figure shows the spectra taken in geometry II with circularly polarized light, averaged over the magnetization directions (R+L) (-> circular, dashed line) and with linearly polarized light (-> linear, solid line). The uppermost spectra of the $Fe_{30}Cr_{18}$ sample are quite similar for linear and circular light excitation, which indicates hardly scattering intensity like in the case of the 50Å Fe film. But in the case of the $Fe_{20}Cr_{18}$ sample both spectra are quite different, just like in Fig. 6.2. This can be understood, because this sample has nearly the same structure as the one shown before. And for the $Fe_{20}Cr_{10}$ film, the scattered intensity is nearly the same. The spectra are normalized to a similar background far above the edges. This is not unambiguous, because the derivative of the background of the two spectra (with circular and linear light) are a little different. The scattering effect exhibits itself by enhanced intensity at the L_2 and L_3 white lines, but more at the L_3 edge. The magnitude of the scattering intensity depends on the Fe thickness but not on the Cr thickness. This shows that the scattering must take place within the Fe layers. The dichroism of these samples (not shown) is similar to that of the 50Å Film for the $Fe_{30}Cr_{18}$ system and to that of the Fe/Cr multilayer (Fig. 6.2-3) for the $Fe_{20}Cr_{18}$ systems. The $Fe_{20}Cr_{10}$ system

did not show dichroism effects at all. This is probably caused by antiferromagnetic coupling of the adjacent Fe layers. In multilayers like this, with relatively thin layers, the magnetic fields for aligning the layers ferromagnetically, can be in the range of 1 Tesla and more. The magnetic field induced by the permanent magnets in our case is only in the range of 0.1 T.

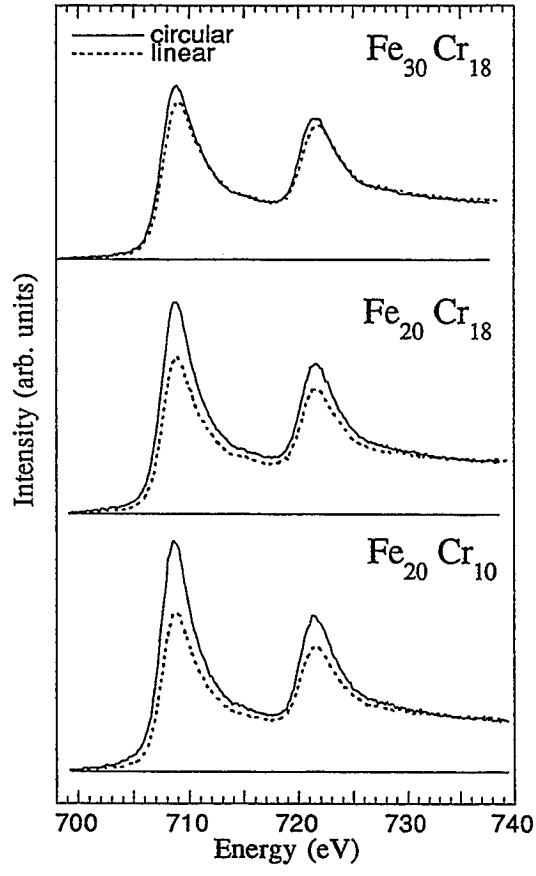

Fig. 6.4. Fe $L_{2,3}$ absorption spectra of Fe/Cr multilayers with different Fe and Cr thicknesses (numbers in Å).

It is not clear yet, whether the light scattering is a pure multilayer effect, which needs several periods of alternating layers, or whether it is already seen in a single film. As a test of this, we have compared the spectra of single Fe films with different film thicknesses, namely with 50Å and with 20Å. We have compared these two thicknesses, because in one of them there is no scattered intensity (50Å), which has been seen already and the thickness of the other film is the same as the one in the presented Fe/Cr multilayer systems, where strong scattering effects are visible. The spectra of both samples, taken again in geometry II, are presented in Fig. 6.5. The spectrum of the 50Å film is shown on the left side. As already discussed, this spectrum does hardly have additional scattering intensity, and the spectra taken in both geometries are nearly identical. Compared to this, on the right side the spectrum of the 20Å film is shown. One can clearly see that there is an enhanced intensity in the fundamental spectra R and L, in the dichroism spectrum, as well as in the comparison of the spectra taken with

circularly and linearly polarized light, just like for the Fe_{20} Cr_{18} multilayer (Fig. 6.2). So, it is demonstrated, that the resonant X-ray scattering depends mainly on the single film thickness.

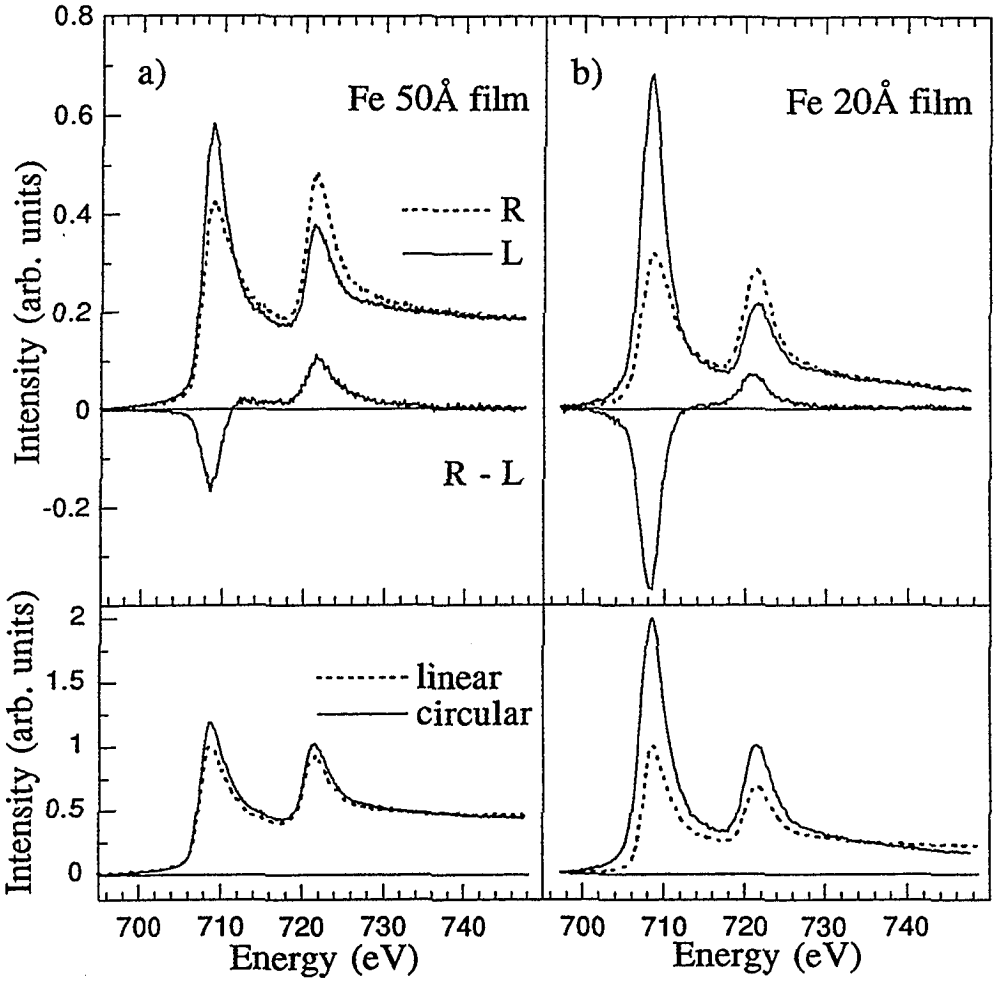

Fig. 6.5 Fe $L_{2,3}$ absorption spectra of Fe films with 50Å (left) and 20Å (right) film thickness, taken in geometry II. Top: fundamental spectra R, L, and the corresponding MCD spectra (R-L); Bottom: comparison of spectra taken with linearly and circularly polarized light

Now it is interesting to see, how the scattering depends on the polarization of the incident light. Already in Fig. 6.2 it could be seen, that the scattering with linearly polarized light under the measuring conditions does not occur. This can be understood as following: synchrotron radiation is linearly polarized in the plane of the storage ring with the electrical field vector (**E**) lying in this plane. This is the x,z plane according to Fig.4.3. Therefore, the linearly polarized light is p-polarized in the case of geometry II (**E** is in the scattering plane) and s-polarized in the case of geometry I (**E** is perpendicular to the scattering plane). From Fig. 2.6 we know, that the reflectivity of p-polarized light is always smaller than the reflectivity of s-polarized light, especially at an reflection angle of 45°, where the reflection intensity of the p-polarized light nearly vanishes. So it can be understood, that even scattered p-polarized light should have

much lower intensity than scattered s-polarized light, and thus it can be understood that there is no scattering intensity in the spectrum for linearly polarized light (degree of circularly polarization P = 0) in geometry II. But with increasing circularly polarization ($|P| > 0$) the light intensity with the electrical field vector perpendicular to the storage ring increases (see chapter IV), this means, there is also s-polarized light intensity in geometry II, which has a higher reflection (and thus scattering) coefficient than the p-polarized light. Therefore the scattered intensity is visible with circularly polarized light in our case, but not with linearly polarized light. But this assumption needs to be verified. We do this by comparing spectra taken with linearly polarized light in p-polarization (as it was shown until now) and in s-polarization. If the explanation is correct, the spectrum taken with p-polarized light should represent the absorption spectrum, while the one taken with s-polarized light should show additional scattered intensity. This comparison is not very simple in our case. We cannot rotate the electrical field vector by 90° (from the x,z plane to the x,y plane), because its direction is strictly defined by the storage ring (in the case of a crossed undulator, E can be rotated, see for example ref. [Roth 93]); and we also cannot simply rotate the fluorescence detector by 90°, because it has a fixed position in the chamber. Therefore, we have taken the p-polarized spectra as usual in geometry II with the Si(Li) detector. For taking the s-polarized spectrum, we have changed the sample into geometry I and put a channeltron underneath the sample (like shown in Fig. 4.3). The channeltron was prepared in a way to detect only photons but not electrons or positive ions. It is shown schematically in Fig. 6.6:

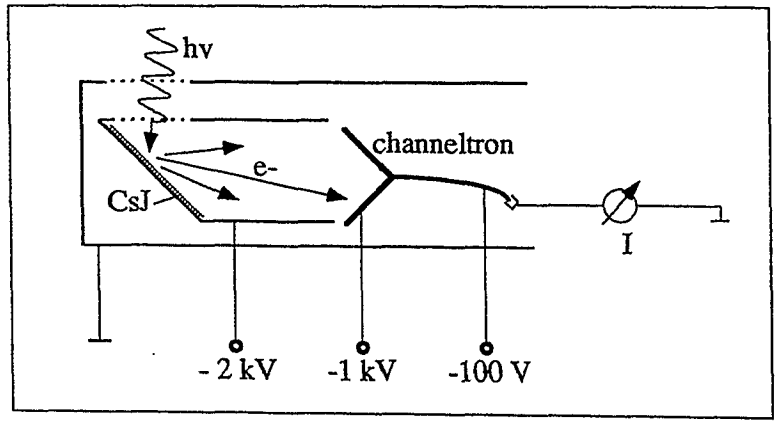

Fig. 6.6: Schematic setup of the channeltron used for Fluorescence Yield detection. The stainless steal plate in front of the channeltron is covered with approx. 3000 Å CsJ. Photons reaching this film, excite electrons, which are detected by the channeltron. The channeltron current is measured with a picoamperemeter.

The whole channeltron is covered by a grounded stainless steal tube, with a mesh in the upper part. Photons passing this mesh, have to pass another mesh which is on -2 kV

potential to keep electrons off. Then the photons reach a stainless steal plate which is covered with approx. 3000Å CsJ. Here, secondary electrons are excited, which are collected by the channeltron. The amplified channeltron current is then measured by a Keithley picoamperemeter, which is grounded on one end. With the help of this channeltron we are able to detect the fluorescence yield emission in the total fluorescence yield mode.

In Fig. 6.7 the comparison between resonant scattering of s- and p-polarized light (both times linearly polarized light!) with detection in and out of the scattering plane is shown. The spectra with s-polarized incidence light are taken in geometry I (left side of the figure). In this geometry, the Si(Li) detector is out of the scattering plane (z-direction) and the channeltron in in the scattering plane (-y-direction). To achieve p-polarized light, geometry II was chosen (right side of the figure). Here, the Si(Li) detector is in the scattering plane and the channeltron is out of this plane. For an overview of the setup see also Fig.4.3.

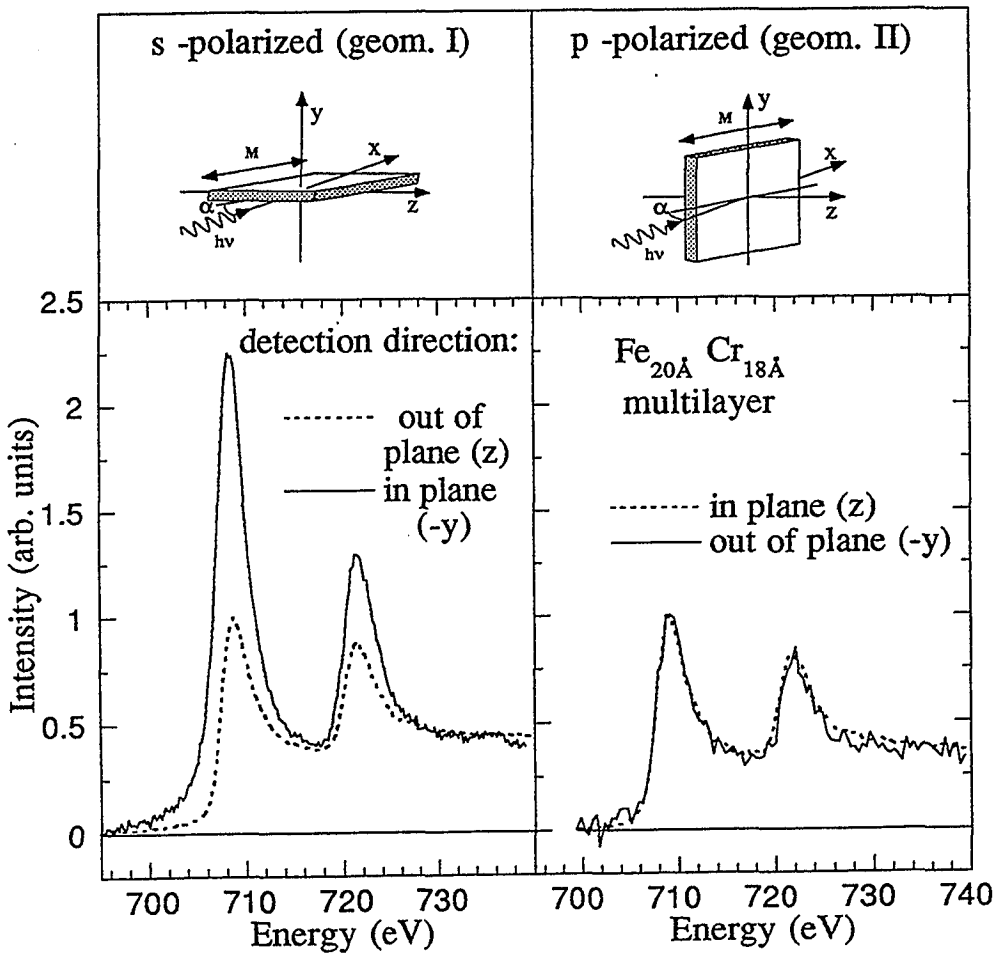

Fig. 6.7. Fe $L_{2,3}$ absorption spectra from a $Fe_{20}Cr_{18}$ multilayer taken with linearly polarized light of s- and p-polarization, respectively.

On top of Fig.6.7 the corresponding sample geometries are shown. On the bottom the spectra of a $Fe_{20Å}Cr_{18Å}$ multilayer are shown (like in Fig. 6.2) taken with the Si(Li) detector (z) and with the channeltron (y). For p-polarized light, both spectra are quite identical and represent the normal absorption shape. But for s-polarized light the spectra are completely different. The out of plane (z) spectrum again represents the absorption curve, while the in plane spectrum (y) shows a very strongly enhanced intensity at the edges, especially at the L_3 edge. The scattered intensity is even stronger than the one with circularly polarized light, see Fig.6.2. This can be understood, because in the case of circularly polarized light, the s-polarized part can be at most 50% of the light (and for a circular polarization of P = 70%, the s-polarized part is only about 1/6 = 16%, see chapter IV), while here we are working with completely s-polarized light.

Therefore it is obvious, that the scattering strongly depends on the polarization of the incidence light and that it is caused by the s-polarized part of the light. One question remains, how the angular dependence of the scattering looks like. Until now we have compared only two distinct geometries. But how is scattering influenced by different angles of incidence? To test this, we have measured a sample which shows scattering in geometry II with the Si(Li) detector. But now we have varied the incidence angle α. Because the detector is always at 90° relative to the incidence light, the emission angle is also changed in this investigation. We have done this at the Cr $L_{2,3}$ absorption edge of a Fe/Cr/Ag multilayer. The structure of this multilayer is (see Fig.6.1) [$Fe_{50Å}$ Cr_{3ML} $Ag_{30Å}$ Cr_{3ML}]4 $Fe_{50Å}$, and it is covered with 500 Å ZnS to avoid oxidation. On this sample, the scattering at the Cr absorption edge has already been observed by Böske et al. [Böske 94b,c]. Fig 6.8 shows the angular dependence of the Cr $L_{2,3}$ absorption spectra taken with circularly and linearly polarized light.

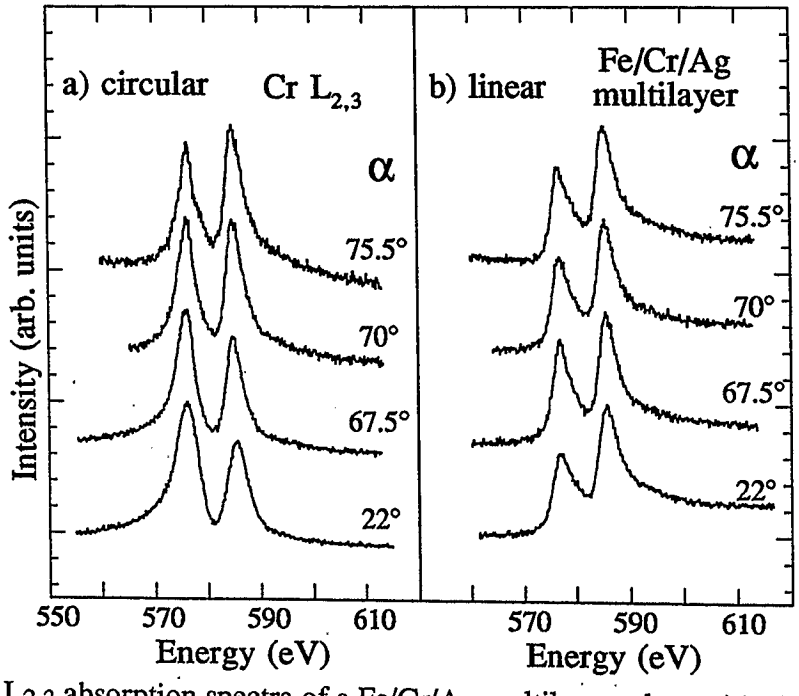

Fig. 6.8. Cr $L_{2,3}$ absorption spectra of a Fe/Cr/Ag multilayer taken with circularly (left) and linearly (right) polarized light at different incidence angles α in geometry II.

On the left side of the figure the spectra taken with circularly polarized light are shown and on the right side the ones taken with linearly polarized light. The spectra are taken in geometry II at different incidence angles α. The spectra on the bottom are taken at $\alpha = 22°$, which is the incidence angle of the spectra discussed above taken in geometry II. Here one can see very clearly the influence of the scattered intensity. The spectrum taken with linearly polarized light represents the conventional absorption spectrum, see for comparison Fig.5.1. Varying the incidence angle with circularly polarized light hardly changes the shape of the spectrum. The L_3/L_2 intensity ratio remains nearly constant, only the peak to background ratio changes a little. In this series we avoided the reflection measurement, which would be at $\alpha = 45°$; this will be discussed below. The incidence angle of $\alpha = 75.5°$ corresponds to nearly normal incidence and grazing emission. Compared to the spectra taken with linearly polarized light, the ones taken with circularly polarized light change their shape drastically. At $\alpha = 22°$ the L_3/L_2 intensity ratio is greater than one, and the intensity in the spectrum is increasing already long before the L_3 edge. There is also no edge-jump in the spectrum, the intensity above the L_2 edge is even lower than before the edges. But with increasing incidence angle, these effects change. The L_3/L_2 intensity ratio becomes smaller and for $\alpha > 70°$ the L_2 peak is even larger than the L_3 peak, like in the normal absorption spectrum. Also the intensity in front of the edges decreases, it is again more like an absorption "edge". Thus it has been shown, that the scattering intensity also depends on the incidence angle of the light and not only on the portion of s-polarized light. For normal in - grazing out geometry (α near 90°) the scattering intensity is small, but not as small as in geometry I.

Scattering and reflection are analogous effects. Therefore one can expect similar spectra in specular reflection to those we have seen until now for the cases where scattering contributes to the spectra. The reflection spectra from a 37Å Co film has been investigated recently by Kao et al. [Kao 94] for grazing incidence angles of 2° - 25°. They found strongly changing spectral shapes and increasing dicroism asymmetry at the edges. We have performed reflection measurements on Fe/Cr multilayers in geometry II with an incidence angle of 45°. For reflection of soft X-rays, this is quite a large angle, where the reflection intensity is quite small. Especially the intensity for p-polarized light nearly vanishes in this case, see Fig. 2.6. Therefore we can expect also in the reflection big changes in the shape of the spectra for linearly and circularly polarized light. Also dichroism effects at the absorption edges will be discussed.

Fig. 6.9 shows the reflection measurement for the $Fe_{20Å}Cr_{18Å}$ multilayer. On the right side the spectra are shown taken at an incidence angle of $\alpha = 42°$, which means 3° off the specular reflectivity; and on the right side there are shown the spectra for the specular reflection at $\alpha = 45°$. The spectra on top are averaged over the magnetization directions (R+L) for circularly (solid line) and linearly (dashed line) polarized light. There is no background subtracted in the spectra. The shape of the Cr edge for 42° is

the same as the one shown in Fig. 6.8 for linear polarized light. In specular reflection (α = 45°), its intensity is drastically enhanced for circular light compared to the iron signal. But now the overall shape remains the same even with linear light. The shape of the spectrum at the Cr edge is analogue to the one with scattered intensity (Fig. 6.8). The shape of the Fe edge represents the normal absorption spectrum if taken with linear polarized light. By excitation with circularly polarized light, it also has the same structure as the one with scattered intensity (see Fig. 6.2), especially an enhanced L_3/L_2 intensity ratio, and a smaller edge jump. But in contrast to the Cr edge, the overall intensity at the Fe edge is not changed.

The influence on the magnetic dichroism in reflection is shown on the bottom of the figure. There the dichroism asymmetry (R-L)/(R+L) is shown.

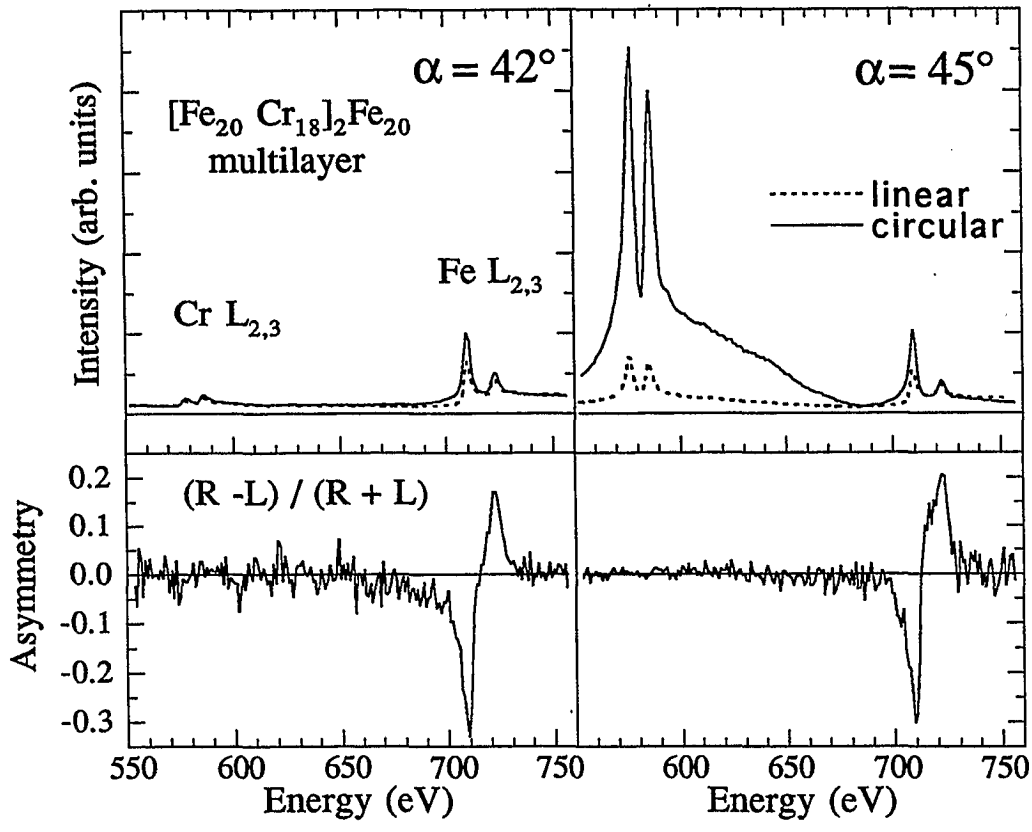

Fig. 6.9. 45° reflection spectrum at the Cr and Fe $L_{2,3}$ absorption edges of a [Fe20Å Cr18Å]2 Fe20Å multilayer. left. not complete reflection α = 42°. right: reflection at α = 45°. solid line: circularly polarized light; dashed line: linearly (p-) polarized light.

There is no asymmetry at the Cr edge, which can be understood, because the Cr is antiferromagnetic and the measurements average over approx. 12 layers of Cr. On the other hand, the asymmetry at the Fe edge is very strong, and it is approximately equal for both angles. It is about -40% at the Fe L_3 edge and +20% at the L_2 edge. So, also in the reflection intensity, the dichroism signal is enhanced, just as in the case of

scattering. This shows, that from the shape of the spectra, it cannot be distinguished between scattering effects and specular reflection (at least at 45° reflection). This is the case for the magnetization averaged as well as for the dichroism spectra. Therefore it is shown, as estimated before, that scattering and reflection are very similar in the corresponding films, and that scattering implies reflection not only for specular reflection but also over a broad variation of angles.

To show, how strong the dichroism effects can be enhanced in the reflection mode, in Fig.6.10 there are shown Fe $L_{2,3}$ spectra in 45° reflection for different degrees of circularly polarization of the incidence light. The spectra are taken from the same Fe/Cr multilayer as before.

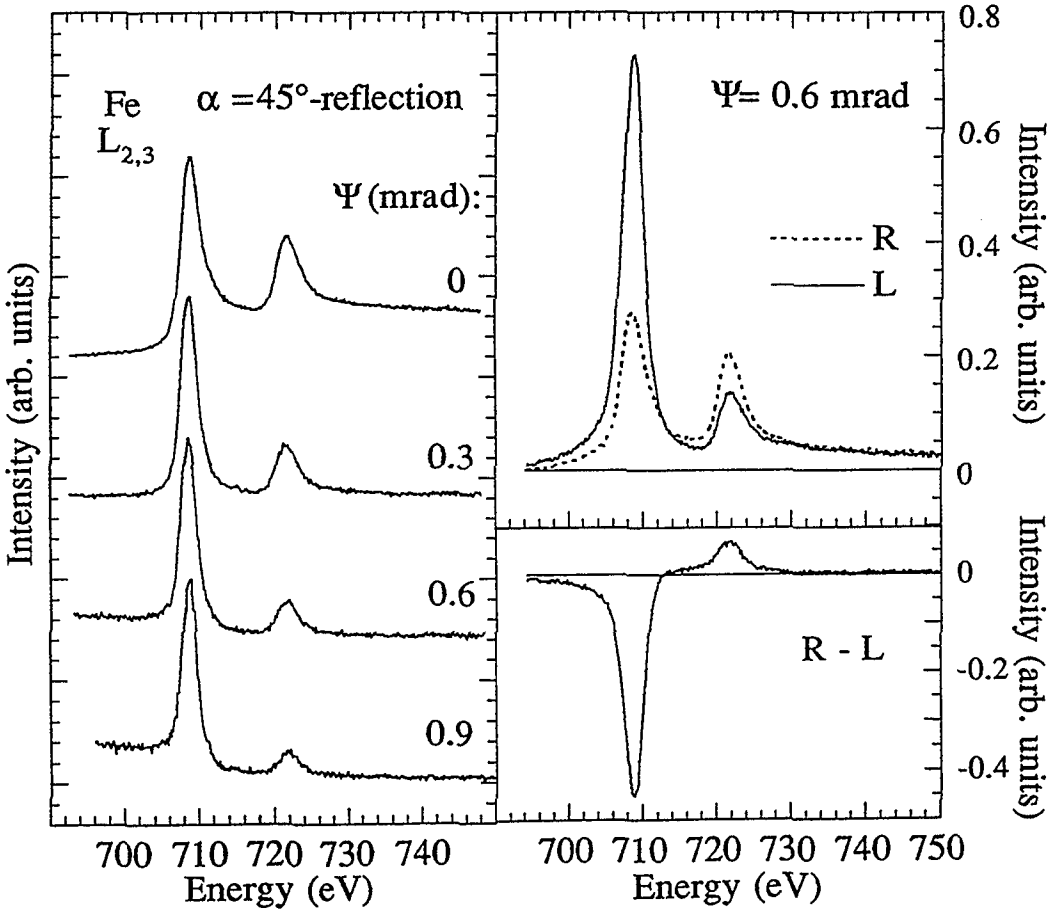

Fig. 6.10. *Fe $L_{2,3}$ absorption edges from a [Fe20Å Cr18Å]2 Fe20Å multilayer taken in specular reflection at 45° incidence angle. The spectra are taken at different off plane angles of the synchrotron light Ψ.*

The spectra on the left side of Fig. 6.10 show the Fe $L_{2,3}$ spectra summed over the two magnetization directions (R+L) for different off plane angles Ψ of the synchrotron light (and thus for different degrees of circular polarization of the light). On top of the left side there is the Fe $L_{2,3}$ absorption spectrum taken with linearly (p-) polarized light,

which corresponds to synchrotron radiation taken directly from the plane of the storage ring (off plane angle $\Psi = 0$). As discussed above, this spectrum represents the conventional absorption spectrum. The spectra below are taken at off plane angles Ψ of -0.3, -0.6 and -0.9 mrad, which means at increasing degree of circularly polarization P. At -0.6mrad P is approximately 70% as discussed above. . For the summed spectra one can see the development of the additional reflection (or scattering) intensity and change of the spectrum. On the right side the dichroism spectra R, L and the differrence R-L for $\Psi = 0.6$ mrad are shown. Because the summed spectra are normalized to 1 at the L_3 peak maximum, one can directly see the dichroism asymmetry in the difference spectrum. It is -45% at the L_3 edge and 18% at the L_2 edge.

The 45° reflection is furthermore studied on the Fe/Cr/Ag multilayer (structure see above). Fig. 6.11 shows the spectra at the Cr and Fe edges from this sample taken with circularly polarized light (now again at an off plane angle of -0.6mrad), and the corresponding MCD asymmetry.

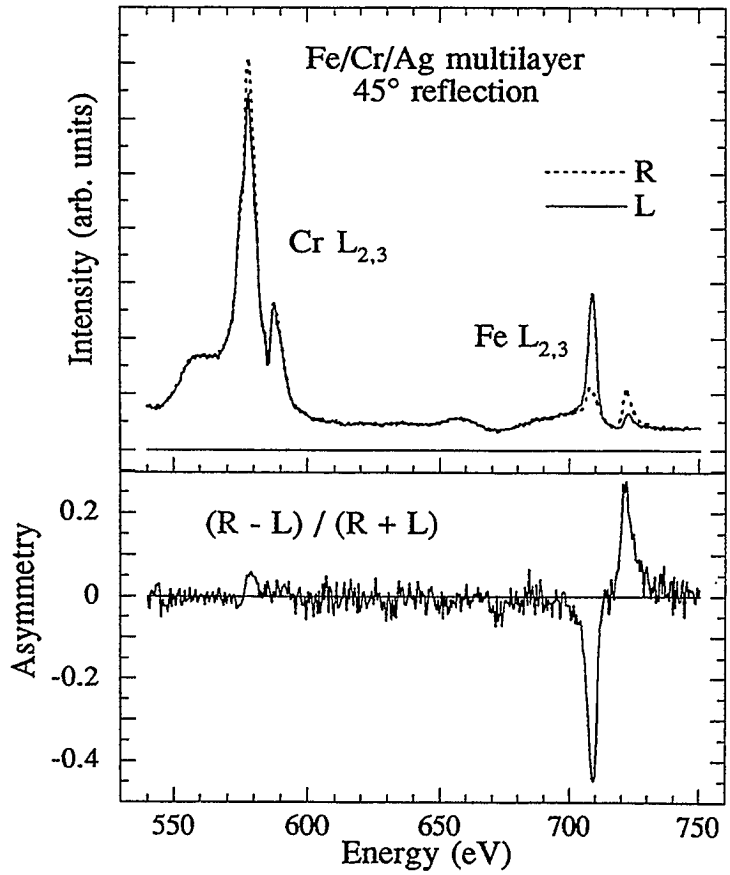

Fig. 6.11. Reflection intensity for 45° reflection of a Fe/Cr/Ag multilayer taken with circularly polarized light. Top: Spectra for parallel and antiparallel magnetization. Bottom: MCD asymmetry.

The Cr and Fe absorption spectra both show additional intensity due to reflection as already seen for the Fe/Cr multilayer above. But here the shape of the Cr spectrum is even more strongly enhanced. The dichroism asymmetry, shown on the bottom of the

figure, shows again a strongly enhanced effect at the Fe edge, -45% at the L_3 and +27% at the L_2 edge.

A longer energy scan of the same sample under the same conditions is shown in Fig.6.12. Here the scan is taken from 300 to 800 eV, for circularly (solid line) and linearly (dashed line) polarized light. Apart from the Cr and Fe absorption edges one can see very strong additional structures, especially around 400 and around 500 eV photon energy and also some smaller structures at different energies. These structures are clearly not due to absorption edges, because the absorption edges of the elements, which are in the sample, are not in this energy range. The small peak around 350 eV photon energy is the second order peak of the iron absorption. The intensity of the additional structures also depends strongly on the light polarization, but they do not show dichroism asymmetry. They are about 4 times larger in circularly polarized light than in linearly polarized light. These additional structures are due to conventional multilayer reflections. Because of interference in the films, the reflected light intensity has maxima or minima depending on the reflection angle or on the light energy (respectively the light wavelength)

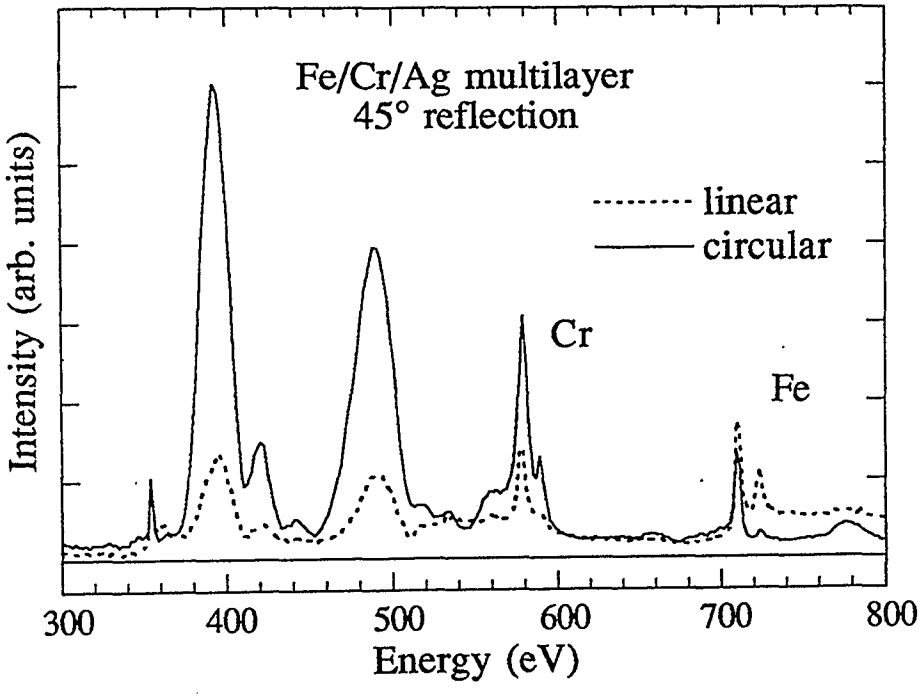

Fig. 6.12. 45° reflection from a Fe/Cr/Ag multilayer (structure see text). Solid line: linearly (p-) polarized light, dashed line: circularly polarized light.

For a better understanding of the multilayer reflection peaks, we have performed calculations of the reflection intensities of this multilayer [Friedrich 94]. The

calculations are done on the basis of the Fresnel formalism described in chapter 2. The corresponding optical parameters are taken from the tables of Henke et al. [Henke 82], and the interfaces have been taken as ideally flat (no roughness). The optical parameters vary with the photon energy, especially near the absorption edges there is a strong variation. The tabulated parameters are valid for energies quite away from the absorption edges, while they are very unprecise near the absorption edges. Therefore we have performed calculations not exactly for the same spectrum as the measured one, but at a fixed photon energy of 500 eV and varying the reflection angle. The energy is far enough away from the Cr and Fe absorption edges, so that the optical parameters can be taken from the table. If one varies the photon energy at a fixed incidence angle, the wavelength is automatically changed, too, and herewith the interference conditions in a film. This is similar to the case, where the photon energy is kept constant and the incidence angle is varied, because the optical thickness of the film changes with the incidence angle.

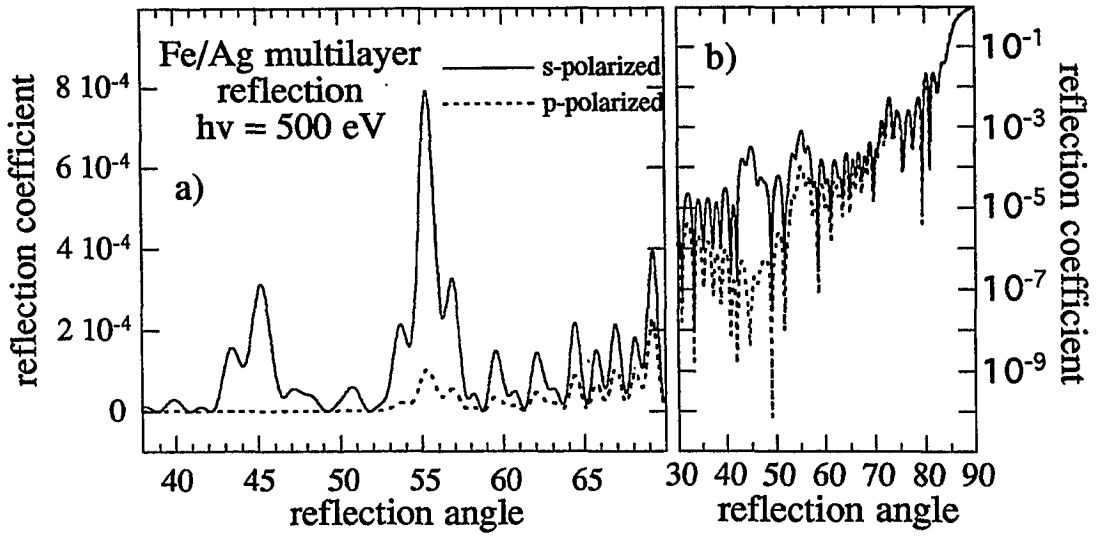

Fig. 6.13. Calculated reflection spectrum of the Fe/Cr/Ag multilayer at a photon energy of hv = 500 eV for s- and p-polarized light as a function of the incidence angle. a) linear scale ; b) logarithmic scale

Fig.6.13 shows the calculation of the reflection at a photon energy of 500eV as a function of the incidence angle. At this energy the optical constants of Fe and Cr are nearly the same, therefore we treated both elements as one in the calculations. So the structure of the multilayer in the calculation is [Fe/Cr$_{58Å}$ Ag$_{30Å}$]$_4$ on a Ag substrate, covered with 300Å ZnSe. The solid line is due to reflection of s-polarized light and the dashed one is due to p-polarized light. In part a) the reflection coefficient on a linear scale is shown in the angle range from 40 - 70° of the reflection angle. The large structures in the spectrum at about 45° and 55° are due to reflection from the Fe/Cr - Ag multilayer, while the small structures with a shorter periodicity of about 2° are due to

the cover layer. One can clearly see, that the reflection coefficient for p-polarized light is nearly vanished at 45°, as expected. In part b) of the figure there is shown the reflection coefficient on a logarithmic scale from 30° - 90°. Here one can see, that the structures in s- and p-polarization are quite the same in the whole spectrum, mainly the intensities are quite different (especially around 45°). For more normal (small angles) and more grazing incidence (larger angles) the intensities for both polarizations become more identical, as it has been seen in fig. 2.6 on the reflection of an Au surface.

The calculations show, that the additional structures in the reflection spectrum from the multilayer are due to multilayer reflections, independent of the edge structures. For the understanding of the change in the spectra at the absorption edges due to scattering or reflection, energy dependent calculations must be performed, which is much more effort, because the optical parameters near the absorption edges must be determined. This can in principle be done with the help of the Kramers Kronig relations described in chapter II.

6.2 Co/Mn-Multilayers and Single Mn-Films

Until now we have discussed the effect of scattered and reflected light on the shape of the absorption spectrum on the Fe/Cr multilayer systems, which has served as a model system. Here we want to show that these effects are not limited to Fe/Cr systems, but can also seen in other systems. We have studied Co/Mn multilayers and single Mn films, where analogous effects are seen in the absorption spectra of Mn.

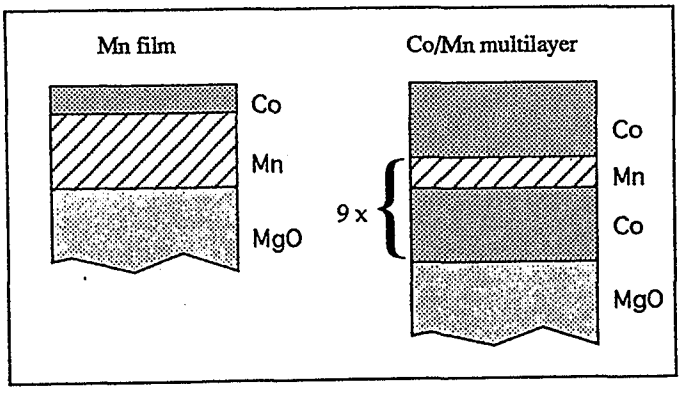

Fig. 6.14. Schematic structure of the Mn film and the Co/Mn multilayers. For details see text.

Fig. 6.14. shows the schematical setup of the structure of the Mn film and the Co/Mn multilayers. The layers are deposited by sputtering onto an MgO single crystal substrate. The thickness of the Mn film is 40Å and it is covered with 20Å Co. The

Co/Mn multilayers have the structure $[Co_n\ Mn_m]_9\ Co_n$, with different values of n and m (in Å).

The scattering in the Mn $L_{2,3}$ absorption edges is studied in comparison with a single Mn film of 40Å thickness for Co/Mn multilayers with different Co and Mn layer thicknesses. Fig.6.15 displays the Mn $L_{2,3}$ absorption spectra for the different samples taken in geometry II ($\alpha = 22°$) with the Si(Li) fluorescence detector.

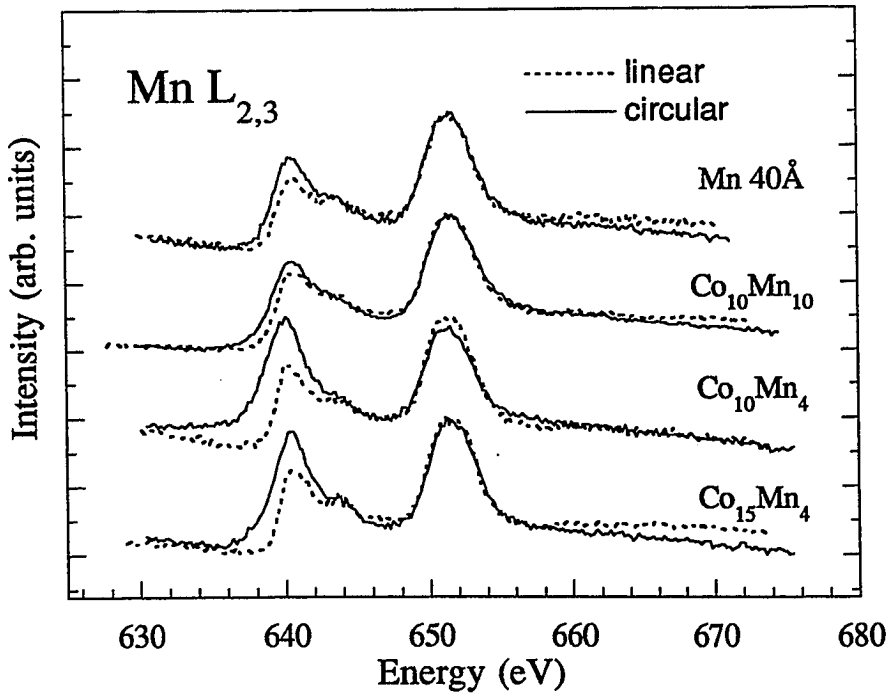

Fig. 6.15. Mn $L_{2,3}$ absorption spectra taken in geometry II for a 40Å Mn film compared to different Co/Mn multilayers (the numbers indicate the film thickness in Å). solid line: excitation with circularly polarized light; dashed line: excitation with linearly polarized light.

On top of Fig.6.15 the spectrum of the single Mn film is shown. The solid line corresponds to the spectra taken with linearly polarized light and the dashed line to the one taken with linearly (p-)polarized light. The spectra are nearly identical in this case, which demonstrates that the Mn film does not show scattering effects. Below the spectra of different Co/Mn multilayers are shown, having a structure as described above. The first one below the Mn film consists of Co layers of n = 10Å and Mn layers

also of m=10Å. The comparison between the spectra taken with linear and circular light shows, that also in this sample there is hardly any scattering visible. But the spectra for the n=10Å, m=4Å, below, look quite different for the two polarizations. As in the case of the Fe/Cr films, the intensity at the L_3 edge is enhanced for circularly polarized light. The same is true for the last sample shown on the bottom, with n = 15Å and m = 4Å.

This shows that there is resonant X-ray scattering also is observed at the Mn absorption edge and it depends mostly on the thickness of the Mn film, not on the thickness of the other elements of the multilayer (Co). So, this is quite analogous to the Fe/Cr layers. And also the shape of the scattered intensity is the same; always the intensity at the edges, especially at the L_3 edge is enhanced compared to the absorption spectrum.

We have also performed reflection measurements on the Co/Mn multilayers. Fig. 6.16 shows the reflection spectrum at 45° from the $Co_{10Å}$ $Mn_{4Å}$ sample, which shows scattering intensity.

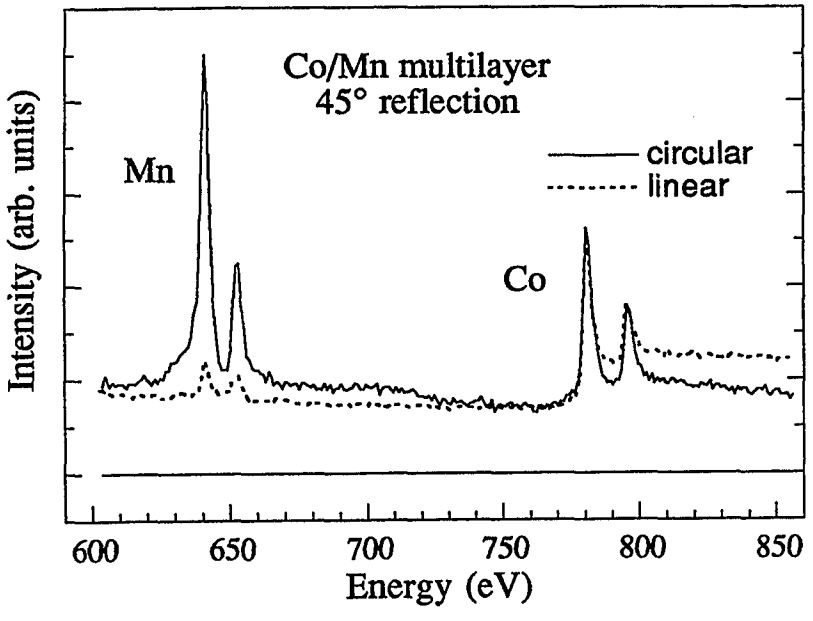

Fig. 6.16. 45° reflection spectrum of a $[Co_{10Å}\ Mn_{4Å}]_9\ Co_{10Å}$ multilayer in geometry II. Top: spectrum taken with linearly (p-) polarized light; bottom: spectrum taken with circularly polarized light.

Fig. 6.16 shows the reflection spectrum at 45° incidence of a $[Co_{10Å}\ Mn_{4Å}]_9\ Co_{10Å}$ multilayer, which exhibits scattering, as seen in fig 6.15. The spectra show the Mn as well as the Co L edges taken with linearly (p-) and with circularly polarized light. The spectra taken with linearly polarized light represent the normal absorption spectrum, while the spectrum for circularly polarized light is quite different. Here the typical

scattering shapes at the L_3 edges are visible, but also the intensities of the Mn and Co emission have changed drastically. While the Mn emission with linear light is very small compared to Co, it is much larger than Co with circular light. In the reflection spectra taken with circularly polarized light, also the shape of the Co edge is different from the one taken with linearly polarized light. Again this is analogous to the Fe/Cr case.

Next we have investigated the Mn absorption spectrum in 45° reflection from the same Co/Mn multilayer as just discussed, in dependence on the degree of circular polarization. The degree of circular polarization can only be influenced by changing the off plane angle Ψ, where $\Psi = 0$ is linearly polarized light. This variation for four different angles, $\Psi = 0$, 0.3, 0.6 and 0.9 mrad is shown in Fig. 6.17.

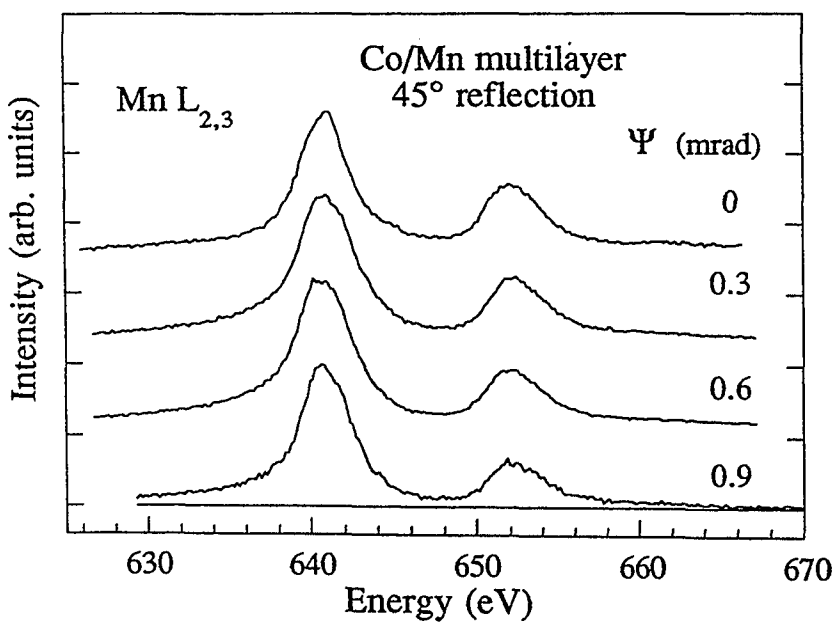

Fig. 6.17. Mn $L_{2,3}$ absorption spectrum from the $[Co_{10Å}\ Mn_{4Å}]_9\ Co_{10Å}$ multilayer in 45° reflection. The spectra for different off plane angles Ψ of the synchrotron radiation are shown.

The spectrum on top of the figure shows the spectrum taken with linearly polarized light $\Psi = 0$, where no scattering is visible. With increasing off plane angle Ψ the degree of circular polarization is also increasing, so that the emission at the L_3 edge increases, too. The L_3/L_2 intensity ratio increases with increasing Ψ. We have also performed the measurements for negative angles Ψ , and also for different magnetization directions, but there are no differences in the spectra, thus there is no circular dichroism in the Mn spectra, because it is not ferromagnetic. The changes in the $L_{2,3}$ peak ratio are plotted in Fig. 6.18 as a function of the angle Ψ. The peak intensities are obtained by integrating the spectra over the L_3 or L_2 peak, respectively, without subtracting a steplike background as it was done in chapter 5. The errorbars come from the fact that it is not very clear where the peak ends, so the integration areas are varied by some eV.

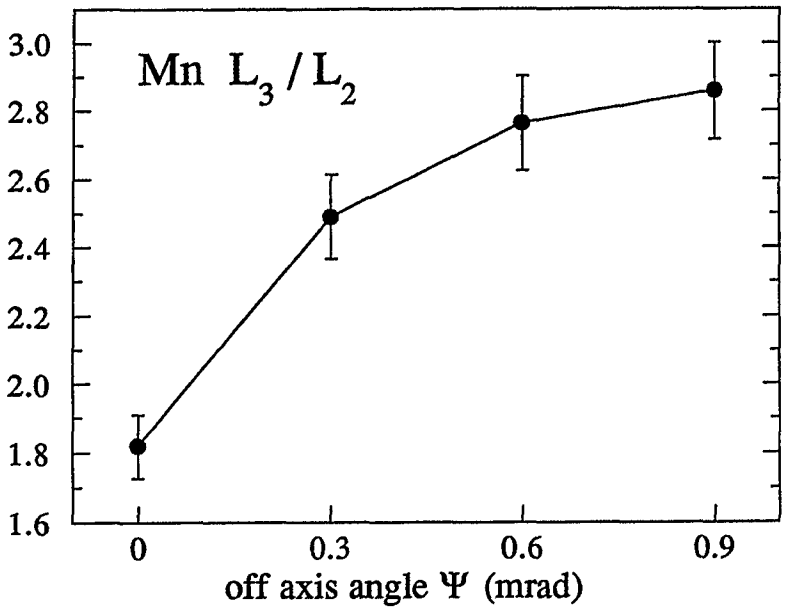

Fig. 6.18. L_3/L_2 intensity ratios of the Mn $L_{2,3}$ absorption spectra shown in figure 6.17, plotted as a function of the off plane angle Ψ.

For linearly polarized light, the ratio is about 1.8, and it increases monotonously with increasing Ψ. Increasing Ψ means increasing degree of circular polarization. So this measurement could be used as a simple calibration of the degree of circular polarization. It is not easy to determine the exact degree of circular polarization in this energy range, as discussed above. But with this measurement one would be able at least to check quite fast, if the polarization is the same or if it has changed compared to an earlier measurement. This can be important, because the conditions at a synchrotron light source are not constant over a long time; so variations in the degree of circular

polarization from one day to the other may occur. With this measurement, one could easily test the intensity ratio and compare it to an earlier one.

In summary we observe that in the fluorescence yield detection, the absorption of thin films can be influenced by X-ray scattering. The scattering is found for several samples. The intensity of the scattering depends mainly on the degree of s-polarized light in the incident radiation. The scattering mainly increases the intensity at the L_3 absorption edge. The magnetic dichroism is also influenced by the scattering. In the Fe spectra there was always seen an enhancement of the dichroism asymmetry. The influence of the shape of the spectra at the absorption edges due to scattering effects and 45° reflection are analogous, so that the scattering can be understood as a largely increased reflection. The scattering depends on the film thickness of the corresponding element, so it is not caused by the atomic structure of the system. If one wants to measure the absorption spectra without any scattering effect, one has to choose the correct geometry; that is a geometry, where the detector is out of the scattering plane, best perpendicular to it, like geometry I in our case. The enhancement of the dichroism effect in the scattering and in the reflection might be used for a polarization filter, where linearly (s-) polarized light is reflected from the magnetized sample. First experiments of this kind show strong evidence that such a polarization filter works. Until now such polarization filters exist only up to the photon energy of the Carbon K-edge (about 270 eV) [Fonzo 94].

VII. Summary and Outlook

We have studied magnetic circular dichroism (MCD) at the $L_{2,3}$ absorption edges of 3d transition elements in thin films and magnetic multilayers. MCD exhibits itself in differences of the absorption coefficient at the absorption edges depending on the relative orientation of the magnetization of the sample to the polarization of the exciting light. The experiments have been performed with circularly polarized synchrotron radiation in the soft X-ray range from the SX700/3 beamline at the BESSY synchrotron light source, Berlin.

Recently derived sum rules, based on an atomic model, relate the intensity of the measured MCD absorption spectra of ferromagnets to the local spin- and orbital magnetic moments. The absorption spectra can be measured with different detection methods. We have compared the spectra of Fe, Co and Ni taken in electron yield (EY) and in fluorescence yield (FY) detection mode. The detected signal in both modes should be proportional to the absorption coefficient, but we find differences in the related spectra, which express themselves in the isotropic spectra (averaged over all polarizations) by a different $L_{2,3}$ branching ratio and in differences in the corresponding MCD spectra (the difference between spectra taken with magnetization parallel and antiparallel to the light helicity). The validity of the sum rules for the ferromagnets Fe, Co and Ni has been tested by applying them to the measured absorption spectra in FY and EY mode and to first-principle calculations. We find different results in the EY and FY spectra, especially in the case of Fe, while the ones for Co and Ni are consistent within about 20%. The data obtained in the EY mode are more reliable than the ones in the FY mode, especially in the case of Fe. Thus for systems where one can use the electron yield for taking the absorption spectra one should prefer it. But there are a lot of systems where one cannot use it, for example in buried films or impurities or in experimental setup with strong magnetic fields. Here only the fluorescence yield can be applied and therefore it is important to know the differences that occur in this case.

The fluorescence yield detection is a suitable (and sometimes the only possible) method for the detection of the absorption spectra in buried structures and dilute systems and for measurements in applied magnetic fields. However one must be aware of complications due to X-ray scattering effects and fundamental differences in the absorption spectra. For quantitative measurements one should use reference samples. A very powerful application of MCD in FY detection is of course the element specific determination of magnetic hysteresis loops, especially in heteromagnetic systems, as it has been shown by Chen et al. [Chen 93].

The magnetic coupling of Cr to Fe inside a Fe/Cr multilayer with one atomic layer of Cr between adjacent ferromagnetically coupled Fe films is shown to be antiparallel with a magnetic moment of Cr of about -0.3 μ_B. The dichroism signal of two atomic Cr layers in the same systems nearly vanishes, obviously due to magnetic frustration in the Cr film. In the fluorescence yield detection mode, resonant X-ray scattering effects are observed at

Fe/Cr and Co/Mn multilayer systems and single Fe films depending on their thickness and on the geometry of measurement. These effects express themselves in additional intensity at the L_3 absorption peak, and the dichroism asymmetry can be enhanced drastically. X-ray reflection measurements on these systems have shown, that the dichroism signal can be strongly enhanced at the absorption edges in reflection. Apart from the absorption edges, additional structures are observed in the energy dependent spectrum, which are related to multilayer reflection peaks. This was modelled by reflection calculations on these systems.

The strong enhancement of the dichroism effects in scattered and reflected light might be useful for several applications, for example determination of the degree of circularly polarization of the exciting light (after a calibration of the spectra) or as a polarization filter. First experiments give strong indications, that the reflected light from a magnetic Fe/Cr multilayer changes the polarization of incoming linearly polarized light into light with a reasonably high degree of circular polarization at the Fe L_3 absorption edge. For this high energy (about 707 eV) there is no other polarization filter available until now.

Appendix

i) Abbreviations

BESSY	Berliner Elektronenspeicherringgesellschaft für Synchrotronstrahlung mbH
CDAD	Circular Dichroism in the Anglular Distribution
CMXD	Circular Magnetic X-ray Dichroism
EXAFS	Extended X-ray Absorption Fine Structure
EY	Electron Yield
FLAPW	Fully linearize augmented plane wave method
FY	Fluorescence Yield
KFA	Forschungszentrum Jülich
LCAO	Linear Combination of Atomic Orbitals
LMTO	linear muffin-tin orbital method
MCD (MLD)	Magnetic Circular (Linear) Dichroism
MXD	Magnetic X-ray Dichroism
NEXAFS	Near Edge X-ray Absorption Fine Structure
SPR-LMTO	spin polarized, relativistic LMTO
SQUID	Superconducting Quantum Interference Device

ii) Soft X-Ray Absorption Energies for some Selected Elements

Conversion between photon energy hν and wavelength l: hν (eV) * l(Å) = 12398.52

Element [Z]	**K edge (eV)**		
C, carbon [6]	283.84 (283.87)		
N, nitrogen (gas) [7]	(409.5)		
O, oxygen (gas)[8]	(546.2)		
3d - elements	**L_2 edge (eV)**	**L_3 edge (eV)**	**$M_{2,3}$ edge (eV)**
Ca, calcium [20]	[350.2]	[347.2]	
Sc, scandium [21]	[403.5]	[399.5]	
Ti, titanium [22]	[460.1]	454.4 (452.9) [454.5]	
V, vanadium [23]	[520.1]	(511.3) [512.0]	≈36.8
Cr, chromium [24]	(583.2) [583.4]	(573.98) [575.4]	≈40.0
Mn, manganese [25]	[650.2]	[639.5]	≈45.0
Fe, iron [26]	720.8 (720.89) [720.1]	707.4 (707.55) [707.5]	53.8
Co, cobalt [27]	793.8 (793.65) [793.6]	779.0 (778.85) [778.9]	61.0
Ni, nickel [28]	870.6 (870.73) [869.2]	853.6 (853.71) [852.4]	65.81
Cu, copper [29]	952.68 (952.94)	933.06 (933.21)	74.7
Zn, zink [30]	1045.23 (1045.32)	1022.01 (1022.07)	86.2

Table A1. Absorption energies: 1st value: [Bearden 67]; 2nd value (in brackets): [Bourcier]; 3rd value [in brackets]: [Fink 85] (from ref [Fink 85] took the mean value of the given values for the edge appearance energy and the peak maximum.)

iii) Dipole Matrix Elements for p -> d Optical Transitions in the Erskine-Stern Model of MCD

The quantities A, B, and C of this table are defined according to ref [Smith 92] as

$$\begin{aligned} A &= |\langle Y_{2\pm2} | (x \pm iy)/r | Y_{1\pm1} \rangle|^2 R^2 , \\ B &= |\langle Y_{2\pm1} | (x \pm iy)/r | Y_{1\,0} \rangle|^2 R^2 , \\ C &= |\langle Y_{2\,0} | (x \mp iy)/r | Y_{1\pm1} \rangle|^2 R^2 , \end{aligned} \tag{A1}$$

where R is the standard integral

$$R = \int r^2 R_p(r) R_d(r)\, dr , \tag{A2}$$

and where $R_p(r)$ and $R_d(r)$ are the 2p and 3d radial wave functions.

	$p_{3/2}$				$p_{1/2}$	
	$\left\|\frac{3}{2}\,\frac{3}{2}\right\rangle$	$\left\|\frac{3}{2}\,\frac{1}{2}\right\rangle$	$\left\|\frac{3}{2}\,-\frac{1}{2}\right\rangle$	$\left\|\frac{3}{2}\,-\frac{3}{2}\right\rangle$	$\left\|\frac{1}{2}\,\frac{1}{2}\right\rangle$	$\left\|\frac{1}{2}\,-\frac{1}{2}\right\rangle$
			$\mu^+ = \|\langle \|(x+iy)/r\| \rangle\|^2$			
$Y^{\downarrow}_{2\,2}$	0	$\frac{1}{3}A$	0	0	$\frac{2}{3}A$	0
$Y^{\downarrow}_{2\,1}$	0	0	$\frac{2}{3}B$	0	0	$\frac{1}{3}B$
$Y^{\downarrow}_{2\,0}$	0	0	0	C	0	0
$Y^{\downarrow}_{2\,-1}$	0	0	0	0	0	0
$Y^{\downarrow}_{2\,-2}$	0	0	0	0	0	0
			$\mu^- = \|\langle \|(x-iy)/r\| \rangle\|^2$			
$Y^{\downarrow}_{2\,2}$	0	0	0	0	0	0
$Y^{\downarrow}_{2\,1}$	0	0	0	0	0	0
$Y^{\downarrow}_{2\,0}$	0	$\frac{1}{3}C$	0	0	$\frac{2}{3}C$	0
$Y^{\downarrow}_{2\,-1}$	0	0	$\frac{2}{3}B$	0	0	$\frac{1}{3}B$
$Y^{\downarrow}_{2\,-2}$	0	0	0	A	0	0

Table A2. Dipole-matrix elements (squared) for p → d optical transitions in the Erskine-Stern model of CMXD [Smith 92], with the relativistic states $|j,m_j\rangle$ for the p - core states and the spherical harmonics $Y^{\downarrow}_{l\,m}$ for the unoccupied $d^{\downarrow}$ valence states.

iv) MCD Sum Rules

In the last few years sum rules have been developed for the absorption of circularly polarized light in ferromagnets. With the help of these sum rules one obtaines the ground state expectation values of $\langle L_z \rangle$ [Thole 92] and $\langle S_z \rangle$ [Carra 93].

$$\rho = \frac{\int_{j^+ + j^-} dE(\mu^+ - \mu^-)}{\int_{j^+ + j^-} dE(\mu^z + \mu^+ + \mu^-)} = \frac{1}{2} \frac{l(l+1) + 2 - c(c+1)}{l(l+1)\,(4l + 2 - n)} \langle L_z \rangle \qquad \text{(A3)}$$

$$\delta = \frac{\int_{j^+} dE(\mu^+ - \mu^-) - \frac{(c+1)}{c} \int_{j^-} dE(\mu^+ - \mu^-)}{\int_{j^+ + j^-} dE(\mu^z + \mu^+ + \mu^-)} \qquad \text{(A4)}$$

$$= \frac{l(l+1) - 2 - c(c+1)}{3c\,(4l + 2 - n)} \langle S_z \rangle + \frac{l(l+1)[l(l+1)+2c(c+1)+4] - 3(c-1)^2\,(c+2)^2}{6lc\,(l+1)\,(4l + 2 - n)} \langle T_z \rangle$$

Here μ^+, μ^-, and μ^z denote the absorption coefficients according to the fundamental spectra R, L, and Z, respectively; c denotes the quantum number of the core hole, and l the quantum number of the valence state. n is the number of occupied 3d states and n_h = (4l+2-n) the number of unoccupied 3d states, respectively. $\langle T_z \rangle$ is magnetic dipole operator $T = \frac{1}{2}[S - 3r(r \cdot S)]$ with $T_z = S_z\,(1 - 3\cos^2\frac{\Theta}{2})$.

For the $L_{2,3}$ absorption edges of the 3d elements one uses c=1 (p - core hole) and l=2 (d - valence state), thus the formula are:

$$\rho = \frac{\int_{L_3 + L_2} dE(\mu^+ - \mu^-)}{\int_{L_3 + L_2} dE(\mu^z + \mu^+ + \mu^-)} = \frac{1}{2n_h} \langle L_z \rangle \qquad \text{(A5)}$$

$$\delta = \frac{\int_{L_3} dE(\mu^+ - \mu^-) - 2 \int_{L_2} dE(\mu^+ - \mu^-)}{\int_{L_3 + L_2} dE(\mu^z + \mu^+ + \mu^-)} = \frac{2}{3\,n_h} (\langle S_z \rangle + \frac{7}{2} \langle T_z \rangle) \qquad \text{(A6)}$$

Literature

[Alouani 94] M.Alouani, *" Final-state rule and the absorption spectra of 3d ferromagnets"* , Phys. Rev. B **49**, 16038 (1994)

[Altarelli 72] M. Altarelli, D. L. Dexter, H.M Nussenzweig, D.Y.Smith, *"Superconvergence and sum rules for the optical constants"* , Phys. Rev. B **6**, 4502 (1972)

[Altarelli 93] M.Altarelli, *"Orbital-magnetization sum rule for x-ray circular dichroism: A simple proof"* , Phys. Rev. B **47**, 597 (1993)

[Baibich 88] M.N. Baibich, J.M Broto, A. Fert, F.N.v. Dau, F. Petroff, P. Etienne, G. Creuzet, A. Friederich, and J. Chazelas, *"Giant magnetoresistance of (001)Fe/(001)Cr magnetic superlattices"* , Phys. Rev. Lett. **61**, 2472 (1988)

[Baumgarten 90] K. Baumgarten, C.M. Schneider, H. Petersen, F. Schäfers, and J. Kirschner, *"Magnetic X-ray dichroism in core-level photoemission from ferromagnets"* , Phys. Rev. Lett. **65**, 492 (1990)

[Bearden 67] J. A. Bearden, *"X-ray wavelengths"* ; Rev. of Modern Physics **39**, 78 (1967)

[Bennett 65] H. S. Bennett, E. A. Stern, *"Faraday effects in solids"* , Phys. Rev. **137**, A448 (1965)

[Binasch 89] G. Binasch, P.Grünberg, F.Saurenbach, W.Zinn, *" Enhanced magnetoresistance in layered magnetic structures with antiferromagnetic interlayer exchange"* , Phys. Rev. B **39**, 4828 (1989)

[Blume 88] M.Blume and Doon Gibbs, *"Polarization dependence of magnetic x-ray scattering"* , Phys. Rev. B **37**, 1779 (1988)

[Böske 94a] T.Böske, W. Clemens, C. Carbone, and W. Eberhardt, *"Circular magnetic x-ray dichroism of 3d impurities in Ni "*, Phys. Rev. B **49**, 4003 (1994)

[Böske 94b] T.Böske, *"Zirkulardichroismus im Röntgenbereich an Übergangsmetallen als Fremdatome in Nickel und in Schichtsystemen"* , Berichte des Forschungszentrums Jülich, Jül-2880 (1994)

[Böske 94c] T.Böske, W.Clemens, D.Schmitz, J.Kojnok, M.Schäfer, V.Cros, W.Eberhardt, G.Y.Guo, *"The coupling of Cr to Fe in Fe/Cr-multilayers studied by circular magnetic x-ray dichroism in fluorescence-yield mode"* , to be published

[Carbone 87] C. Carbone, S.F. Alvarado, *"Antiparallel coupling between Fe layers separated by a Cr interlayer: Dependence of the magnetization on the film thickness"* , Phys. Rev. B **36**, 2433 (1987)

[Carlson 75] T.A.Carlson, *"Photoelectron and Auger Spectroscopy"* , Plenum Press, New York, 1975

[Carra 93] P. Carra, B. T. Thole, M. Altarelli, X. Wang; *"X-ray circular dichroism and local magnetic fields"* ; Phys. Rev. Lett. **70**, 694 (1993)

[Chen 90] C.T.Chen, F.Sette, Y.Ma, S.Modesti, *"Soft-x-ray magnetic dichroism at the $L_{2,3}$ edges of nickel"* , Phys. Rev. B **42**, 7262 (1990)

[Chen 91] C.T.Chen, N.V.Smith, S.Sette, *"Exchange, spin-orbit, and correlation effects in the soft-x-ray magnetic-circular-dichroism spectrum of nickel"* , Phys. Rev. B **43**, 6785 (1991)

[Chen 93] C.T.Chen, Y.U.Idzerda, H.J.Lin, G.Meigs, A.Chaiken, G.A.Prinz, G.H.Ho, *"Element-specific magnetic hysteresis as a means for studying heteromagnetic multilayers"* , Phys. Rev. B **48**, 642 (1993)

[Ebert 88a] H.Ebert, P.Strange, B.L.Gyorffy, *"Theory of circularly polarized x-ray absorption by ferromagnetic Fe"* , J. Appl. Phys. **63**, 3055 (1988)

[Ebert 88b] H. Ebert, *"Two ways to perform spin-polarized relativistic linear muffin-tin-orbital calculations"* , Phys. Rev. B **38**, 9390 (1988)

[Eisebitt 93] S. Eisebitt, T. Böske, J.E. Rubensson, and W. Eberhardt, *"Determination of absorption coefficients for concentrated samples by fluorescence detection "* , Phys. Rev. B **47**, 14103 (1993)

[Eriksson 90] O. Eriksson, B. Johansson, R.C. Albers, A.M. Boring, and M.S.S. Brooks, *"Orbital magnetism in Fe, Co, and Ni "* , Phys. Rev. B **42**, 2707 (1990)

[Erskine 75] J. L. Erskine, E. A. Stern; *"Calculation of the $M_{2,3}$ magneto-optical absorption spectrum of ferromagnetic nickel"* ; Phys. Rev. B**12**, 5016 (1975)

[Etienne 90] P.Etienne, S.Lequien, F.N.v.Dau, R.Cabanel, G.Creuzet, A.Friederich, J.Massies, A.Fert, A.Barthélémy, F.Petroff, *"A comparative study of the molecular-beam epitaxial growth of Ag/Fe, Ag/Cr, and Fe/Cr superlattices on GaAs (001)"* , J. Appl. Phys. **67**, 5400 (1990)

[Feder 85] R. Feder (ed.), *"Polarized Electrons in Surface Physics"* , World Scientific, Singapore (1985)

[Fink 85] J. Fink, T. Müller-Heinzerling, B. Scheerer, W. Speier, F. U. Hillebrecht, J.C. Fuggle, J. Zaanen, G.A.Sawatzky; *"2p absorption spectra of the 3d elements"* ; Phys. Rev. B **32**, 4899 (1985); ;

[Fischer 89] D.A. Fischer, J. Colbert, J.L. Gland, Rev. Sci. Instrum. **60**, 1596 (1989)

[Fonzo 94] S.D.Fonzo, W.Jark, F.Schäfers, H.Petersen, A.Gaupp, J.H.Underwood, *"Phase retardation and full polarization analysis of soft X-ray synchrotron radiation close to the carbon K-edge using a multilayer transmission filter"* , submitted to Applied optics

[Freiser 68] M.J.Freiser, *"A Survey of Magnetooptic Effects"* , IEEE Transactions on Magnetics, Vol. Mag-**4**, 152 (1968)

[Friedrich 94] J. Friedrich, DESY Hamburg, private communication

[FS 92] 23. IFF-Ferienkurs, *Synchrotronstrahlung zur Erforschung kondensierter Materie*, 23. March - 3. April 1992, Forschungszentrum Jülich

[FS 93] 24. IFF-Ferienkurs, *Magnetismus von Festkörperrn und Grenzflächen*, 8. - 19. March 1993, Forschungszentrum Jülich

[Grünberg 86] P. Günberg, P. Schreiber, Y. Pang, M.B. Brodsky, and H. Sowers, *"Layered Magnetic Structures: Evidence for Antiferromagnetic Coupling of Fe Layers across Cr Interfaces"* , Phys. Rev. Lett. **57**, 2442 (1986)

[Guo 94a] G.Y. Guo and H. Ebert, *"First-principles calculation of magnetic x-ray dichroism in Fe and Co multilayers"* , Phys. Rev. B **50**, 3861 (1994)

[Guo 94b] G.Y. Guo, H. Ebert, W. M. Temmerman and P. J. Durham, *"Band theoretical investigation of circular magnetic x-ray dichroism in Fe and Co multilayers "* , to be published in J. Mag. Mag. Mat., 1994

[Hagemann 74] H.J. Hagemann, W. Gudat, C. Kunz, *"Optical constants from the far infrared to the X-ray region: Mg,Al, Cu, Ag, Au, Bi, C, and Al_2O_3"* , DESY SR-74/7 (1974)

[Hague 93] C.F.Hague, J.M.Mariot, P.Strange, P.J.Durham, B.L.Gyorffy, *"Observation of magnetic circular dichroism in Fe $L_{2,3}$ x-ray-fluorescence spectra"* , Phys. Rev. B **48**, 3560 (1993)

[Hasegawa 91] H.Hasegawa, *"Calculation of electronic and magnetic structures of Fe/Cr, Co/Cr and Ni/Cr multilayers"* , Phys. Rev. B **43**, 10803 (1991)

[Henke 82] B.L. Henke, P. Lee, T.J. Tanaka, R.L. Shimabukuro, and B.K. Fujikawa, *"Low-energy x-ray interaction coefficients: Photoabsorption, Scattering, and Reflection (E = 100 - 2000 eV, Z = 1 - 94)"* ,At. Data Nucl. Data Tables **27**, 1 (1982)

[Hubbel 80] J.H.Hubbel, H.A.Gimm, J.Øverbø, *"Pair, triplet, and total atomic cross sections (and mass attenuation coefficients) for 1 MeV - 100 GeV photons in elements Z = 1 to 100"* , J. Phys. Chem. Ref. Data **9**, 1023 (1980)

[Idzerda 93] Y.U.Idzerda, L.H.Tjeng, H.J.Lin, C.J.Gutierrez, G.Meigs, C.T.Chen, *"Magnetic structure of Fe/Cr/Fe trilayers"* , Phys. Rev. B **48**, 4144 (1993)

[Jo 92] T.Jo, *"Theoretical interpretation of magnetic dichroism measured with soft X-rays"* , Synchrotron Radiation News, Vol. **5**, 21 (1992)

[Jungblut 91] R. Jungblut, C.Roth, F.U.Hillebrecht, E.Kisker, *"Magnetic properties of Cr overlayers on Fe"* , J. Appl. Phys. **70**, 5923 (1991)

[Kachel 94] T.Kachel, W.Gudat, K.Holldack, *"Element specific magnetic domain imaging from an antiferromagnetic overlayer system"* , Appl. Phys. Lett. **64**, 665 (1994)

[Kanamori 63] J. Kanamori, in *Anisotropy and Magnetostriction of Ferromagnetic and Antiferromagnetic Materials*, Magnetism Vol. **I**, ed. by G. T. Rado and H. Suhl, Academic Press, New York, 1963

[Kao 90] C.Kao, J.B.Hastings, E.D.Johnson, D.P.Siddons, G.C.Smith, G.A.Prinz, *"Magnetic-Resonance Exchange Scattering at the Iron L_2 and L_3 Edges"* , Phys. Rev. Lett. **65**, 373 (1990)

[Kao 94] C.C.Kao, C.T.Chen, E.D.Johnson, J.B.Hastings, H.J.Lin, G.H.Ho, G.Meigs, J.M.Brot, S.L.Hulbert, Y.U.Idzerda, C.Vettier, *"Dichroic interference effects in circularly polarized soft X-ray resonant magnetic scattering"*, Phys. Rev. B **50**, 9599 (1994)

[Kessler 76] J. Kessler, *"Polarized electrons"*, 2nd ed., Springer (Berlin), 1976

[Krause 79] M.O.Krause, *" Atomic radiative and radiationless yields for K and L shells"* , J. Chem. Ref. Data **8**, 307 (1979)

[Laan 86] G.v.d.Laan, B.T.Thole, G.A.Sawatzky, J.B.Goedkoop, J.C.Fuggle, J.M.Esteva, R. Karnatak, J.P.Remeika, H.A.Dabkowska, *"Experimental proof of magnetic x-ray dichroism"* , Phys. Rev. B **34**, 6529 (1986)

[Laan 90] G.v.d.Laan, B.T.Thole, *"Magnetic dichroism in the x-ray absorption branching ratio"* , Phys. Rev. B **42**, 6670 (1990)

[Laan 91a] G.v.d.Laan, *"Magnetic circular dichrois in core-level photoemission of localized magnetic systems"* , Phys. Rev. Lett. **66**, 2527 (1991)

[Laan 91b] G .v.d. Laan, B. T. Thole; *"Strong magnetic x-ray dichroism in 2p absorption spectra of 3d transition-metal ions"* , Phys. Rev B **43**, 13401 (1991)

[Landes 90] J.Landes, C.Sauer, R.A.Brand, W.Zinn, S.Mantl, Z.Kajcsos, *"Magnetic hyperfine fields near the Fe/Cr (100, 110) interface studied by CEMS"* , J. Mag. Mag. Mat. **86**, 71 (1990)

[Mott 49] N.F.Mott, *"The basis of the electron theory of metals, with special reference to the transition metals"* , Proc. Phys. Soc. A **62**, 416 (1949)

[Muto 92] S.Muto,Y.Kagoshima, T.Miyahara, S.Yamamoto, H.Kitamura, *"Influence of fano effect on magnetic circular dichroism due to core electron transition in Ni and Gd metals"* , Sol. St. Comm. **83**, 41 (1992)

[Palik 91] A. D. Palik, *Handbook of optical constants of solids*, Academic Press, New York, 1991

[Parkin 90] S.S.P.Parkin, N.More, K.P.Roche, *"Oscillations in exchange coupling and magnetoresistance in metallic superlattice structures: Co/Ru, Co/Cr, and Fe/Cr"* , Phys. Rev. Lett. **64**, 2304 (1990)

[Petersen 93] H. Petersen, M. Willmann, F. Schäfers, and W. Gudat, *"Circularly polarized soft X-rays in the photon energy range 300 - 2000 eV at the BESSY SX700/3"* , Nucl. Instr. and Meth. in Phys. Res. A **333**, 594 (1993)

[Rennert 93] P.Rennert, *"Theoretical analysis of magnetic dichroism in the x-ray-resonance scattering of cubic systems at the K and L edges"* , Phys. Rev. B **48**, 13559, (1993)

[Roth 93] C.Roth, F.U.Hillebrecht, H.B.Rose, E.Kisker, *"Linear magnetic dichroism in angular resolved Fe 3p core level photoemission"*, Phys. Rev. Lett. **70**, 3479 (1993)

[Rudolf 92] P.Rudolf, F.Sette, L.H.Tjeng, G.Meigs, C.T.Chen, *"Magnetic moments in a gadolinium iron garnet studied by soft-X-ray magnetic circular dichroism"* , J. Mag. Mag. Mat. **109**, 109 (1992)

[Samant 94] M.G.Samant, J.Stöhr, S.S.P.Parkin, G.A.Held, B.D.Hermsmeier, F.Herman, M.v.Schilfgaarde, L.C.Duda, D.C.Mancini, N.Wassdahl, R.Nakajima, *"Induced spin polarization in Cu spacer layers in Co/Cu multilayers"* , Phys. Rev. Lett. **72**, 1112 (1994)

[Schäfers 93] F.Schäfers, *"Transmission multilayers as circular polarization analyzers"* , Workshop on Applications of Circular Polarization, BESSY, Nov. 3rd and 4th, 1993

[Schmitz 94] D.Schmitz, *"Magnetischer Röntgendichroismus an Co/Cr - Vielfachschichten"* , Berichte des Forschungszentrums Jülich, Jül-2941 (1994)

[Schneider 94] C.M. Schneider, K.Meinel, J. Kirschner, M.Neuber, M.Grunze, *"Elementspezifische Abbildung magnetischer Mikrostrukturen"* , Phys. Bl. **50**, 939 (1994)

[Schneider 94] C.M.Schneider, K.Meinel, J.Kirschner, M.Neuber, M.Grunze, "Elementspezifische Abbildung magnetischer Mikrostrukturen" , Phys. Bl. **50**, 939 (1994)

[Schütz 87] G.Schütz, W.Wagner, W.Wilhelm, P.Kienle, R.Zeller, R.Frahm, G.Materlik, *"Absorption of circularly polarized X rays in Iron"* , Phys. Rev. Lett. **58**, 737 (1987)

[Schütz 90] G.Schütz, *"Zirkular polarisierte Röntgenstrahlung - eine neue Sonde zum Studium des Magnetismus"* , Phys. Bl. **46**, 475 (1990)

[Smith 92] N. V. Smith, C. T. Chen, F. Sette, and L. F. Mattheiss; *"Relativistic tight-binding calculations of x-ray absorption and magnetic circular dichroism at the L_2 and L_3 edges of nickel and iron"* ; Phys. Rev. B **46**, 1023 (1992)

[Stähler 93] S. Stähler, G. Schütz, H. Ebert, *"Magnetic K-edge absorption in 3d elements and its relation to local magnetic structure"* , Phys. Rev. B **47**, 818 (1993)

[Starke 93] K.Starke, E.Navas, L.Baumgarten, G.Kaindl, *"Strong magnetic circular dichroism in 4f photoemission from gadolinium metal"* , Phys. Rev. B **48**, 1329 (1993)

[Stearns 86] M. B. Stearns, in Landolt-Börnstein Numerical Data and Functional Relationships in Science and Technology, ed. by H.P.J. Wijn, Springer Verlag, Berlin, 1986), Group3, Vol. **19**, Pt.a.

[Stoeffler 91] D.Stoeffler, F.Gautier, *"Interface roughness, magnetic moments, and couplings in $(A)_m/(Cr)_n$ (001) superlattices (A = Fe, Co, Ni)"* , Phys. Rev. B **44**, 10389 (1991)

[Stöhr 92] J. Stöhr, *NEXAFS Spectroscopy*, Springer Verlag, Berlin (1992)

[Stöhr 93] J.Stöhr, Y.Wu, B.D.Hermsmeier, M.G.Samant, G.R.Harp, S.Koranda, D.Dunham, B.P.Tonner, *"Element-specific magnetic microscopy with circularly polarized x-rays"* , Science, Vol. 259, 658 (1993)

[Strange 91] P.Strange, P.J.Durham, B.L.Gyorffy, *" Dichroic X-Ray Fluorescence"* , Phys. Rev. Lett. **67**, 3590 (1991)

[Thole 85] B.T.Thole, G.v.d.Laan, G.A.Sawatzky, *"Strong magnetic dichroism predicted in the $M_{4,5}$ x-ray absorption spectra of magnetic rare-earth materials"* , Phys. Rev. Lett. **55**, 2086 (1985)

[Thole 88] B.T.Thole, G.v.d.Laan, *"Branching ratio in x-ray absorption spectroscopy"* , Phys. Rev. B **38**, 3158 (1988)

[Thole 92] B. T. Thole, P. Carra, F. Sette, G. v.d. Laan; *"X-ray circular dichroism as a probe of orbital magnetization"* ; Phys. Rev. Lett. **68**, 1943 (1992)

[Timothy 83] J.G. Timothy, R.P. Madden, in *"Photon detectors for the ultraviolet and x-ray region"* , Handbook on Synchrotron Radiation, Vol. 1a, p.315, ed. by E.E. Koch, North Holland, Amsterdam 1983

[Turtur 94] C.Turtur, G.Bayreuther, *"Magnetic moments in ultrathin Cr films on Fe(100)"* , Phys. Rev. Lett. **72**, 1557 (1994)

[Unguris 91] J. Unguris, R.J. Celotta, D.T. Pierce, *"Observation of two different oscillations in the exchange coupling of Fe/Cr/Fe(100)"* , Phys. Rev. Lett. **67**, 140 (1991)

[Unguris 92] J.Unguris, R.J.Celotta, D.T.Pierce, *"Magnetism in Cr thin films on Fe (100)"* , Phys. Rev. Lett. **69**, 1125 (1992)

[Veigele 73] W.J. Veigele, *"Photon cross sections from 0.1 keV to 1 MeV for elements Z = 1 to Z = 94"* , At. Data Tables **5**, 51 (1973)

[Vettier 94] C.Vettier, *"Resonant X-ray scattering from magnetic materials"* , J. Mag. Mag. Mat. **129**, 59 (1994)

[Vogel 94] J.Vogel, M.Sacchi, *"Polarization and angular dependence of the L2,3 absorption edges in Ni (110)"* , Phys. Rev. B **49**, 3230 (1994)

[Walker 92] T.G.Walker, A.W.Pang, H.Hopster, S.F.Alvarado, *"Magnetic ordering of Cr layers on Fe (100)"* , Phys.Rev. Lett. **69**, 1121 (1992)

[Weller 94] D. Weller, Y.Wu, J. Stöhr, M.G.Samant, B.D. Hermsmeier, C.Chappert, *"Orbital magnetic moments of Co in multilayers with perpendicular magnetic anisotropy"* , Phys, Rev. B **49**, 12888 (1994)

[Wu 92] Y.Wu, J.Stöhr, B.D.Hermsmeier, M.G.Samant, D. Weller, *"Enhanced orbital magnetic momemt on Co atoms in Co/Pd multilayers: a magnetic circular X-ray Dichroism study"* , Phys. Rev. Lett. **96**, 2307 (1992)

[Wu 94a] R. Wu, D. Wang, A.J. Freeman, *"First principles investigations of MCD spectra and sum rules for 3d transition metal surfaces"* , J. Mag. Mag. Mat. **132**, 103 (1994)

[Wu 94b] R.Wu, A.J.Freeman, *"Limitation of the magnetic-circular-dichroism spin sum rule for transition metals and importance of the magnetic dipole term"*, Phys. Rev. Lett. **73**, 1994 (1994)

[Xu 93] J.Xu, A.J.Freeman, *"Interlayer-coupling magnetism and electronic structure of Fe/Cr (001) superlattices"* , Phys. Rev. B **47**, 165 (1993)

Acknowledgements

This thesis has been performed at the *Institut für Elektronische Eigenschaften* (IEE) within the *Institut für Festkörperforschung* (IFF) of the *Forschungszentrum Jülich* (KFA). Firstly I want to thank all the members of the institute for their collaboration and for the pleasant atmosphere. I sincerely want to thank Professor Wolfgang Eberhardt, who has suggested this work, for his encouragement and support. He was always available for many helpful discussions.

Many thanks to Thomas Böske, with whom I started the dichroism project and with whom I have discussed a lot about absorption and dichroism. Special thanks to Carlo Carbone, from whose experience and knowledge, especially about magnetism, I have profited very much. Jan Eric Rubensson (Ruben) was always there when I had questions concerning the absorption and fluorescence data. Theoretical support was given by Stefan Blügel, with whom I could discuss any time. Thanks to Detlef Schmitz who was a great help not only in performing the measurements. The experience of Stefan Cramm concerning everything which has to do with spectroscopy and synchrotron radiation was very helpful, too. Lutz Baumgarten has also helped me a lot, in discussions about dichroism as well as experimentally. Technical support was given by Josef Keppels, Dieter Hoffmann, Bernd Küpper, who produced and organized parts for the experiment, by Heinz Pfeifer (and his coworkers) concerning electronics and by Jürgen Lauer, who solved the computer problems. Technical support was also given by Herbert Feilbach, who made constructions and by the IFF workshop, where things were produced fast enough for the next beamtime. Thanks also to the other colleagues from the IEE, especially Matthias Neeb, Kevin Colbow and Elio Vescovo.

The work was done in collaboration with Josef Kojnok from the Eötvös University Budapest; it was a pleasure to work with him.

The Fe/Cr - samples have been produced and characterized by Markus Schäfer, Vincent Cros, and Reiner Schreiber from the IFF. The Co/Mn and Ni - samples have been produced and characterized by Qi Wang, in cooperation with Naoto Metoki and Wolfgang Donner, and the Co/Cu/Co sample was produced by Katharina Bröhl from the Ruhr Universität Bochum. They all have spent a lot of time and effort for me, I am greatly indepted to them.

The first-principles calculations were performed by Guang Yu Guo from the Daresbury Laboratory, Warrington. I want to thank him a lot, especially for his engagement in performing the calculations for the same systems that I have measureed. The reflection calculations on the Fe/Cr/Ag multilayer have been done by Jan Friedrich from DESY, Hamburg. Gratitudes to him for his friendly collaboration.

The measurements have been carried out at the Berliner Elektronenspeicherring-Gesellschaft für Synchrotronstrahlung (BESSY) mbH. Thanks to the BESSY staff, who have given help in many situations; especially I want to thank Manfred Willmann, who has put the SX700/3 beamline in a very good shape. Furthermore, I want to thank Oliver Rader, I was always happy to meet him again at BESSY.

Special thanks to Jutta Gollnick for all her help with any bureaucracy and for her great contributions to the friendly atmosphere in our group.

I want to thank Prof. G. Dietz for his willingness to co-assess this thesis.

Last but not least I want to thank my parents who made my studies possible and Claudia, who had to miss me a lot during the beamtimes.

FORSCHUNGSZENTRUM JÜLICH GmbH

KFA

Jül-2994
December 1994
ISSN 0944-2952